NUMERICAL ANALYSIS ON FAILURE PRESSURE OF PIPELINES WITH
MULTI-CORRODED REGION

NG YEW KEONG

Report submitted in partial fulfillment of requirements
for award of the Degree of
Bachelor of Mechanical Engineering

Faculty of Mechanical Engineering
UNIVERSITI MALAYSIA PAHANG

JUNE 2013

UNIVERSITI MALAYSIA PAHANG
FACULTY OF MECHANICAL ENGINEERING

I certify that the project entitled "*Numerical Analysis on Failure Pressure of Pipelines With Multi-Corroded Region*" is written by *Ng Yew Keong*. I have examined the final copy of this project and in my opinion, it is fully adequate in terms of language standard and report formatting requirement for the award of the degree of Bachelor of Mechanical Engineering. I herewith recommend that it be accepted in partial fulfilment of the requirements for the degree of Bachelor of Mechanical Engineering.

NUR AZHANI ABD RAZAK

Examiner   Signature

SUPERVISOR'S DECLARATION

I hereby declare that I have checked this report and in my opinion, this report is adequate in terms of scope and quality for the award of the degree of Bachelor of Mechanical Engineering.

Signature   :

Name of supervisor   : NASRUL AZUAN BIN ALANG

Position   : LECTURER

Date   : 27 JUNE 2013

STUDENT'S DECLARATION

I hereby declare that the work in this project report "*Numerical Analysis on Failure Pressure of Pipelines With Multi-Corroded Region*" is my own except for quotations and summaries which have been duly acknowledged. The report has not been accepted for any degree and is not contently submitted in candidate of any other degree.

Signature   :

Name   : NG YEW KEONG

ID Number   : MA09029

Date   : 27 JUNE 2013

Dedicated to my beloved

Father: Ng Peng Fook

Mother: Lee Lian See

Brothers

For your support and prayers…

It means a lot to me…

From my deepest heart, I love you all so much

Thank you very much

ACKNOWLEDGEMENT

I am grateful and would like to express my sincere gratitude to my supervisor Mr. Nasrul Azuan Bin Alang for his germinal ideas, invaluable guidance, continuous encouragement and constant support in making this research possible. He has always impressed me with his outstanding professional conduct and his time waste to conduct me.

Besides that, I would like to acknowledge with much appreciation the crucial role of staff in Analysis Room Faculty of Mechanical Engineering, for their valuable comments, sharing their time and knowledge on this research project during the project was carried out and giving a permission to use all the necessary tools in the laboratory. They have contributed towards my understanding and thoughts.

Last but not least, an expression of thanks is extended to everyone who has offered their help and support especially to my family and friends. All of their helps are very significant to the success of this project. I cannot find the appropriate words that could be properly described my appreciation for their devotion, support and faith in my ability to attain my goal.

ABSTRACT

The underground gas pipeline is vulnerable which can explode any time. The percentage of the pipeline fails due to the pressure may cause fatal destruction. Hence, the predictions of pipeline burst pressure in the early stage are very important in order to provide assessment for future inspection, repair and replacement activities. This thesis is to study the effect of multiple corrosion defects on failure pressure for API X42 steel and validate the results with available design codes. The project implicates analysis by using MSC Patran 2008 r1 software as a pre-processor and MSC Marc 2008 r1 software as a solver. Half of the pipe was simulated by fully applying symmetrical condition. The pipe is modeled in 3-D with outer diameter 381 mm, wall thickness of 17.5 mm and different defect parameter. In this analysis, SMCS and von Mises stress used to predict the failure pressure. The result shows that the failure pressure increases when the distance between defect increases but decreases when the defect length increases. SMCS always shows a higher value compared to von Mises. The design codes applied only when the distance between defect is small enough that multiple defects acts as a single defect. Meanwhile, value of FEA is the highest among all the design codes.

ABSTRAK

Saluran paip gas bawah tanah terdedah yang boleh meletup bila-bila masa. Peratusan perancangan gagal kerana tekanan boleh menyebabkan kerosakan maut. Oleh itu, ramalan-ramalan saluran paip tekanan pecah pada peringkat awal adalah amat penting dalam usaha untuk memberikan penilaian untuk pemeriksaan masa depan, pembaikan dan aktiviti penggantian. Karya ini adalah untuk mengkaji kesan pelbagai kecacatan hakisan pada tekanan kegagalan API X42 keluli dan mengesahkan keputusan dengan kod reka bentuk boleh didapati. Projek ini membabitkan analisis dengan menggunakan perisian Patran 2008 r1 MSC sebagai pra-pemproses dan Marc 2008 perisian MSC r1 sebagai penyelesai. Separuh daripada paip adalah simulasi dengan menggunakan sepenuhnya keadaan simetri. Paip ini dimodelkan dalam 3-D dengan diameter luar 381 mm, ketebalan dinding sebanyak 17.5 mm dan parameter kecacatan yang berbeza. Dalam analisis ini, SMC dan von Mises tekanan digunakan untuk meramalkan tekanan kegagalan. Hasilnya menunjukkan bahawa tekanan kegagalan meningkat apabila jarak antara kenaikan kecacatan tetapi berkurangan apabila kenaikan panjang kecacatan. SMC sentiasa menunjukkan nilai yang lebih tinggi berbanding dengan von Mises. Kod reka bentuk digunakan hanya apabila jarak antara kecacatan cukup kecil bahawa pelbagai kecacatan bertindak sebagai kecacatan tunggal. Sementara itu, nilai FEA adalah yang tertinggi di kalangan semua kod reka bentuk.

TABLE OF CONTENTS

CHAPTER 3   METHODOLOGY

CHAPTER 4   RESULTS AND DISCUSSION

CHAPTER 5   CONCLUSION AND RECOMMENDATION

LIST OF TABLES

LIST OF FIGURES

LIST OF SYMBOLS

M	Bulging stress magnification factor
D	Outer diameter of the pipe
t	Wall thickness
σ_y	Yield strength of the material
σ_u	Ultimate tensile strength
l	Length of defect
d	Defect depth
W	Distance between defects
ε_f	Equivalent fracture strain
ε_f^*	Equivalent fracture strain for smooth specimen
σ_m	Hydraulic stress
σ_e	Equivalent stress
K	Strength coefficient
n	Strength hardening exponent

LIST OF ABBREVIATIONS

2D	Two Dimension
3D	Three Dimension
API	American Petroleum Institute
ASME	American Society of Mechanical Engineer
ASTM	American Society for Testing and Materials
FEA	Finite Element Analysis
HSS	High Speed Steel
SMCS	Stress Modified Critical Strain
VGM	Void Grow Model

CHAPTER 1

INTRODUCTION

1.1   BACKGROUND

Nowadays, offshore and onshore pipelines are the highest capacity and the safest means of gas or oil transmission in the world. Trans Thailand-Malaysia Gas Pipeline (TTM) is a gas pipeline linking suppliers in Malaysia to consumers in Thailand. It is a part of the Trans-ASEAN Gas Pipeline project to transport and process natural gas.

However, underground gas pipelines are often damaged due to surrounding and third-party accidents throughout the years as well as increasing of ages. The most common defects in the pipelines are corrosion and dents. Hence, the probability of gas leaking or bursting of the pipeline has increased. The aging pipelines also known as underground time bombs can cause fatal destruction.

Failure due to internal and external corrosion defects has been a major concern in maintaining pipeline integrity. As a pipeline ages, it can be affected by a range of corrosion mechanism, which lead to a reduction in its structural integrity and eventual failure. Corrosion occurs as individual pits, colonies of pits, general wall-thickness reduction, or in combinations. For the pipe with colonies of pits, they begin to interact reducing the burst strength of the pipe as the distance between two corrosion pits decreases.

Naturally, the corrosion started at the point of cracking. The dents and gouges also participate in the formation of corrosion. However, the outer corroded surface of pipelines with desired size and orientation is quite difficult to get in a short time.

Therefore, the artificial defects with desired shape is created to have a different type of analysis. The determination of burst pressure for underground gas pipelines is critical to prevent accidents. Throughout this research the effect of multiple corrosion defects on failure pressure and validation of results with available design codes can be determined.

1.2   PROBLEM STATEMENT

The underground gas pipeline is vulnerable which can explode any time. The defects on the surface of the pipeline further increase the danger. The percentage of the pipeline fails due to the pressure may cause fatal destruction. The main defects that caused the pipes to fail are corrosion and third party such as dents and gouges. The dimension of the defects plays important role in the pipeline failure. The depth, width, and length are vital to determine the burst pressure. The effect of these parameters on burst pressure must be analyzed in order to predict the failure of the pipes. The multiple corroded defects aligned longitudinally are located at outer surface of the pipe. The corroded defects are made artificially with desired dimension for simulation.

1.3   OBJECTIVES

The objectives of the study are as follows:

  i.   To study the effect of multiple corrosion defects on failure pressure.
  ii.   To validate the results with available design codes.

1.4   SCOPES

The scopes of the study are as follows:

  i.   Machining: tensile test specimens
  ii.   Spectrometry analysis
  iii.   Uniaxial tension test according to ASTM E8 for smooth and notched specimens
  iv.   Development of failure criteria
  v.   Structural modelling: model the pipe with multi corroded region using MSC Patran software
  vi.   Analysis: A 3D Non-linear FEA using MSC Marc software

CHAPTER 2

LITERATURE REVIEW

2.1   INTRODUCTION

This chapter will briefly explain about the properties, material, design, failure, and cause of failure in the pipeline. The sources are taken from journals, articles, and books. Besides, the information about the software that will be used also included in this chapter. The purpose of literature review is to provide information on previous research and that can help to run this project smoothly. All this information is important before furthering to the analysis and study later.

2.2   PIPELINES ISSUES IN MALAYSIA

Underground pipelines transport large quantities of product from the source to the marketplace. The first oil pipeline, which measured at 175 km in length and 152 mm in diameter, was laid from Bradford to Allentown, Pennsylvania in 1879 (Thompson and Beavers, 2006). Since the late 1920s, virtually all oil and gas pipelines have been made of welded steel.

Malaysia has the one of the most extensive natural gas pipeline networks in Asia (EIA, 2011). The Peninsular Gas Utilization (PGU) project expanded the natural gas transmission infrastructure in Peninsular Malaysia. The PGU project is an integral part of Malaysia's economic development plan and involves the construction and installation of facilities for production, processing, and transmission of gas to customers throughout peninsular Malaysia (Gas Technology, 1998). The PGU pipeline project, with a total distance of 1,688 km is supplying Peninsular Malaysia and Singapore with a total of 56

million cubic meters a day, with an additional standby capacity of 21 million cubic meters a day (APERC, 2000). The figure 2.1 shows the major existing and planned domestic gas pipelines in Malaysia.
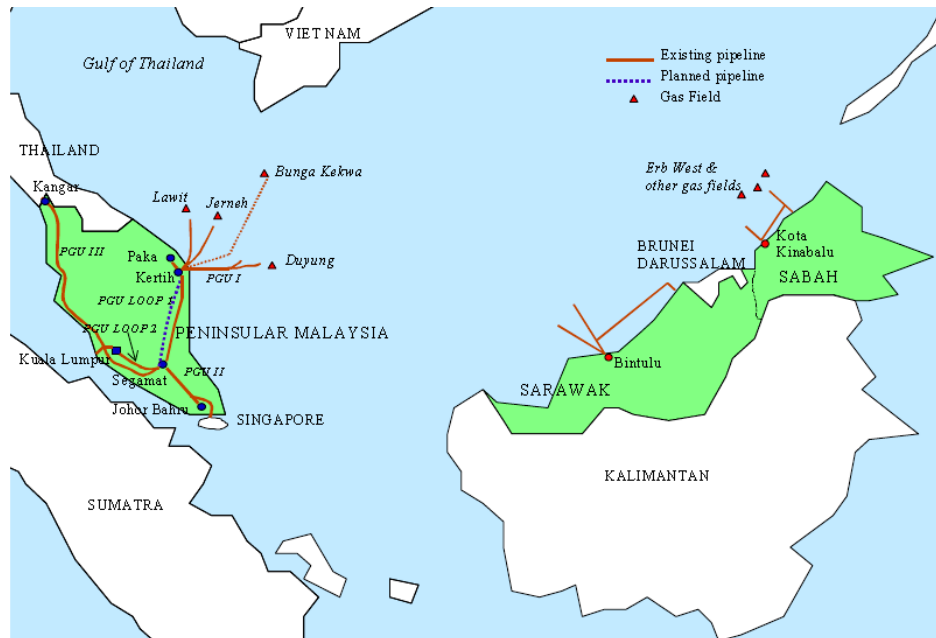
Figure 2.1: Existing and planned gas pipelines in Malaysia

Source: APERC (2000)

The RM4.6 billion Sabah-Sarawak gas pipeline project linking Kimanis in Sabah and Bintulu in Sarawak, expected to be completed by the end of 2013, will be successful as the North-South Expressway (PLUS) linking the Peninsular Malaysia states (New Straits Times, 2011). This project would transport gas from the Sabah Oil and Gas Terminal in Kimanis to customers in Sabah and Petronas LNG complex in Bintulu. Once operational, the terminal will be able to receive, store, and export up to 300,000 bbl/d of crude oil, as well as receive, process, compress, and transport up to 1.25 Bcf/d of gas produced from the Gumusut/Kakap, Kinabalu Deep and East, Kebabangan, and Malikai field (Pipelines In International, 2012; EIA, 2011; Petronas, 2012). The 512 km, 36 inch diameter Sabah Sarawak Gas Pipeline (SSGP) will transport 750 MMcf/d of gas from the Sabah Oil and Gas Terminal (SOGT) to the Petronas LNG Complex. Figure 2.2 shows the location of SOGT and SSGP. It's being

constructed using API 5L X70 steel grade pipe, with a thickness of 14,17, and 20 mm, and will have a design pressure of 96 bar.

Malaysia was the third exporter of LNG in the world after Qatar and Indonesia in 2010, exporting over 1 Tcf of LNG, which accounted for 10 percent of total world LNG exports (EIA, 2011). The Bintulu LNG complex in Sarawak is the main hub for Malaysia's natural gas industry. SOGT will supply gas for domestic use in Sabah, largely for a new electric power plant slated for completion in 2014. A reported 500,000 cubic feet per day will be piped to Bintulu complex to be exported as LNG.

Figure 2.2 Location of SOGT and SSGP

Source: Sedia (2012)

2.3   MATERIAL

Most of the pipe used for oil and gas pipelines, particularly in the United States, is either seamless or longitudinal welded pipe. But spiral weld pipe has been used increasingly in oil and gas service in many areas of the world (Kennedy, 1993). Pipe furnished to API Spec 5L may be heat treated using one of several processes: rolled, normalized, normalized and tempered, quenched and tempered, subcritically stress-

relieved, or subcritically age-hardened. Heat treating processes are used to modify the steel's characteristic to give it specific physical properties. The Table 2.1 shows the physical properties of the API 5L line pipe.

Table 2.1: Physical properties of the API 5L line pipe

API 5L Grade	Yield Strength min. (MPa)	Tensile Strength min. (MPa)	Yield to Tensile Ratio (max.)	Elongation min. %
A	206.84	330.95	0.93	28
B	241.32	413.68	0.93	23
X42	289.58	413.68	0.93	23
X46	317.16	434.37	0.93	22
X52	358.53	455.05	0.93	21
X56	386.11	489.53	0.93	19
X60	413.68	517.11	0.93	19
X65	448.16	530.90	0.93	18
X70	482.63	565.37	0.93	17
X80	551.58	620.53	0.93	16

Source: Woodco USA

The chemical composition of steels is varied to provide specific properties. API specifications give a detailed listing of the amount of each element that can be contained in a given grade of steel used for line pipe. Carbon is a key component in all steels. The amount of carbon affects the strength, ductility, and other physical properties of steel. Maximum carbon content ranges from 0.21%-0.31%, depending on the grade of steel used and the method of pipe manufacture. In general, the amount if manganese required in line pipe steel increases as the grade (strength) increases. For instance, the maximum manganese in Grade A pipe is 0.90% and the maximum content in Grade X70 is 1.60% (Kennedy, 1993). The chemical properties of the API 5L line pipe indicates in Table 2.2.

Table 2.2: Chemical properties of the API 5L line pipe

Grade & Class	Carbon, Max	Manganese, Max	Phosphorus		Sulfur, Max	Titanium, Max
			Min	Max		
A25, C1 I	0.21	0.60		0.030	0.030	
A25, C1 II	0.21	0.60	0.045	0.080	0.030	
A	0.22	0.90		0.030	0.030	
B	0.28	1.20		0.030	0.030	0.04
X42	0.28	1.30		0.030	0.030	0.04
X46, X52, X56	0.28	1.40		0.030	0.030	0.04
X60	0.28	1.40		0.030	0.030	0.04
X65, X70	0.28	1.40		0.030	0.030	0.06

Source: API (2004)

2.4   TYPES OF DEFECT

The possibility defects in the pipeline can be occurred during manufacturing, transportation, fabrication and installation, and occur both due to deterioration and due to external interference. The main factor cause of damage and failures in transmission pipelines in Western Europe and North America is external interference (Cosham and Kirkwood, 2000), e.g. a farmer accidentally gouging a pipeline or a boat denting an offshore pipeline by dragging an anchor across it. The main defects considered in the pipeline are listed as below.

   i.   Corrosion

  ii.   Gouges

 iii.   Dents

 iv.   Third-party defects

2.4.1   Corrosion

Corrosion is an electrochemical process. It is a time dependent mechanism and depends on the local environment within or adjacent to the pipeline (Cosham, Hopkins and Macdonald, 2007). NACE International (NACE) states that corrosion is the deterioration of a material, usually a metal, which results from a reaction with its

environment. Corrosion usual appears as either general corrosion or localized (pitting) corrosion. Corrosion causes metal loss. In regards to external corrosion, the environment would be groundwater or moist for onshore pipelines and seawater for offshore pipelines. Figure 2.3 shows the corroded pipeline. For internal corrosion, the environment would be water containing sodium chloride (salt), hydrogen sulphide, and/or carbon dioxide (Baker, 2008). Data for onshore gas transmission pipelines in Western Europe in the period from 1970 to 1997 indicates that 17% of all incidents resulting in a loss of gas were due to corrosion (Cosham, Hopkins and Macdonald, 2007).

Figure 2.3: Corroded pipeline

Source: David Daring

2.4.2   Dents and Gouges

A pipe can be mechanically damaged during transport, construction, while in service, or during maintenance. Mechanical damage can take the form of accidental bends, buckles (surface ripples), dents (deformation of the cross section), gouges (sharp, knife like groove), or fatigue failure (Antaki, 2005). A gouge normally results in a highly deformed, work hardened surface layer and may involve metal removal as shown in Figure 2.4. These damages can result in immediate failure of the pipe, delayed failure or no failure over the design life of the pipeline (Panetta et al., 2001). A dent in a

pipeline is a permanent plastic deformation of the circular cross section pipe which have a gross distortion of the pipe cross-section. A dent causes a local stress and strain concentration and a local reduction in the pipe diameter. The dent depth is the most significant factor affecting the burst strength and the fatigue strength of a plain dent (Cosham and Hopkins, 2003).

Figure 2.4: Defects of dents and gouges

Source: Pipelines OZ (2012)

2.5   TYPES OF CORROSION

It is convenient to classify corrosion by the forms in which it manifests itself, the basis for this classification being the appearance of the corroded metal. Each form can be identified by mere visual observation. In most cases the naked eye is sufficient, but sometimes magnification is helpful or required. Valuable information for the solution of a corrosion problem can often be obtained through careful observation of the corroded specimens or failed equipment. However, all the forms of corrosion are more or less interrelated (Fontana and Greene, 1967 as cited in Corrosion Doctors).

2.5.1   Uniform Attacks

Uniform attack is the most common form of corrosion. It is normally characterized by a chemical or electrochemical reaction which proceeds uniformly over the entire exposed surface or over a large area. The metal becomes thinner and eventually fails which shown in Figure 2.5. For example, a piece of steel or zinc immersed in dilute sulphuric acid will normally dissolve at a uniform rate over its entire surface. A sheet iron roof will show essentially the same degree of rusting over its entire outside surface. General attack corrosion accounts for the greatest amount of metal destruction by corrosion, but is considered as a safe form of corrosion, due to the fact that it is predictable, manageable and often preventable (About.com).

Figure 2.5: Generalized corrosion

Source: Corrview

2.5.2   Galvanic or Two Metal Corrosion

A potential difference usually exists between two dissimilar metals when they are immersed in a corrosive or conductive solution. If theses metals are placed in contact (or otherwise electrically connected), this potential difference produces an electron flow between them (Corrosion Doctors). Figure 2.6 shows the generalized corrosion. Corrosion of the less corrosion resistant material is decreased, as compared

with the behaviour of these metals when they are not in contact. The farther apart the metals are in the galvanic series, the greater the galvanic corrosion effect or the rate will be (David Darling). New steel pipe installed during a repair or renovation is often more electronegative than older existing pipe, and therefore may suffer from some degree of galvanic attack (Corrview).

Figure 2.6: Galvanic corrosion

Source: Corrview

2.5.3   Pitting Corrosion

Passive metals, such as stainless steel, resist corrosive media and can perform well over long periods of time. However, if corrosion does occur, it forms at random in pits (David Darling). Pits are sometimes isolated or so close together that they look like a rough surface as shown as Figure 2.6. Generally a pit may be described as a cavity or hole with the surface diameter about the same as or less than the depth. Pitting is the most common form of corrosion found where there are incomplete chemical protective films, and insulating or barrier deposits of dirt, iron oxide, organic, and the other foreign substances at the pipe surface (Corrview).

Figure 2.7: The rust indicates the pitting is occurring.

Source: David Darling

2.5.4   Erosion Corrosion

Erosion corrosion is the acceleration or increase in rate of deterioration or attack on a metal because of relative movement between a corrosive fluid and the metal surface (Corrosion Doctors) which shown in Figure 2.8. Erosion is similar to impingement attack, and is primarily found at elbows and tees, or in those areas where the water sharply changes direction. Softer metals such as copper and brass are inherently more susceptible to erosion corrosion than steel (Corrview). Many people assume that erosion corrosion is associated with turbulent flow. This is true, because all practical piping systems require turbulent flow, the fluid would not flow fast enough if laminar flow were maintained (David Darling).

Figure 2.8: Erosion Corrosion

Source: David Darling

2.5.5   Microbiologically-influenced Corrosion (MIC)

MIC also known as microbial corrosion is the corrosion that is caused by the presence and activities of microbes. This corrosion can take many forms and can be controlled by biocides or conventional corrosion control methods. Figure 2.9 represents the microbiologically-influenced corrosion. Most MIC takes the form of pits that form underneath colonies of living organic matter and mineral and biodeposits (David Darling). A MIC presence usually signals a very severe threat to the entire system requiring extensive and repeated cleaning and sterilization at great expense. For many affected systems, MIC cannot be eliminated, and an elevated corrosion and pitting condition will exist for the remainder of system life.

Figure 2.9: Microbiologically-influenced Corrosion

Source: Corrview

2.5.6   Intergranular Corrosion

Intergranular corrosion is an attack on or adjacent to the grain boundaries of a metal or alloy. A highly magnified cross section of most commercial alloys will show its granular structure as indicates in Figure 2.10. This structure consists of quantities of individual grains, and each of these tiny grains has a clearly defined boundary that chemically differs from the metal within the grain center (David Darling). Corrosion often occurs due to impurities in the metal, which tend to present in higher contents near

grain boundaries (About.com). These boundaries can be more vulnerable to corrosion than the bulk of the metal.
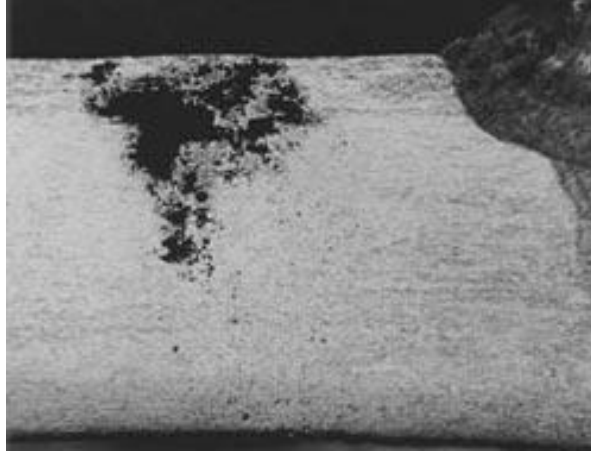
Figure 2.10: Intergranular corrosion

Source: David Darling

2.6   INTERNAL AND EXTERNAL CORROSION

Internal and external corrosion are together one of the major causes of pipeline failures (Cosham, Hopkins, and Macdonald, 2007). According to the Summary of corrosion-related accident reports, the percentage of the accidents due to the external corrosion in natural gas distribution is higher than the accidents due to internal corrosion by 31.3% (Beavers and Thompson, 2006). Although the external corrosion in this case is higher than the internal corrosion, both types of corrosion play important role in the pipeline application. Figure 2.11 and 2.12 represent the internal and external corrosion respectively.

Corrosion on the internal wall of a natural gas pipeline can occur when the pipe wall is exposed to water and contaminants in the gas, such as O_2, HS, CO, or chlorides. The nature and extent of the corrosion damage that may occur are functions of the concentration and particular combinations of these various corrosive constituents within the pipe, as well as the operating conditions of the pipeline. Internal corrosion may also

be caused or facilitated by the activity of microorganisms living on the pipe wall (Corrosion Doctors).

Figure 2.11: Internal corrosion

Source: Indymedia

The presence and activities of microorganisms estimated to have 20-30% relationship of the external corrosion on underground pipelines (Beavers and Thompson, 2006). The stress-corrosion cracking (SCC) is also grouped in the external corrosion. The cracks propagate through the grains in the metal and it is associated with corrosion of the crack faces and, in some cases, with corrosion on the external surface of the pipe as well.
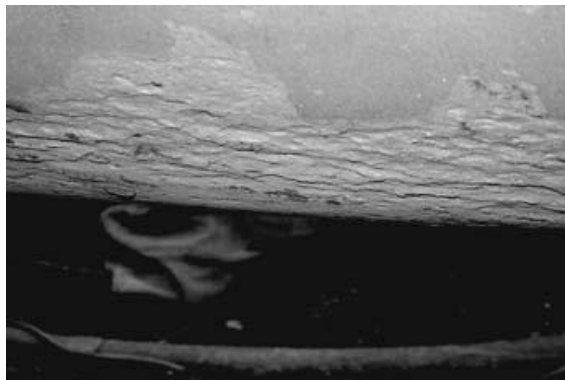
Figure 2.12: External corrosion

Source: Beavers and Thompson (2006)

2.7   FUNDAMENTAL THEORY AND EQUATIONS

In this section, the fundamental theory and equations will be included in converting the data for engineering stress-strain to true stress-strain.

2.7.1   Engineering Stress and Strain

According to (P. Beer, E. Russell Johnston, T. Dewolf, & F. Mazurek, 2009), stress could be defined as the force per unit area or the intensity of the forces distributed over a given section and is denoted by the Greek letter σ(sigma) whereas the strain is defined as the deformation of the member per unit length.

Both stress and strain are expressed as equation shown below in engineering terms.

$$\text{Stress}, \sigma = \frac{\text{Load}}{\text{Cross sectional area}} = \frac{P}{A_o} \qquad (2.1)$$

$$\text{Strain}, \varepsilon = \frac{\text{Change in length}}{\text{Original length}} = \frac{\delta}{l_o} \qquad (2.2)$$

2.7.2   Modulus of elasticity

$$\text{Modulus of elasticity}, E = \frac{\text{Stress}}{\text{Strain}} = \frac{\sigma}{\varepsilon} \qquad (2.3)$$

The coefficient E, which is the modulus of elasticity is defined as the ratio of stress applied to a material with the strain of the material. Besides that, it also can be understood that, stress and strain in this term are directly proportional to each other.

2.7.3   True Stress and Strain

According to (Smith and Hashemi, 2009), since the cross-sectional area of the specimen decreases as P increases, the stress account does not represent the actual stress in the specimen. The difference between the engineering stress and true stress that is the area of cross sectional divided. The area used for the true stress is the cross-sectional area of the deformed specimen.

$$\text{True stress}, \sigma_t = \frac{\text{Load}}{\text{Instantaneous cross sectional area}} = \frac{P}{A_i} \qquad (2.4)$$

$$\text{True strain}, \varepsilon_t = \frac{\text{Instantaneous extended gage length}}{\text{Original gage length}} = \ln\frac{l_i}{l_o} \qquad (2.5)$$

2.7.4   Relationship between Engineering Stress-Strain and True Stress-Strain

True Stress can be related to the engineering stress if assume that there is no volume change in the specimen.

$$\sigma_T = \frac{P}{A_i} = \frac{P}{A_o} \cdot \frac{l_i}{l_0} = \sigma_E(1 + \varepsilon_E) \qquad (2.6)$$

The true strain is defined as the sum of all the instantaneous engineering strains.

$$\varepsilon_T = \ln\frac{l_i}{l_o} = \ln\frac{l_o + \delta}{l_o} = \ln(1 + \varepsilon_E) \qquad (2.7)$$

2.7.5   Relationship between True Stress and True Strain

Power law used to relate true stress and true strain. The flow curve can be expressed using the equation below.

$$\sigma = K\varepsilon^n \qquad (2.8)$$

where:

K = strength coefficient

n = strength hardening exponent

2.8   STRESS IN PRESSURISED CYLINDERS

Cylindrical pressure vessels, hydraulic cylinders, gun barrels, and pipes carrying fluids at high pressures develop both radial and tangential stresses with values that depend upon the radius of the element under consideration (Budynas and Keith Nisbeth, 2011). Therefore, pipelines must be able to withstand a variety load of loads, ranging from the high loads they see during construction (e.g. during laying offshore) and during operation (e.g. due to frost heave).

2.8.1   Hoop Stress

The major stress in the most pipelines is that caused by the internal pressure, and this hoop stress is usually the major design consideration. Figure 2.13 illustrates the hoop stress on a pipe. Most design codes use the following equation for calculating the hoop stress (thin-walled pipeline):

$$\sigma_h = \frac{PD}{2t} \qquad (2.9)$$

where:

P = pipeline pressure

D = outside pipe diameter

t = pipe wall thickness
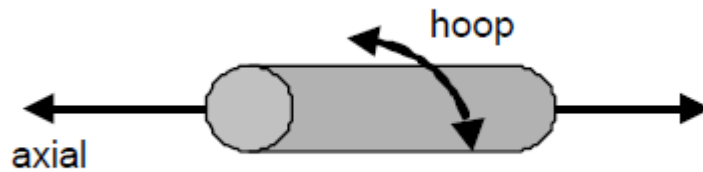
Figure 2.13: Hoop stress

Source: Hopkins (2002)

Hoop stress is defined for rotationally-symmetric objects as the average force exerted circumferentially (perpendicular both to the axis and to the radius of the object) in both directions on every particle in the cylinder. Hoop stress also known as tangential stress, σ_t, assumption was made that the longitudinal elongation is constant around the circumference of the cylinder (Budynas and Keith Nisbeth, 2011). In other words, a right section of the cylinder remains after stressing. The equation 2.10 is for thick-walled vessels. Figure 2.14 shows the cylinder subjected to both internal and external pressures.
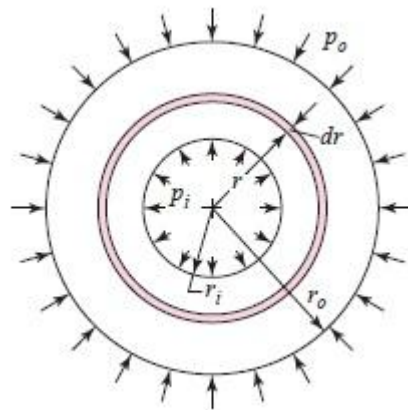
Figure 2.14: Cylinder subjected to both internal and external pressures

Source: Budynas and Keith Nisbeth (2011)

$$\sigma_t = \frac{p_i r_i^2 - p_o r_o^2 - r_i^2 r_o^2 (p_o - p_i)/r^2}{r_o^2 - r_i^2}$$

(2.10)

2.8.2   Radial Stress

It's defined as stress towards or away from the central axis of a curved member. The walls of pressure vessels generally undergo triaxial loading. For cylindrical pressure vessels, the normal loads on a wall element are the longitudinal stress, the circumferential (hoop) stress and the radial stress. The radial stress for a thick walled cylinder is equal and opposite to the gauge pressure on the inside surface, and zero on the outside surface. The circumferential stress and longitudinal stresses are usually much larger for pressure vessels, and so for thin walled cases, radial stress is usually neglected.

$$\sigma_r = \frac{p_i r_i^2 - p_o r_o^2 + r_i^2 r_o^2 (p_o - p_i)/r^2}{r_o^2 - r_i^2}$$

(2.11)

2.8.3   Longitudinal Stress

The stress in the axial direction at a point in the tube or cylinder is the longitudinal stress. In a closed cylinder, the longitudinal stress σ_l exists because of the pressure upon the ends of the vessel. The following equation is assumed that the stress is uniformly distributed over the wall thickness.

$$\sigma_l = \frac{p d_i}{4t}$$

(2.12)

2.9   MATERIAL AND SPECIMEN GEOMETRY

In order to investigate the effect of triaxial stress states on ductility of pipe, (Oh, Kim, Baek, & Kim, 2007; Oh, Kim, Baek, Kim, & Kim, 2007) performed tensile tests using smooth and notched bars with four different notch radii. The tensile bars were extracted from a pipe in the longitudinal direction. The outer diameter, D_o and wall

thickness, t is 762mm and 17.5mm, respectively. The pipe is made from the American Petroleum Institute (API) 5L X65. The minimum specified yield strength and ultimate tensile strength are 448 and 530MPa, respectively based on API specifications. Figure 2.15 shows schematic illustrations for (a) smooth tensile bars, (b) and (c) notched tensile bars. All the units are in mm.
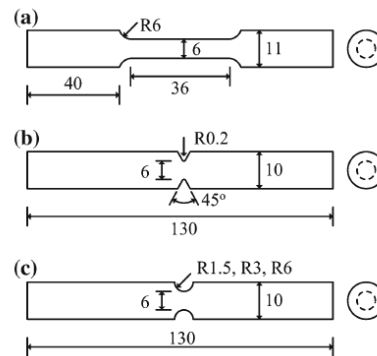
Figure 2.15: Schematic illustration of tensile bars

Source: Oh, Kim, Baek, & Kim (2007)

According to Figure 2.15, it is clearly shown that all specimens have 6 mm diameter at the minimum section. (Oh et al., 2010; Oh, Kim, Baek, Kim, & Kim, 2007) used the same dimension of specimens as above except the specimen with notched R0.2 was excluded from his study. The four machined notched bar with notch radii were 6.0 mm (R6), 3.0 mm (R3), 1.5 mm (R1.5) and 0.2 mm (R0.2). Except for R0.2, the rest of notch radii were machined. The V-notch with a half angle of 45 ° was machined with the notch radius of 0.2 mm.

2.10 EXPERIMENTAL RESULTS

The following two figures, Figure 2.16 and Figure 2.17 show the experimental engineering stress-strain and true stress-strain, respectively. Figure 2.16 indicates the experimental engineering stress-strain of smooth and notched tensile specimens. Meanwhile, Figure 2.17 represents the averaged true stress-strain data of the API X65

resulting from three tensile tests of smooth bars. The Bridgman Corrective factor is applied to correct the stress and strain for data of smooth specimens starting from the point which material has significant changed in cross-sectional area.
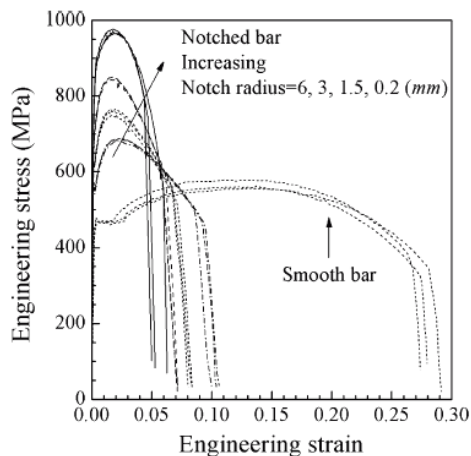
Figure 2.16: Experimental engineering stress-strain data

Source: Oh, Kim, Baek, & Kim (2007)
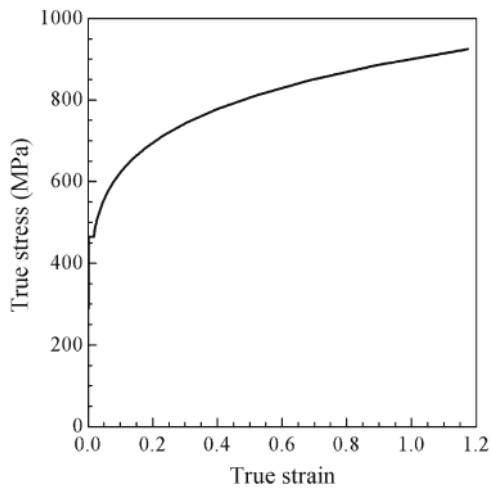
Figure 2.17: True stress-strain for API X65

Source: Oh, Kim, Baek, & Kim (2007)

(Oh et al., 2007) explained that when the notch decreases, the yield and tensile strength increase but the strain to fracture decreases. The trend of the graph above is due to the fact that the triaxial stress increases with decreasing notch radius. Meanwhile, the graph of true stress-strain is taken from the data of three tensile tests of smooth specimen.

2.11   FINITE ELEMENT ANALYSIS

2.11.1 FE model and analysis

In order to determine variations of the triaxial stress and strain within the specimen, detailed elastic-plastic and axi-symmetric FE analysis was performed to simulate tensile tests of smooth and notched specimens (Oh et al., 2010). Figure 2.18 shows FE meshing for notched tensile bars.
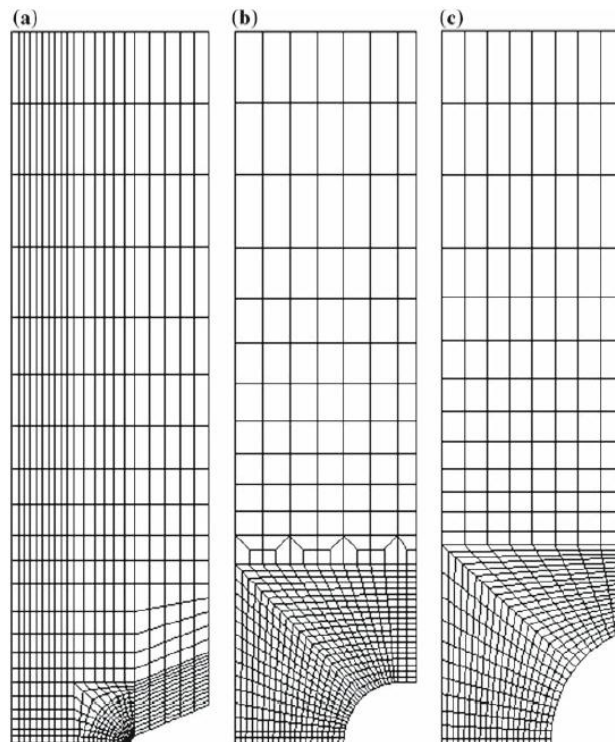
Figure 2.18: FE meshes for notched tensile bars: (a) R0.2, (b) R1.5 and (c) R3

Source: Oh, Kim, Baek, & Kim (2007)

Typically, FE meshes ranges from 484 elements/1557 nodes to 658 elements/2089 nodes. Experimental true stress-plastic strain data were used in FE analyses. Materials were modelled as isotropic elastic-plastic materials that obey the incremental plasticity theory. Symmetric conditions were fully utilized and the second order, reduced integration elements (CAX8R within ABAQUS) were used for efficient computation.

2.11.2 Comparison with experimental results
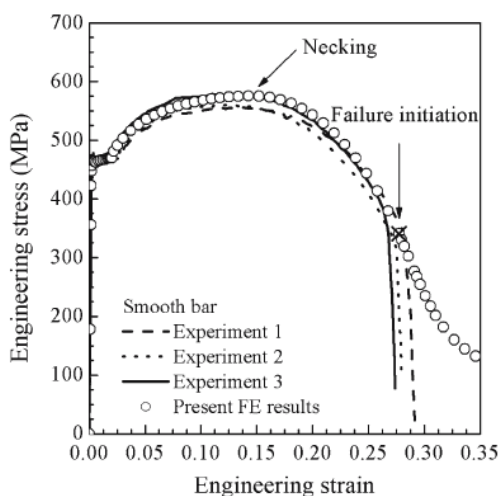
Figure 2.19: Comparison of experimental engineering stress-strain data
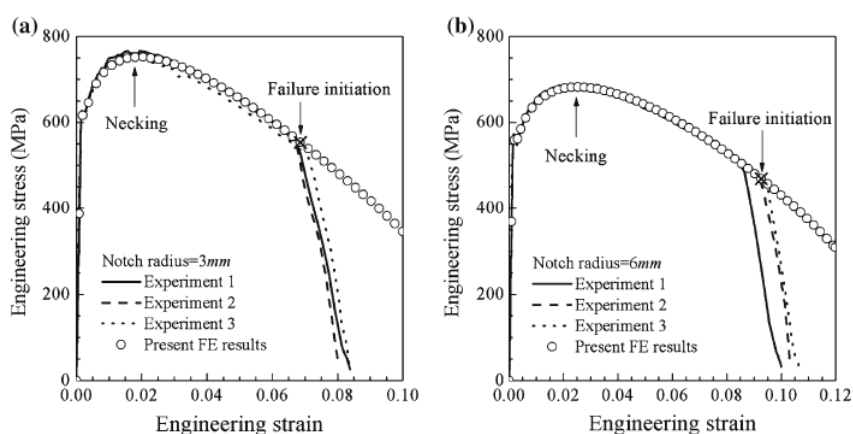
Figure 2.20: Comparison of experimental engineering stress-strain data

Souce: Oh, Kim, Baek, & Kim (2007)

According to Figure 2.19, it compared experimental engineering stress-strain data from the smooth specimen with FE results, which shows excellent agreement. Although the present FE analysis cannot simulate failure of tensile test specimens, it can simulate tensile deformation behaviour even after necking. Figure 2.20 shows the comparison of experimental engineering stress-strain for cases with two different notch radii, R3 mm and R6 mm. As for the smooth bar case, agreements between the test results and FE ones are quite good up to failure initiation points.

2.12   EVALUATION OF FAILURE PRESSURE

2.12.1 Stress Modified Critical Strain (SMCS)

SMCS model used to predict the failure pressure of pipelines with gouge and corrosion defects. The accuracy and validity of the model is acceptable in a wide range of defect geometries. Numerically, SMCS is derived from several equations as shown below. The stress triaxiality is defined by the ratio of the mean normal (hydrostatic) stress, σ_m to the equivalent stress, σ_e.

$$\frac{\sigma_m}{\sigma_e} = \frac{\sigma_1 + \sigma_2 + \sigma_3}{3\sigma_e} \tag{2.13}$$

$$\sigma_e = \frac{1}{\sqrt{2}} [(\sigma_1 - \sigma_2)^2 + (\sigma_1 - \sigma_3)^2 + (\sigma_3 - \sigma_2)^2]^{0.5} \tag{2.14}$$

$$\varepsilon_e = \frac{\sqrt{2}}{3} [(\varepsilon_1 - \varepsilon_2)^2 + (\varepsilon_1 - \varepsilon_3)^2 + (\varepsilon_3 - \varepsilon_2)^2]^{0.5} \tag{2.15}$$

Where the $\sigma_1, \sigma_2, \sigma_3$ and $\varepsilon_1, \varepsilon_2, \varepsilon_3$ are the principle stresses and principle strain respectively. The fracture strain ε_f is determined using the equation proposed by Mackenzie and Hancock:

$$\varepsilon_f = A \, exp\left(-\frac{3}{2}\frac{\sigma_m}{\sigma_e}\right) \tag{2.16}$$

where *A* is the material constant found through tensile test experiment.

2.12.2 Design Codes

There are several design codes used in practice to evaluate the remaining strength of corroded pipelines such as American Society of Mechanical Engineer (ASME) B31G, modified ASME B31G and DNV-RP-F101 codes. Referring to ASME B31G and modified ASME B31G codes, a short longitudinal corrosion defect can be simplified as a parabolic curve whereas long corrosion defect can be simplified to a rectangular shape. According to ASME B31G and DNV-RP-F101 codes, the failure of corroded pipeline is controlled by the defect size as well as the flow stress of the material. The DNV-RP-F101 code can be applied for both defect subjected to internal pressure loading only or internal pressure loading combined with longitudinal compressive stresses. However, the ASME B31G is limited to defects subjected to internal pressure only. DNV RP-F101 design code equations also include the assessment of single and interacting defects, and complex shaped of defects. The burst pressure, P_b based on these codes are expressed as:

$$P_b = \frac{2tS_f}{D} \tag{2.17}$$

ASME B31G:

$$S_f = 1.1\sigma_y \left[\frac{1 - \frac{2}{3}\left(\frac{d}{t}\right)}{1 - \frac{2}{3}\left(\frac{d}{t}\right)/M} \right] \tag{2.18}$$

$$M = \left(1 + 0.8\frac{L^2}{Dt} \right)^{0.5} \tag{2.19}$$

Modified ASME B31G:

$$S_f = (\sigma_y + 69) \left[\frac{1 - 0.85\left(\frac{d}{t}\right)}{1 - 0.85\left(\frac{d}{t}\right)/M} \right] \quad (2.20)$$

$$M = \left[1 + 0.6275\frac{L^2}{Dt} - 0.003375\left(\frac{L^2}{Dt}\right) \right]^{0.5} \quad (2.21)$$

DNV-RP-F101:

$$P_b = 1.05\left(\frac{2t\sigma_u}{D - t}\right) \left[\frac{1 - \left(\frac{d}{t}\right)}{1 - \left(\frac{d}{t}\right)/M} \right] \quad (2.22)$$

$$M = \left(1 + 0.31\frac{L^2}{Dt} \right)^{0.5} \quad (2.23)$$

where:

M = bulging stress magnification factor

D = outer diameter of the pipe

t = wall thickness

σ_y = yield strength of the material

σ_u = ultimate tensile strength

L = length of defect

d = defect depth

2.12.3 PCORCC

For corroded pipes with sufficient ductility, one solution to estimate the burst pressure of pipes with local wall thinning is the so-called PCORRC equation. The relationship of burst pressure may be expressed fitting procedure of FE simulation result. Equation proved to be conservative and closet when using 95% of UTS of tensile test, σ_u.

$$P_{burst} = \sigma_u \frac{2t}{D}\left\{1 - \frac{d}{t}\left[1 - exp\left(-C\frac{L}{\sqrt{Rt^*}}\right)\right]\right\} \qquad (2.24)$$

Where the value of C is a curve fit constant for capture the global behaviour defect failure relationship. When the pit depth is constant, the behaviour of burst pressure with with increasing defect length, L can generate C value by fitting procedure. The resulted C value varies from 0.142 ~0.224 as curve fit constant for whole range of depth. Then, limit solution about a single pit model is as follows.

$$P_{burst} = 0.95\sigma_u \frac{2t}{D}\left\{1 - \frac{d}{t}\left[1 - exp\left(-0.224\frac{L}{\sqrt{Rt^*}}\right)\right]\right\} \qquad (2.25)$$

CHAPTER 3

METHODOLOGY

3.1   INTRODUCTION

This chapter will describe the detail of the methodology used in this study. Methodology is needed to complete any research and development. The main reason to have a methodology is to assure that the project will be done in time and following the planning that has been made until it is finished. By having a good methodology, it will ensure that the project or research is following the objectives that have been stated earlier which mean it will follow the guidance based on the objectives.

3.2   FLOWCHART

The purpose of flow chart is to simplify the entire methodology part that shows the chronology to complete the project. Figure 3.1 represents the flow chart of the study.
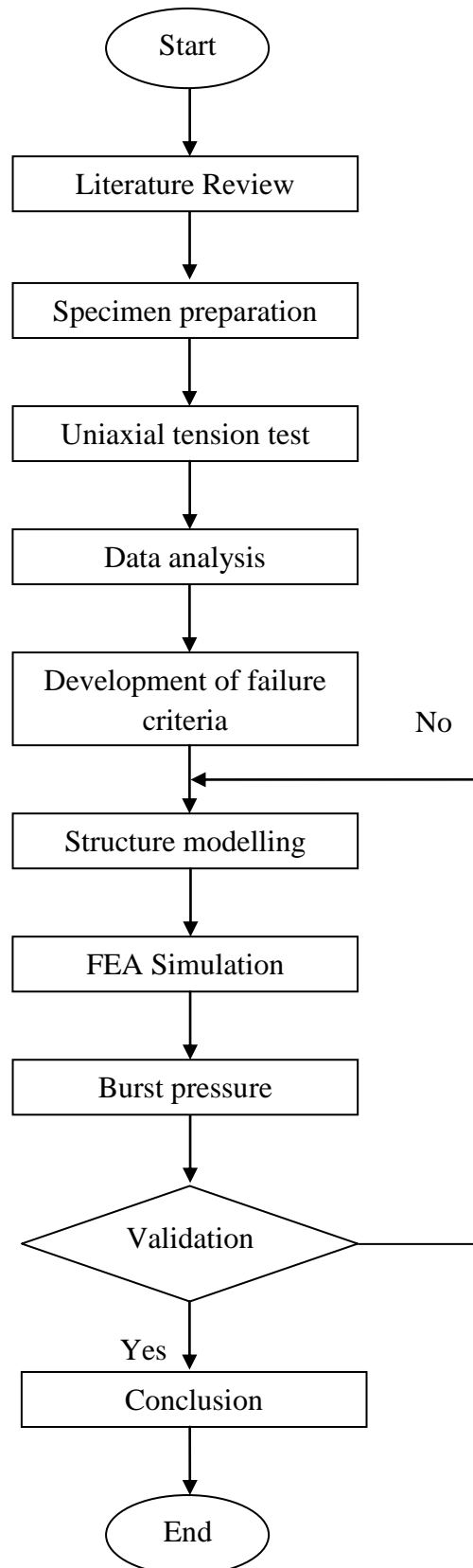
Figure 3.1: Flowchart

3.3   FLOWCHART DESCRIPTION

3.3.1   Literature Review

The literature review is needed to prove the experiment and numerical analysis is correct. Therefore, the study starts with literature review and research about the title. The content of literature review consists of the pipeline issues in Malaysia, types of corrosion, stress and strain, stress on the pipe, material and specimen preparation, experimental results and finite element analysis of the corroded pipelines. These have been done through research on the internet, books, journals and other resources.

3.3.2   Specimen Preparation

Before the specimen preparation stage, the design of the experiment is needed to determine by following the objectives of the project. The experiment design included types of machine to be used, types of material, experiment equipment and parameters needed to key in into the machine. The review dimension of smooth and notched specimen is done according to "ASTM A370". It is done to have a better understanding of the specific parameter of the specimen such as the dimension of the gage length and area of reduction. Meanwhile, the CAD modelling is prepared in engineering drawing format in order to have a detail dimension of specimens when machining. Besides, the drawing is needed to ease the guide and help from the laboratory assistants. There is a total of 13 specimens that need to be machined. The specimens consist of smooth and notched tensile bars. All the specimens are in the form of cylindrical shaped that follow "ASTM E8" standard. The raw material is a pipeline. Then, hydraulic bend saw is used to cut it into rectangular bar shaped. The raw material is cut with dimension of 30 mm width which reserved some place to machining later. The specimens are done by machining using the conventional milling machine and conventional lathe machine.
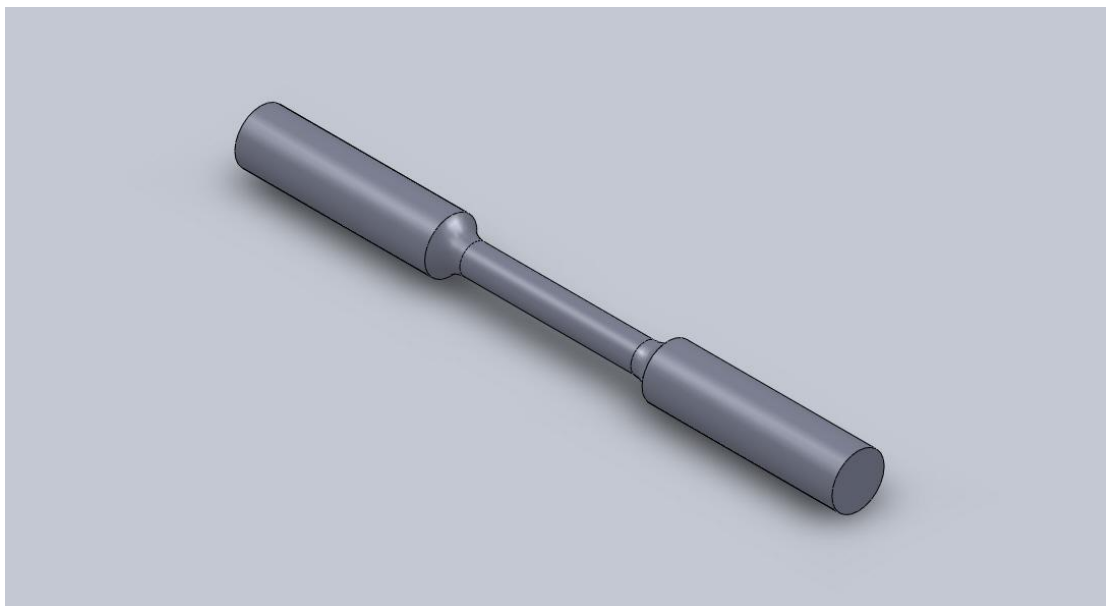
Figure 3.2: Smooth tensile bar


Figure 3.3: 1.5R notched tensile bar
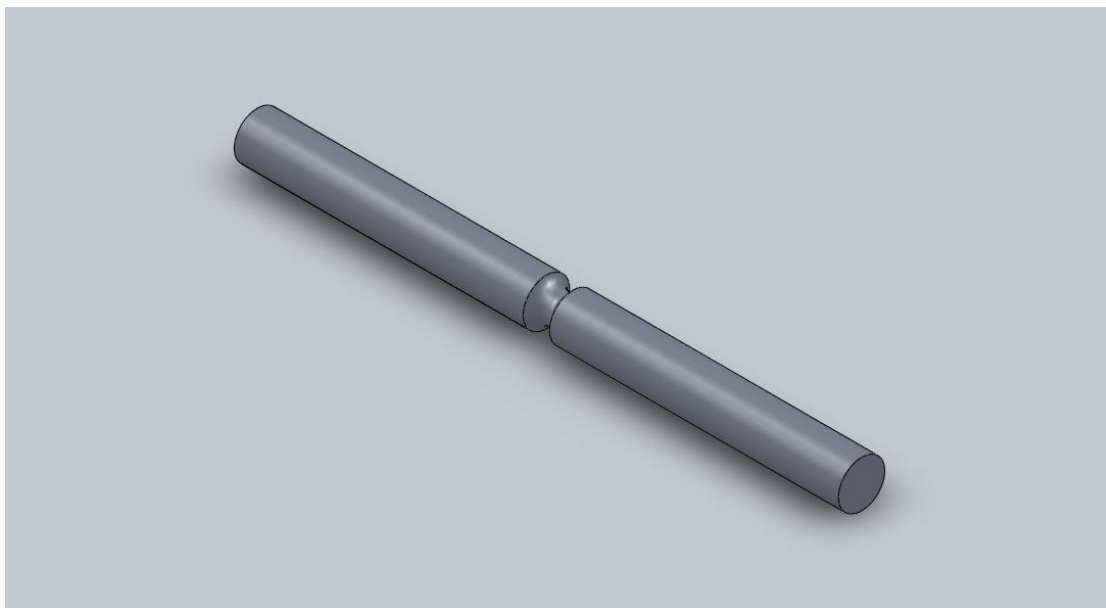
**Figure 3.4:** 3R notched tensile bar
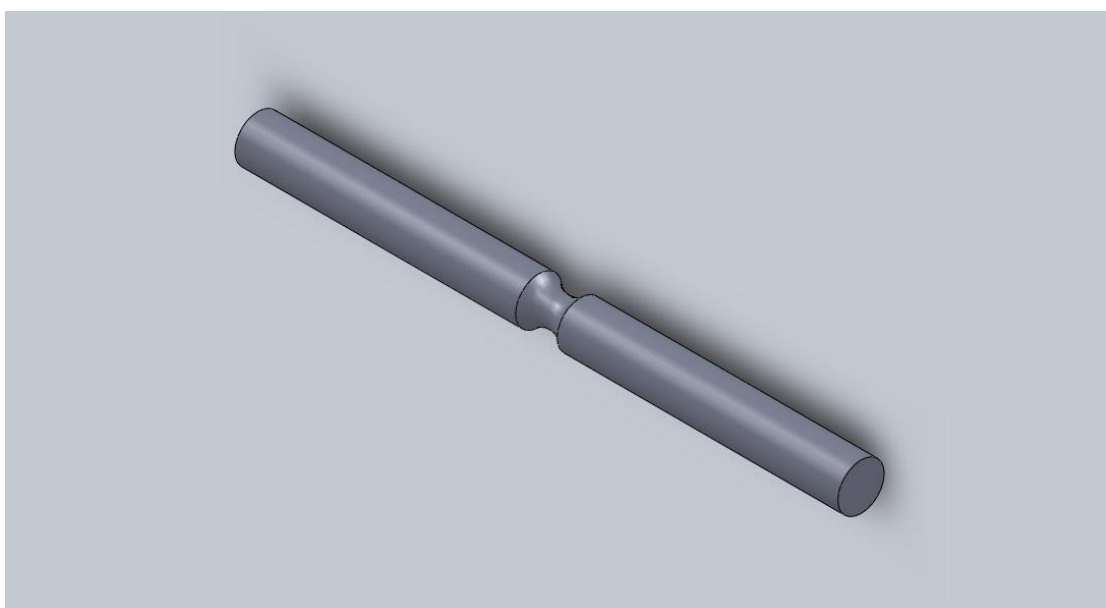
Figure 3.5: 6R notched tensile bar

3.3.3 Material

The material used for this study is API X42. The mechanical and chemical properties of the material are shown in Table 3.1. Due to the similarity of characteristic of API X65 that used in the study (Oh, Kim, Baek, & Kim, 2007; Oh, Kim, Baek, Kim, & Kim, 2007), API X42 can be used to perform similar experiment and simulation.

Table 3.1: Physical and chemical properties of API X42

API X42		
Mechanical properties	Yield Strength min. (MPa)	289.58
	Tensile Strength min. (MPa)	413.68
	Yield to Tensile Ratio (max)	0.93
	Elongation min. %	23
Chemical Properties	Carbon Max	0.28
	Manganese Max	1.30
	Phosphorus Max	0.030
	Sulphur Max	0.030
	Titanium Max	0.030

Source: Woodco USA and API (2004)

3.3.4 Machining Process

The machining process for this study is the turning/lathe process. The specimens need to be machined with 4 different dimensions. The parameters that need to be controlled in the turning process are the spindle speed, the feed rate and also the depth of cut. The unsuitable parameter will affect the surface roughness of the work piece. However, these can be repaired after the end of the process by the surface finishing. The spindle speed can be calculated using the equation below.

$$RPM = \frac{CS \; x \; 1000}{\pi d} \qquad (3.1)$$

where:

CS = cutting speed

d = work piece diameter

The feed rate calculation equation is as shown below.

$$\text{Feed rate, } v_f = f \; x \; N \qquad\qquad (3.2)$$

Where:

f = feed

N = spindle speed

Sample calculation of spindle speed:

Cutting speed $= 100 \; to \; 200 \; m/min$

Diameter of workpiece $= 20 \; mm$

$$RPM = \frac{100 \; x \; 1000}{\pi \; x \; 20} = 1592 \; rpm$$

Sample calculation of feed rate:

Feed $= 0.35 \; mm/rev$

Spinde speed $= 1592 rpm$

$$v_f = f \; x \; N = 0.35 \; x \; 1592 = 557.2 mm/min$$

Calculated machining parameters for lathe operation are shown in Table 3.2:

Table 3.2: Machining parameters

Machining parameters	Types of cutting tool	
	Carbide	**High Speed Steel (HSS)**
Spindle speed (rpm)	1592	637
Feed rate (mm/min)	557.2	95.6
Depth of cut (mm)	0.7	0.1

Below are the procedures of the lathe operation.

i. The lathe machine was set up.

ii. Lathe machine was switched on.

iii. The cutting tool was set up. Dead centre was used to centralize the cutting tool.

iv. The work piece was attached to the spindle and clamped to the chucks. The work piece was held tightly.

v. The spindle speed was set up to the 1592. Set 0,0 point for x and z axis of cutting tool.

vi. The facing processes in x axis was done to ensure the cutting tool is truly centralize. Procedure 4 was repeated if there are any nipples. The x axis was set to zero.

vii. Z axis was set to zero when the cutting tool slightly touched the work piece in z direction.

viii. The work piece was machined following geometry shape in the drawing. Refer Appendix.

ix. The feed rate was set with the value that has been calculated. Refer to Table 3.2.

x. The depth of cut was lathed with the increment of 0.7 mm during the machining process.

xi. The cutting tool was changed to HSS according to the dimension needed for the notched making.

xii. The work piece was measured using vernier calliper after machining process is finished.

xiii. The process for the rest of work piece was repeated.

Figure 3.6 to 3.10 show the process, tools and machine for the specimen preparation.

Figure 3.6: Hydraulic bend saw

Figure 3.7: Conventional lathe machine
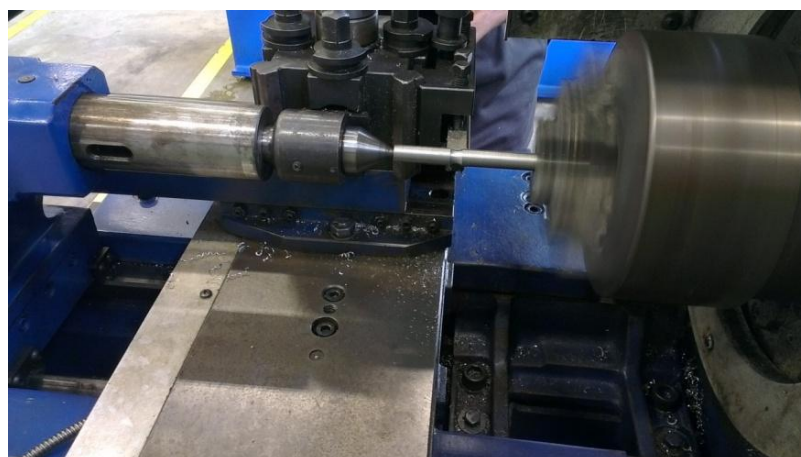
Figure 3.8: Turning process

Figure 3.9: Tool, HSS create the notched part

Figure 3.10: Transformation of raw material to specimen

3.3.5 Notched Dimension

The dimension of the notched specimen as well as the smooth specimen is measured. This was done to ensure the data that account in the calculation does not vary much from the dimension of the notched making cutting tools. Figure 3.11 shows the profile projector to measure the notched dimension.

Below are the steps in the operation of the profile projector.

  i.   The notched part of the specimen was measured after the machining process.
 ii.   The profile projector was switched on.
iii.   The clean specimen was placed on the glass of the table.

iv.   Notched part was focus properly by moving the focusing wheel and work table to obtain correct magnified images of the object.

v.   Horizontal (x axis) measurement was taken by right hand side micrometer and the vertical measurement was taken from front side micrometer.

Figure 3.11: Profile projector to measure the notched dimension

3.3.6   Spectrometry Analysis

In order to confirm the material of the machined specimens, the chemical composition of the specimens need to be checked. The material that left after turning process is used to perform spectrometric analysis. The specimen must be flat and smooth enough so that the spectrometry analysis can be performed. The spectroscopy test was repeated three times and the average data is taken. Figure 3.12 shows the optical emission spectrometry. Refer appendix for the chemical composition of the raw material.

Figure 3.12: Optical emission spectrometry

3.3.7   Uniaxial Tension Test

After finishing the material preparation process, the tension testing was conducted. The tensile test will be started to analyse the maximum of engineering stress-strain, elongation and yield strength of the specimen. The tensile test will be performed by using an equipment named as an Instron Universal Testing machine. The raw data need to be collected are values of engineering stress-strain which vary with time until fracture and displacement/elongation that vary with time as well. The data are used to obtain a true stress-strain graph which will be used to develop and derive the equation.

3.3.8   Experiment Apparatus

The experimental apparatus that is involved in this experiment is Instron 3369 Universal Testing machine as shown in Figure 3.13. This machine is needed to be setup accordingly to the standard "ASTM E8" as the project is using API X42 steel pipe.
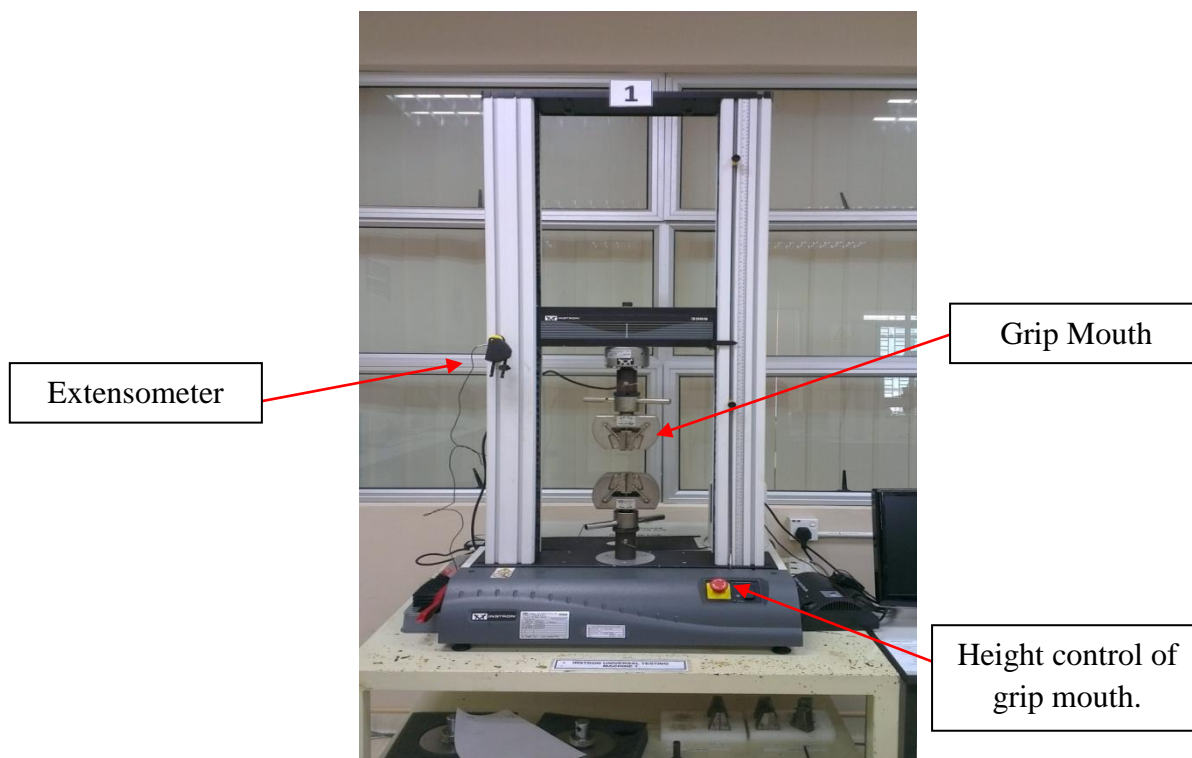

Figure 3.13: Instron 3369 Universal Testing machine

The following steps are the experiment setup for tensile test machine.

    i.   Emergency Off switch was released (pulled out).

   ii.   The machine was switched on.

  iii.   The detail of the testing was reset by using INSTRON software in computer.

  iv.   The height of the grip was adjusted so that the specimen can be placed.

   v.   All the force was reset before testing.

3.3.9   Tensile Specimen

Four type of specimens made by API X42 with different geometries that were used in this experiment are as follows:

    i.   1.5R of notched specimen

   ii.   3R of notched specimen

  iii.   6R of notched specimen

  iv.   Smooth specimen
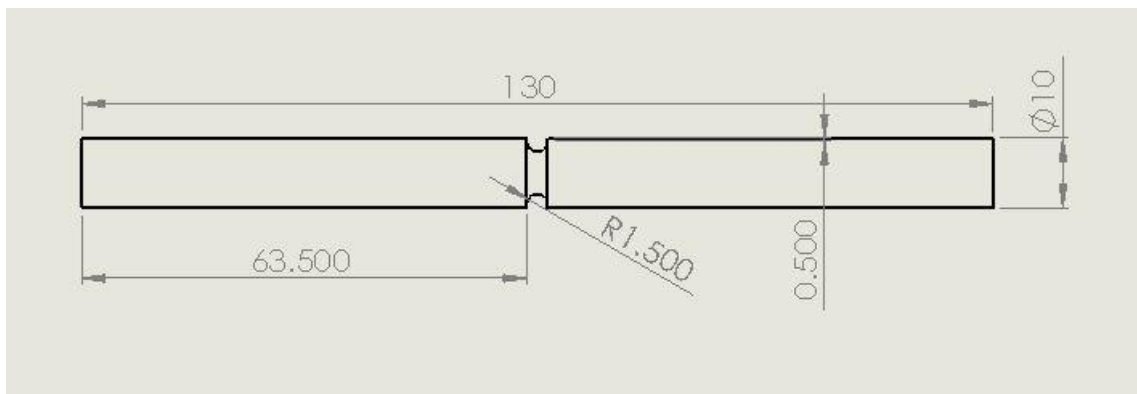
Figure 3.14: 1.5R notched specimen (unit in mm)
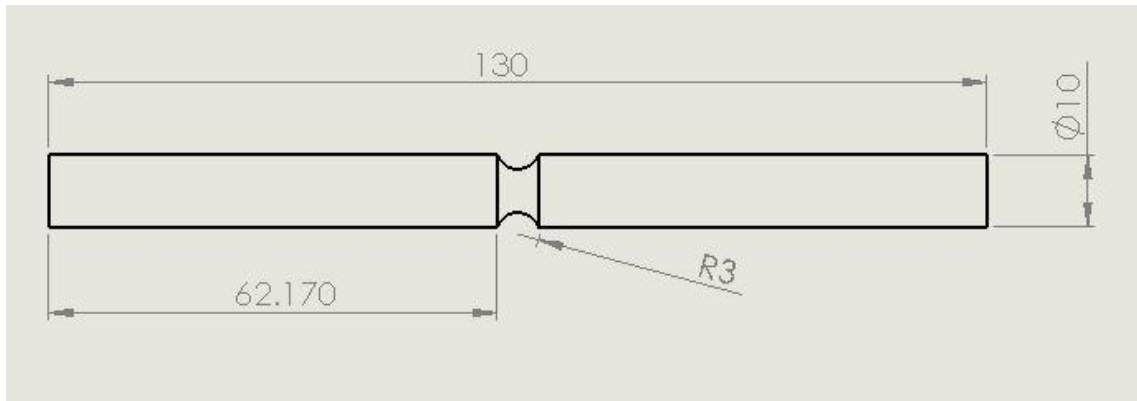
Figure 3.15: 3.0R notched specimen (unit in mm)
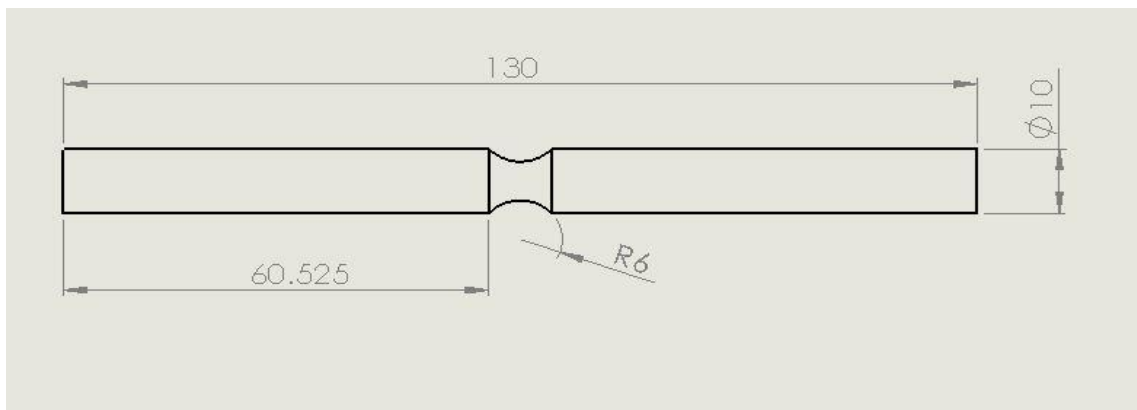
**Figure 3.16**: 6.0R notched specimen (unit in mm)
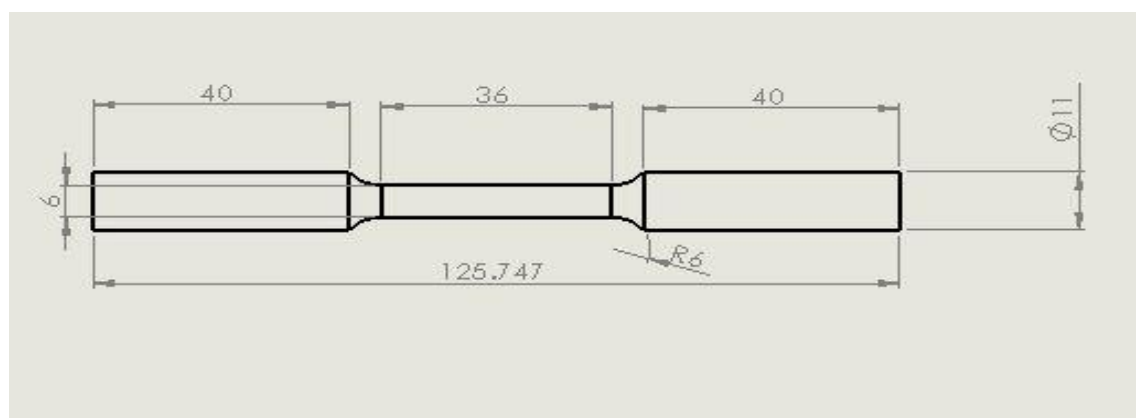
Figure 3.17: smooth specimen (unit in mm)

3.3.10 Experiment Procedure

The experiment was conducted to determine the engineering stress-strain diagram for the specimens. The constant and variable parameters are needed to be decided before the start of the experiment. The experiment parameter for this experiment is shown in Table 3.3.

Table 3.3: Experiment parameters

Parameters	Values
Speed of Testing (mm/mm/min)	0.25
Sensitivity of the end of the test (%)	80%
Gauge length of notched specimen (mm)	50
Gauge length of smooth specimen (mm)	36

After all the experimental parameters have been set, the experiment then was conducted by using the following procedure :

i. The experiment was started with 1.5R notched specimen.
ii. The gauge length of the specimen was measured and put into the grip mouth which each side away of 25 mm from centre specimen then gauge length will be 50 mm.
iii. The force was balance before the test started.
iv. Collect raw data for engineering stress-strain, times and displacement of each specimen.
v. Repeat the above procedure with different specimens.

3.3.11 Measurement of Final Diameter of Rupture Specimens

Measuring Microscope Marvision MM320 is an instrument for measuring For example, points, lines, circles, distances, intersection and etc. The measuring of geometric elements is via automatic edge detection. Quadra-Chek 300 is to display the 2D view of surface specimen so that it is easy for users to measure the geometric accuracy. Figure 3.18 and 3.19 show Microscope Marvision MM320 and Quadra-Chek 300 instruments respectively.
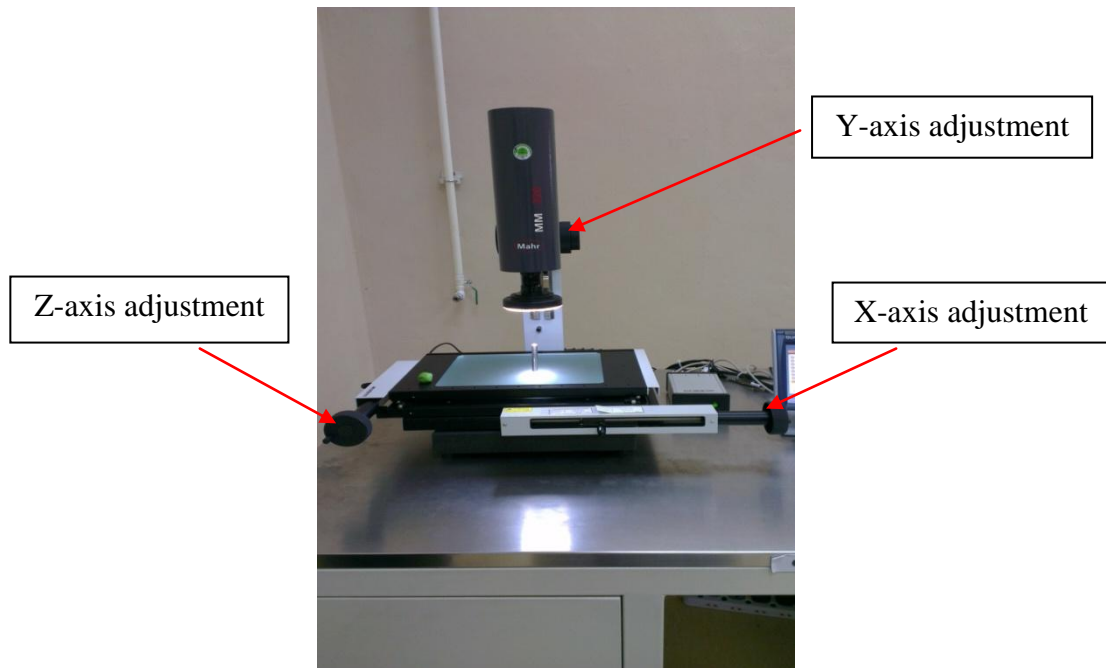
Figure 3.18 : Microscope Marvision MM 320 - Mahr

Figure 3.19 : Quadra-Chek 300

The experiment have been conducted to determine the final diameter of failed specimen after tensile test. In order to obtain the correct values, the experiment will be conducted by using the following procedures :

i.   The desktop that linked the Microscope Marvision MM 320 was switched on.

ii. The measuring Microscope Marvision MM 320 was switched on and followed by Quadra-Chek 300.

iii. The clean specimen was placed on the platform of glass at measuring microscope.

iv. The specimen was focused properly by moving the focusing wheel and work table to obtain correct magnified images of the object and the better view was shown at Quadra-Chek 300.

v. The measuring type of circle with 4 point was chosen.

vi. 4 points around the specimen was found to form a circle.

vii. The best answer for the points that selected was provided.

viii. Steps 3 - 7 for several of specimens was repeated.

3.3.12 Analysis of Tensile Test Data

From the tensile test, the data such as load, extension, stress and strain can be converted into two graphs. These are engineering stress-strain and true stress-strain graphs. The following two equations are used to convert engineering stress-strain to true stress-strain. Refer to equation 2.6 and 2.7 as below.

$$\sigma_t = \sigma_e(1 + \varepsilon_e) \tag{2.6}$$

$$\varepsilon_t = \ln(1 + \varepsilon_e) \tag{2.7}$$

DPLOT software is used to find the yield point of engineering stress-strain. The equation 2.6 and 2.7 is valid from yield stress to ultimate tensile strength. Therefore, power law equation is used to represent the trend line of true stress-strain from yield point to ultimate tensile strength. Refer equation 2.8 as below.

$$\sigma = K\varepsilon^n \tag{2.8}$$

Meanwhile, the true fracture strain can be obtained by measuring the diameter of the specimens after rupture.

$$\varepsilon_f = \ln\frac{A_o}{A_f} \qquad (3.3)$$

$$\varepsilon_f = \ln\left(\frac{D_o}{D_f}\right)^2 \qquad (3.4)$$

where:

D_o = initial diameter of tensile specimen

D_f = final diameter of tensile specimen

Data from the ultimate tensile strength to rupture point of true stress can be calculated by substituting the true strain into the power law. The engineering stress strain and true stress strain are shown in Figure 3.20 and 3.21 respectively.
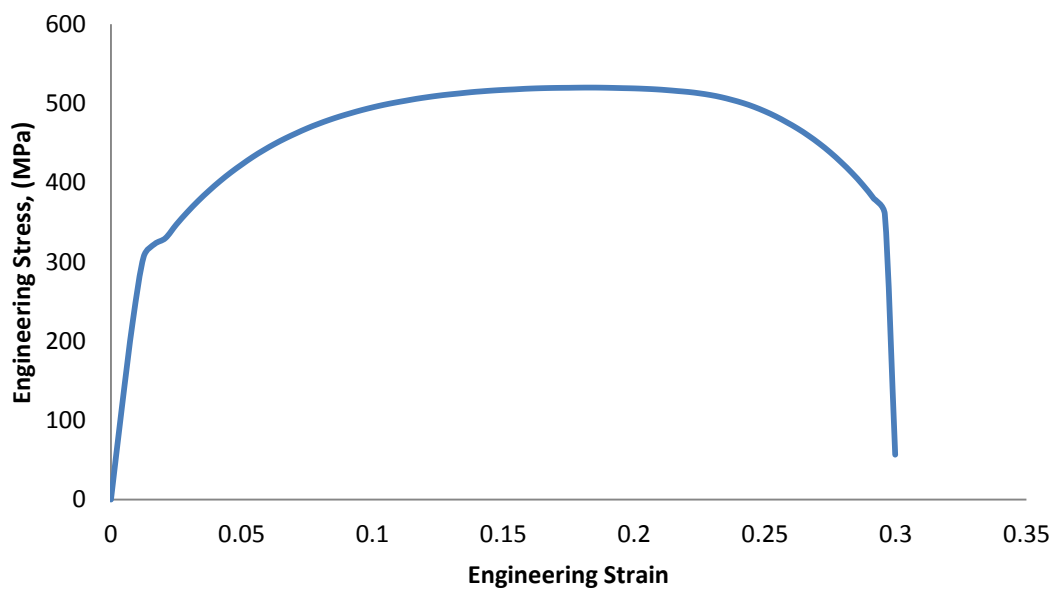

Figure 3.20: Engineering stress-strain for API X42
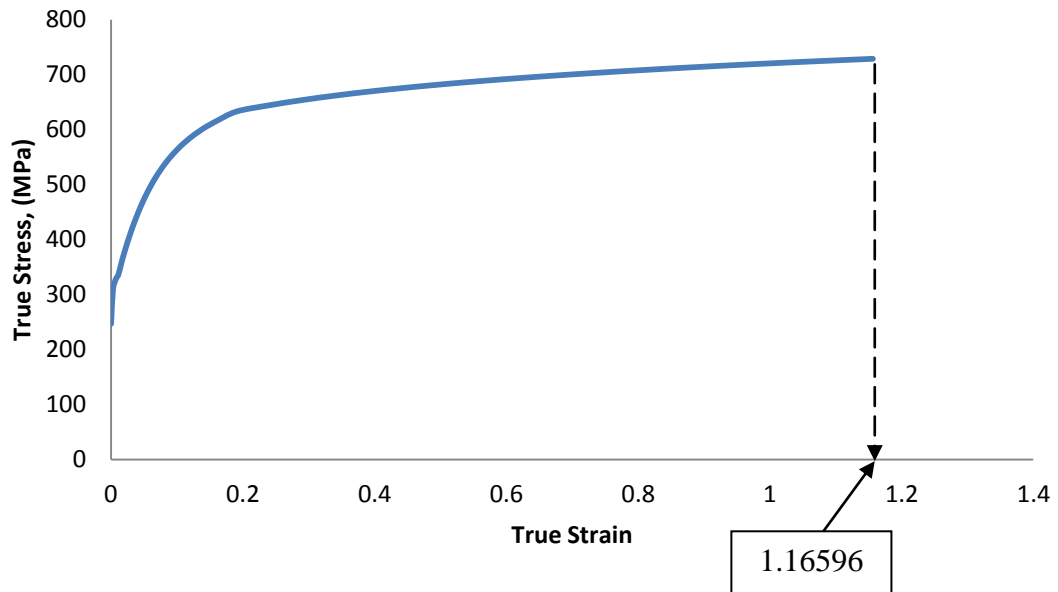
Figure 3.21: True stress-strain for API X42

3.3.13 Development of Failure Criteria Equation

The SMCS model is quite simple since the critical plastic strain as a function of stress triaxiality can be directly calculated and it is not for VGM model where the triaxiality and plastic strain history have to explicitly integrate. Due to its simplicity and accuracy, SMCS model is frequently preferred by researchers to predict the ductile failure of the materials.

$$\frac{\varepsilon_f}{\varepsilon_f^*} = \frac{\exp\left(-\frac{\sigma_m}{\sigma_e}\right)}{\exp\left(-\frac{\sigma_m}{\sigma_e}\right)} \tag{3.3}$$

where

ε_f = equivalent fracture strain

ε_f^* = equivalent fracture strain for smooth specimen

$\frac{\sigma_m}{\sigma_e}$ = stress triaxiality

σ_m = hydraulic stress

σ_e = equivalent stress

According to graph of true stress-strain, the fracture strain of specimen results from the tensile test is 1.16596 (indicated by the arrow in Figure 3.21). The stress triaxiality for smooth specimen is 1/3 (P.W. Bridgman). By substituting both data, the failure criteria based on SMCS equation can be developed.

$$\frac{\varepsilon_f}{1.16596} = \frac{\exp\left(-\frac{\sigma_m}{\sigma_e}\right)}{\exp\left(-\frac{1}{3}\right)}$$

$$\varepsilon_f = \frac{1.16596}{\exp\left(-\frac{1}{3}\right)} \exp\left(-\frac{\sigma_m}{\sigma_e}\right)$$

$$\varepsilon_f = 1.6272 \exp\left(-\frac{\sigma_m}{\sigma_e}\right)$$

3.4   FE ANALYSIS
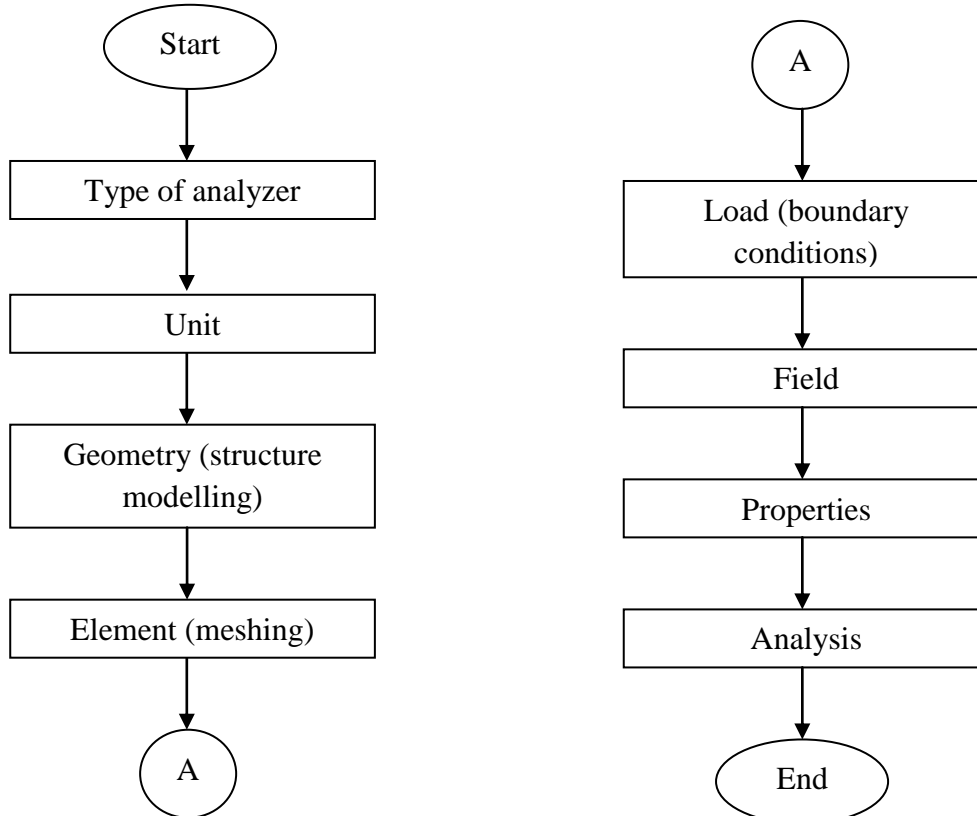
Figure 3.22: Simulation Flowchart

3.4.1 Structure Modelling

The MSC Patran/Marc software were used to model the pipe with multi-corroded region. Due to symmetrical condition, only half of the pipe was simulated. The corroded area was simplified by artificial defects; rectangular shaped on the outer surface of the pipeline. The defects are varying with length and distance between defects. The detail dimensions for modelling the corroded pipeline for the simulation is shown in Table 3.4. Figure 3.23 and 3.24 show the full pipe with multiple defects and closed up view of multiple defects respectively.

Table 3.4 : Pipe and Defect Dimension

Dimensions	Values (mm)
Outer diameter, D	762
Length of the pipe, L	2300
Wall thickness, t	17.5
Defect depth, d	8.75
Length of defect, l	100,200,300
Distance between defects, W	1 to 300
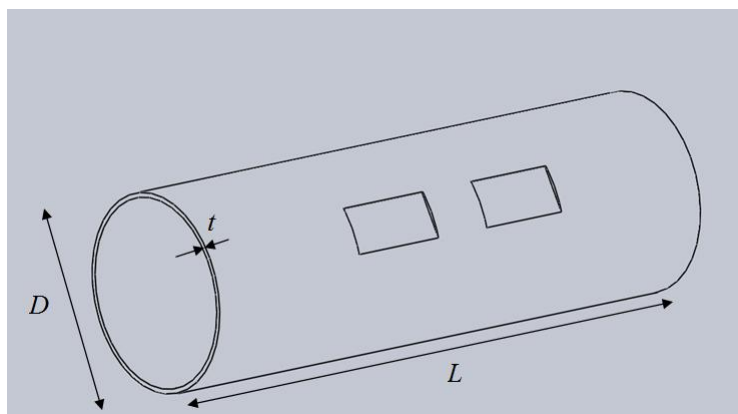
Figure 3.23: Full pipeline with multiple defects

D = Outer diameter

t = Pipe thickness

L = Length of the pipe
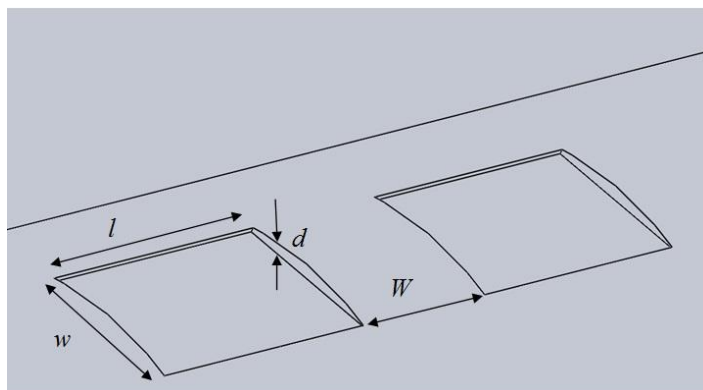
Figure 3.24: Closed up view of multiple defects

l = length of defect

w = width of defect

d = depth of defect

W = distance between defects

3.4.2   Simulation Procedure

MSC Patran 2008r1 was opened. The folder for saving data was renewed. MSC Marc as the analysis code was selected to process the analysis and the parameters was change to the millimetre (mm) as Figure 3.25 below.
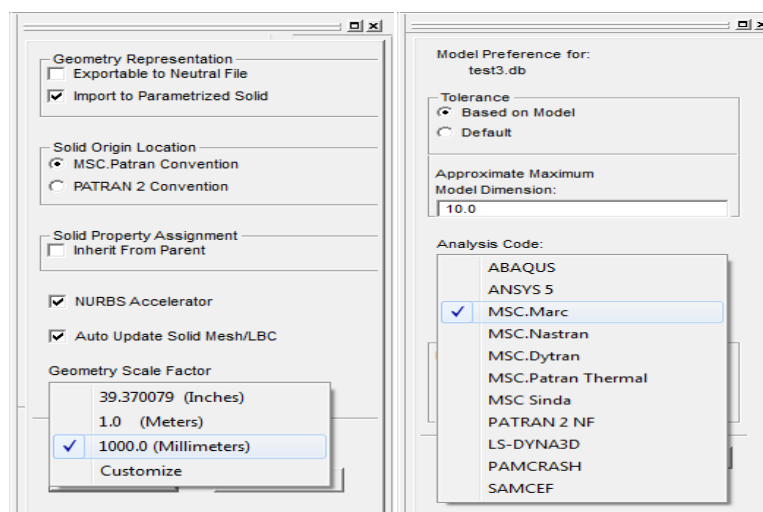
Figure 3.25 : Configuration before starting the MSC Patran

The geometry button was clicked. This button enables to create the pipe sample to be tested. Using the create button, point as the object and the XYZ as the method, point was created using coordinates. Three point showed the upper, middle and the lower of the circle diameter was made. The point for the thickness of the sample pipe was included.

The line created by using the curve as the object and the point as the method. The thickness of the pipe as the pipe is in a half design was lined up. Then, the circle was created using 2D Arc2point. was created The outer circle and the inner point was created to make the inner circle by using the upper point and joint with the lower point. All the line of the pipe will be created by using the translation. Figure 3.26 shows the point, line created and the line linked.
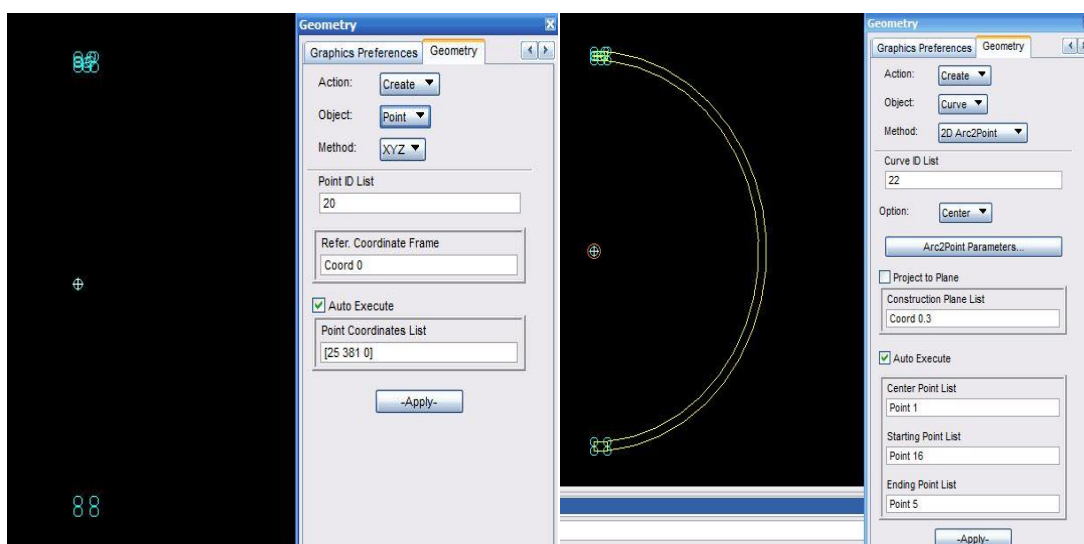
Figure 3.26: Points and lines created

For creating the surface, methods of curve and edge were used. After created the surface, then surface normal force must be checked in order to make sure there is no element errors when running the simulation. All the surface normal force should be show to z-axis direction as shown in Figure 3.27. Action to edit and object to surface was chosen to edit the surface force. Method of reverse and select the region that need to be edit was selected. Figure 3.28 and 3.29 show the full design of a half pipe and multiple defects on pipeline respectively.
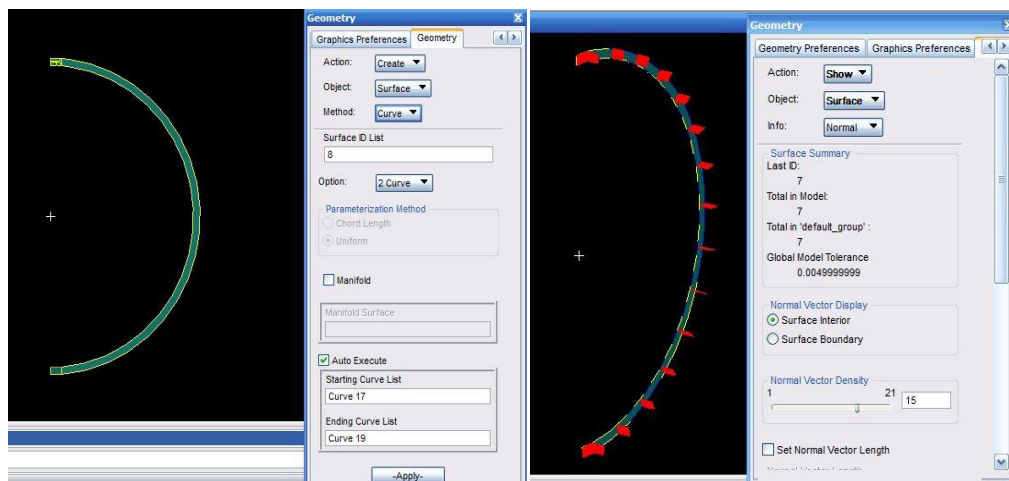
Figure 3.27 : Surfaces and normal forces in z-axis
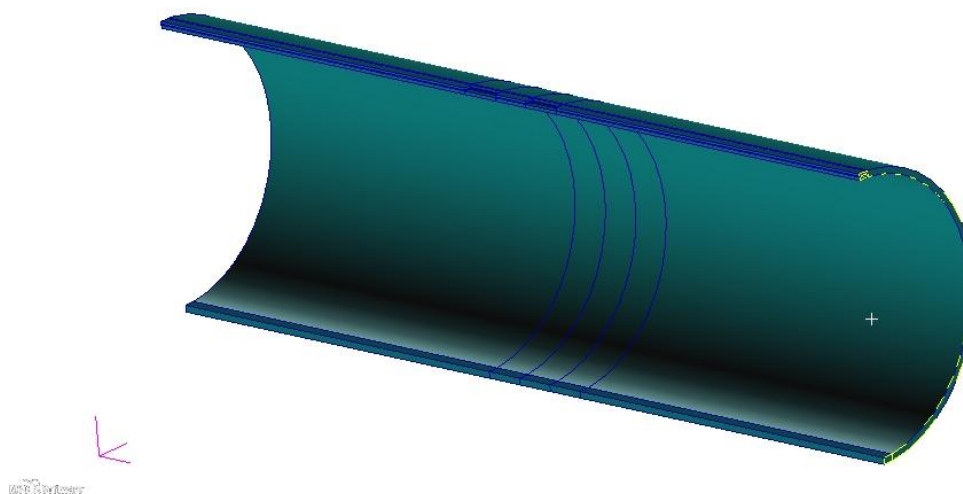
Figure 3.28: Full design of a half of the pipe
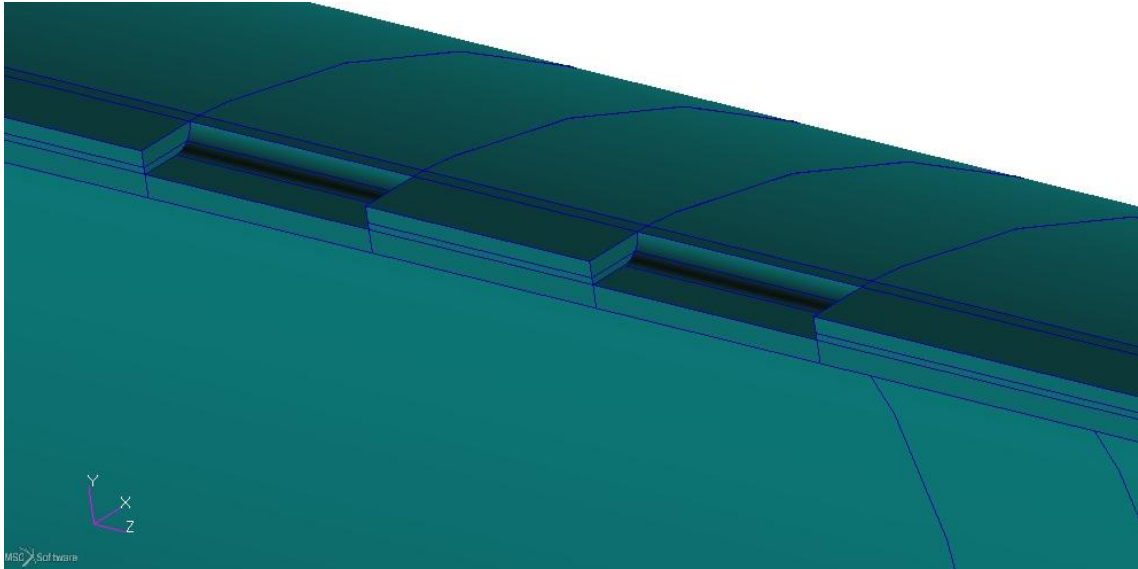
Figure 3.29: Multi defects on pipeline

The next button which is element was clicked after finished the modelling. This button enables the meshing setup. The mesh seed was created and the area was selected that need more focusing on the test or the defects area. There are two methods which to control the mesh. First method is by uniform mesh seed and second method is one way bias. Uniform method was used on place that needed to focus or generate more mesh nodes and one way bias is to mesh simple nodes on an overall model.

Mesh seed can control the number of the mesh and also element (nodes) in the mesh. Then the full mesh was created to enable the mesh on the test sample. HEX value for meshing type was used and the properties for the meshing was filled in. The meshing equivalent in setting was made to make the mesh in the uniform and equivalent with the nodes. The critical part located in the defect length as well as the distance between defect. Therefore, the meshing size for this critical part has high value of meshing compared to others. This is to ensure the simulation for the critical part to be more precise and accurate in order to have a significant value of data. Figure 3.30 shows the meshing process and the view of the HEX meshing.
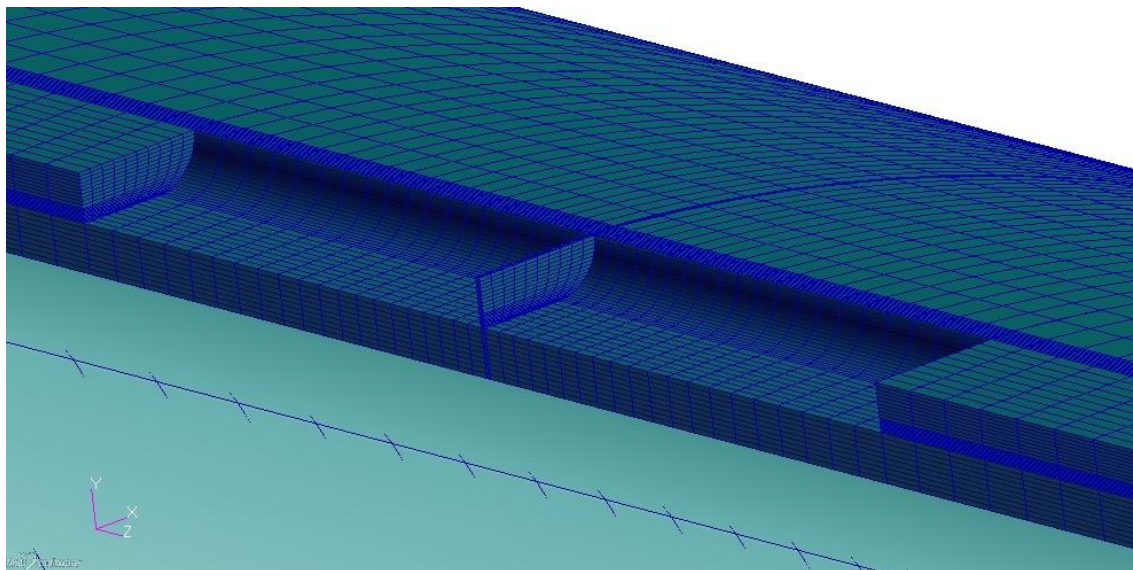
Figure 3.30 : Detail FE Meshing

After the meshing was done, the next step which is to apply load. There was a button load right next to geometry. Function of load enables to create the boundary condition on the model that created at early. There are few boundaries need to be create in order to complete the simulation. Those boundaries are x-axis symmetry, fixed and pressure. Figure 3.31 shows the boundaries conditions that applied.
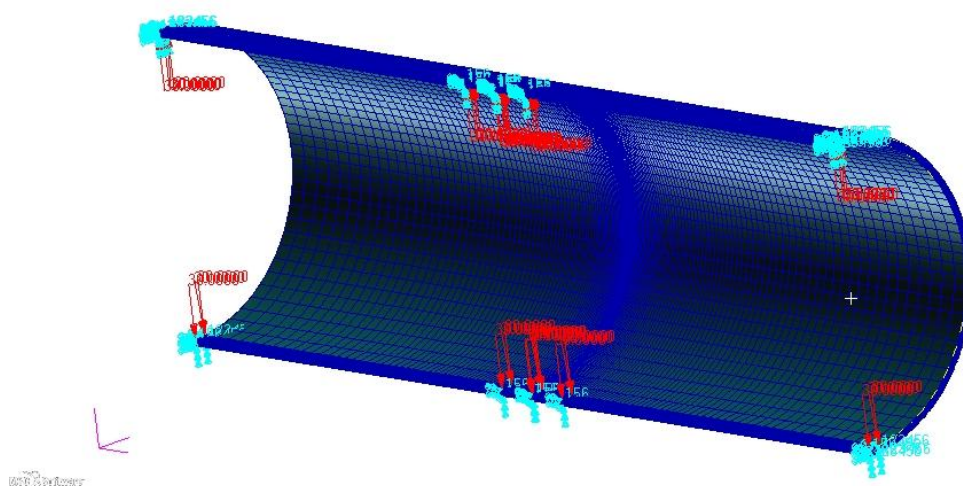
Figure 3.31: Boundaries conditions that applied.

This section was to set up properties. This enables to give the properties for the sample material. The 3D dimension was chosen and also the reduce integration was enabled. Figure 3.32 show the reduce integration setting in material section.
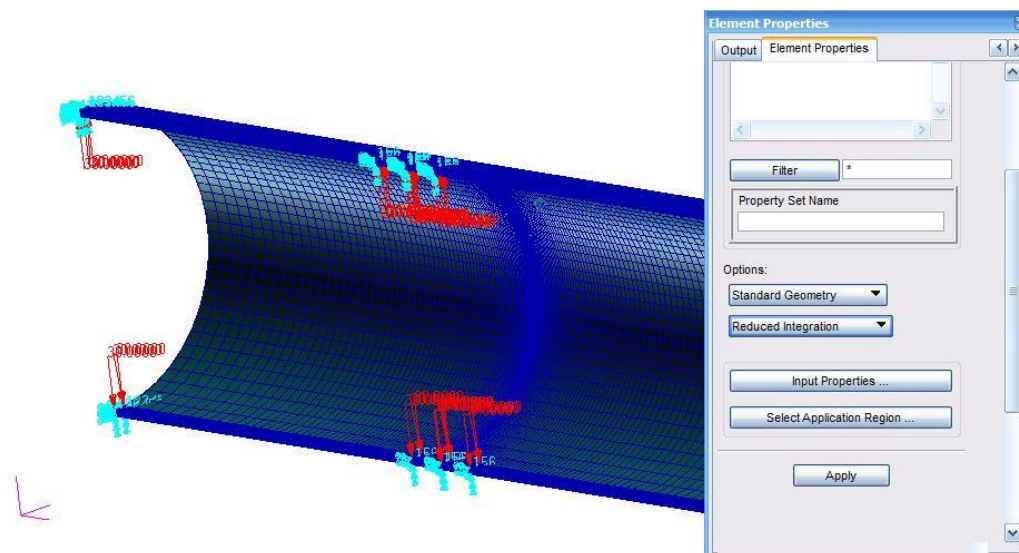
Figure 3.32: Reduce integration

Material property for object was chosen in the field section. The strain box was ticked and true strain stress values that taken from tensile test was imported. The stress strain values was enabled to make sure the data can be used in the material section. Figure 3.33 shows the field data that imported.
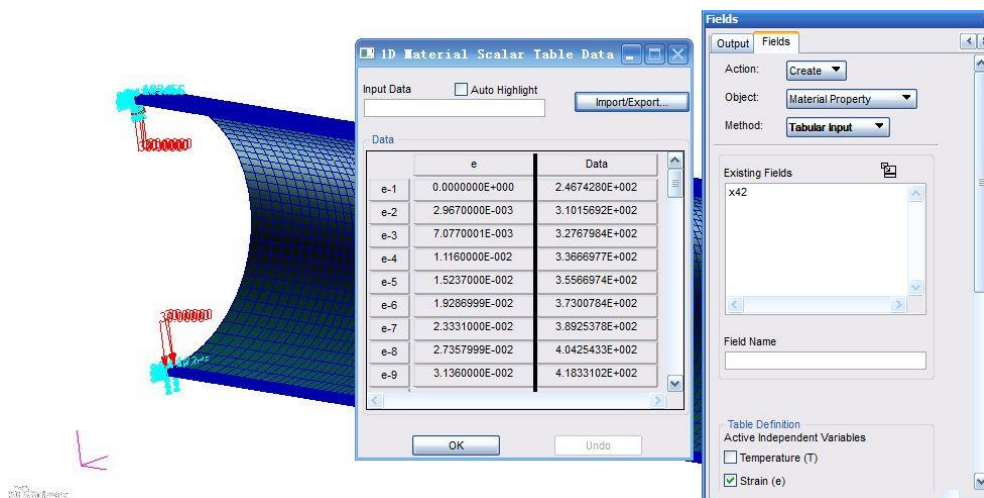
Figure 3.33: True strain and true stress values

For specifying the material properties, the material's section was selected. There were two section need to be create which is elastic and plastic values. However, for elastic values, it is stated as Table 3.5 below.

The plastic values was updated using field data that imported early. The box showed the plastic value was active. The name of properties was noted to avoid error as shown in Figure 3.34.

Table 3.5 : Material data for API X42

Property	Values
Elastic Modulus	210 GPa
Poisson's ratio	0.3
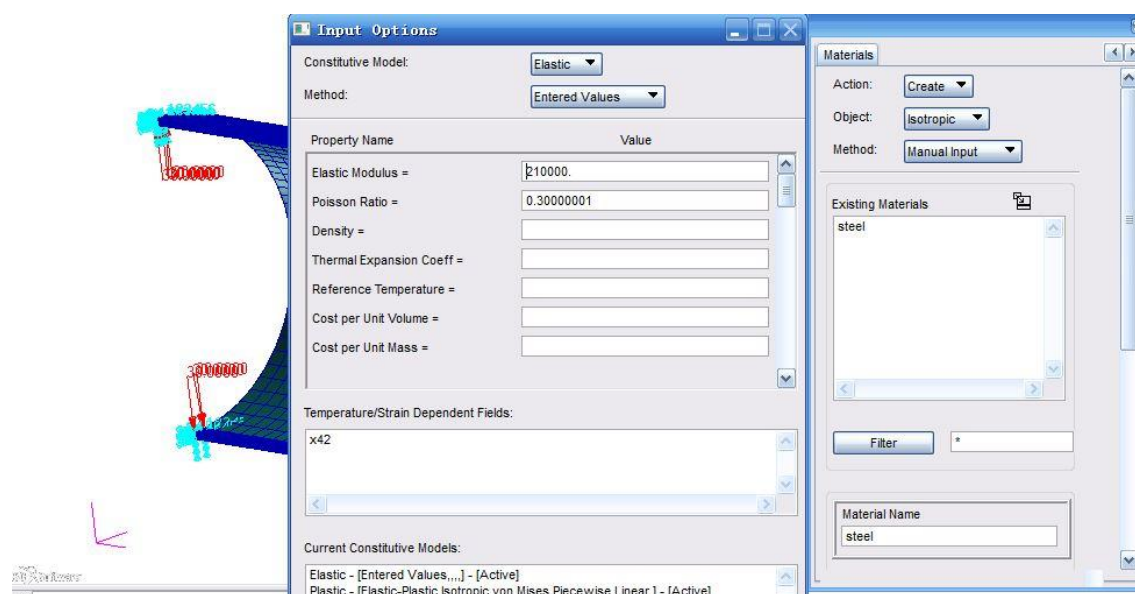
Figure 3.34: Material update

This section was the analysis of the pipeline. The setting to entire models and analysis deck for this option was changed. The non-positive define in solver option at job parameter was enabled. On the load step creation, solution parameter was clicked and the follower force was enabled. On the iteration parameter, the residual force was changed to 0.001 in order to have more accuracy and also better result. Figure 3.35 shows the non-positive define, follower force and also residual force.
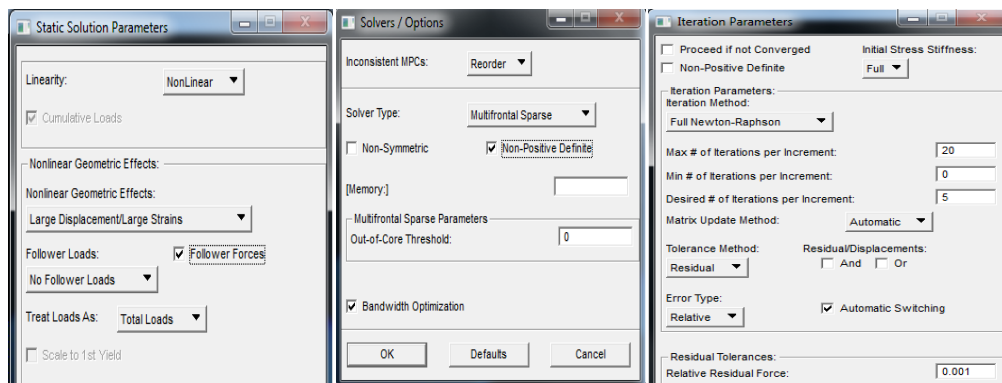
Figure 3.35: Setting of analysis

For run the test, command prompt was used to run the test. If the result ending with the number 3004, the run is succeed.

3.5   SIMULATION

Under simulation, software named as "MSC Patran/Marc" will be used to simulate the multi defects on the plane. It's a nonlinear analysis that involved of equations that derived and values that obtained from tensile test. There are 3 stages of the simulation which is pre-processing, analysis/solving and post-processing.

Pre-processing is a step where to create the geometry for the defects on the plane. Then, it was followed with mesh generation which is to meshed the entire object in order to be analytical. Lastly, is to select the appropriate type of analysis of the defects and boundary condition for the defects.

Secondly, solving is a time consumed step which needed to wait for computer to analyse the boundary and type of defects been set. It is basically based on how complicated the meshing of the object. If more complicated then more times will be required for this to run.

Lastly, which is a post-processing step. This step is where the results and all the graph will be show out. From the result, we can estimate the failure pressure for the different type of defects and different location of defects.

3.6   GANTT CHART

Gantt Chart is a planning schedule for a project to ensure the project are following the planning schedule that have been decided by this Gantt Chart. The detail of the Gantt Chart for this project is shown in Appendix.

CHAPTER 4

RESULTS AND DISCUSSION

4.1   INTRODUCTION

This chapter will discuss about the result obtained from the analysis of corroded defects pipelines using finite element analysis. The material used for this analysis is API X42. There are two objectives for this study which to study the effect of multiple corrosion defects on failure pressure and validate the results with available design codes. The results for different dimensions were analysed and discussed. The failure pressure was predicted using strain-based failure criteria (SMCS) and compared to stress-based criteria (von Mises).

Evaluation of corroded pipeline is an issue for several researches and pipeline operators. Most of the available design codes are only valid for the single defects. The present study is about the multiple defects on corroded pipeline. However, with the small distance between defects, such as 1, 3, 5 and 10 mm as compared to defect length of 100, 200 and 300 mm, it is still acceptable to use design codes with the condition of multiple defects assume as single defect. In this chapter, the evaluation of failure pressure of SMCS model is compared to Von Mises. Meanwhile, the failure pressure obtained from FE analysis were also compared to design codes only for small distance between defects.

4.2   RESULT

In this section, the analysis of the results of different cases will be presented. The results between SMCS and von Mises for different defect length and distance between defects will compared. Table 4.1 summarises the results for cases that were gained from the FE analysis.

Table 4.1: Summarise of failure pressure of different defect dimensions

Case No.	Dimension (mm)		Failure pressure (MPa)	
	Defect length, l	Distance between defects, W	SMCS	von Mises
1	100	1	21.6	16.2
2	100	3	21.6	16.2
3	100	5	21.6	16.2
4	100	10	21.6	16.2
5	100	15	22.8	17.4
6	100	40	24.6	18.5
7	100	50	25.2	18.9
8	100	75	25.8	19.6
9	100	100	26.6	21
10	200	5	18.8	15
11	200	10	18.8	15
12	200	15	19.2	15
13	200	50	20.4	16.2
14	200	75	21	16.8
15	200	100	21.4	17.3
16	200	150	21.8	17.8
17	200	200	22.4	18.4
18	300	5	17.28	13.68
19	300	10	17.64	13.68
20	300	15	17.64	13.68
21	300	50	18.8	14.9
22	300	100	19.5	15.4
23	300	150	20	15.8
24	300	225	20.5	16.2
25	300	300	21	16.6

4.2.1 Comparison of failure pressure between SMCS and von Mises to different distance between defects with same defect length of 100 mm.

The results and analysis of failure pressure predicted using Stress Modified Critical Strain Model and von Mises stress with different distance between defects of the same defect length is presented. The results of failure pressure with different distance between defects are summarized in Figure 4.1 and 4.3. However, for Figure 4.2 and 4.4, the x-axis is represented by a new parameter which smoothen the trend line of the curve. Meanwhile, the comparison of graph for SMCS and von Mises are shown in Figure 4.5. Furthermore, Table 4.1 shows failure pressure for different distance between defects for SMCS and von Mises. The two plots show approximately same pattern where the larger distance between defects have higher values of failure pressure.

Table 4.2: Comparison of failure pressure between SMCS and von Mises to different distance between defects with same defect length of 100 mm

| Defect length, l (mm)	Distance between defects, W (mm)	$\left(\dfrac{\text{Distance between defects}, W}{\text{Defect length}, l}\right)^2$	SMCS Failure Pressure (MPa)	von Mises Failure Pressure (MPa)
100	1	0.0001	21.6	16.2
100	3	0.0009	21.6	16.2
100	5	0.0025	21.6	16.2
100	10	0.0100	21.6	16.2
100	15	0.0225	22.8	17.4
100	40	0.1600	24.6	18.5
100	50	0.2500	25.2	18.9
100	75	0.5625	25.8	19.6
100	100	1.0000	26.6	21
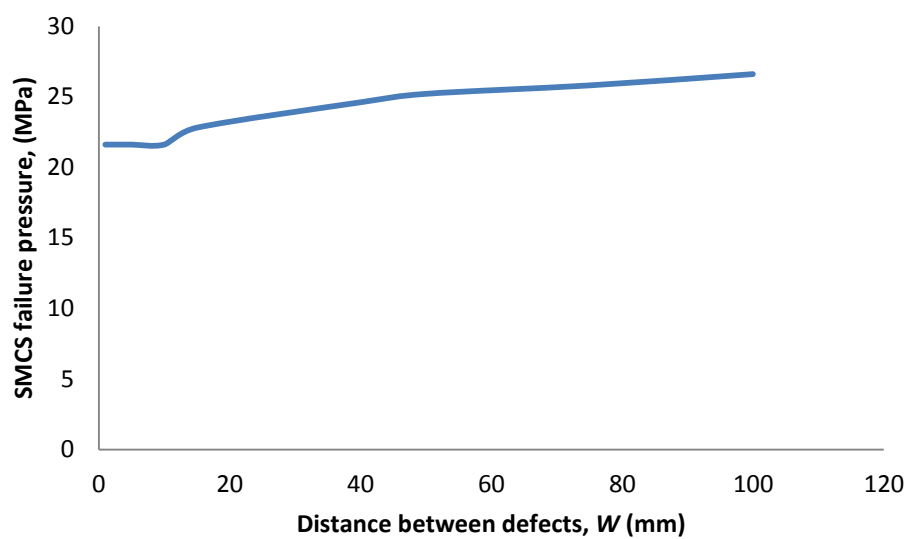
Figure 4.1: Graph of SMCS failure pressure versus distance between defects of 100 mm defect length
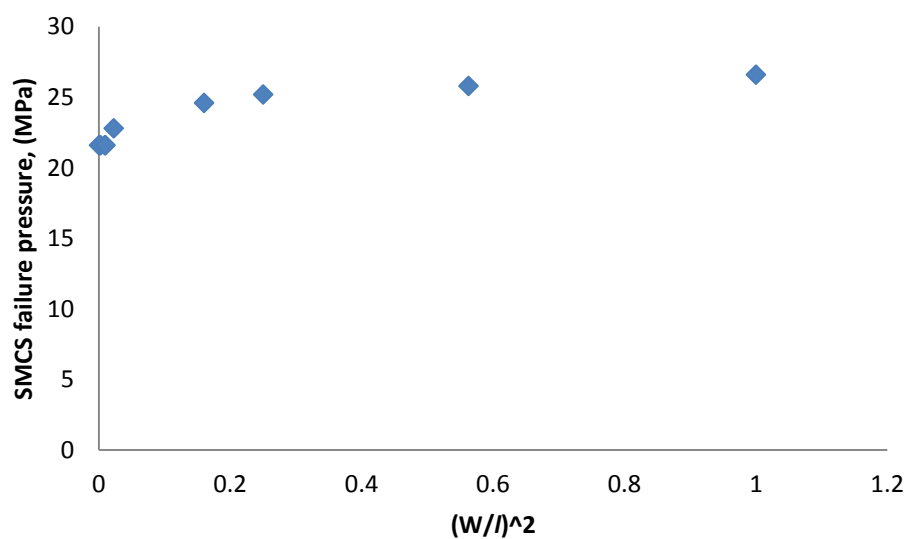
Figure 4.2: Graph of SMCS failure pressure versus $\left(W/l\right)^2$ of 100 mm defect length
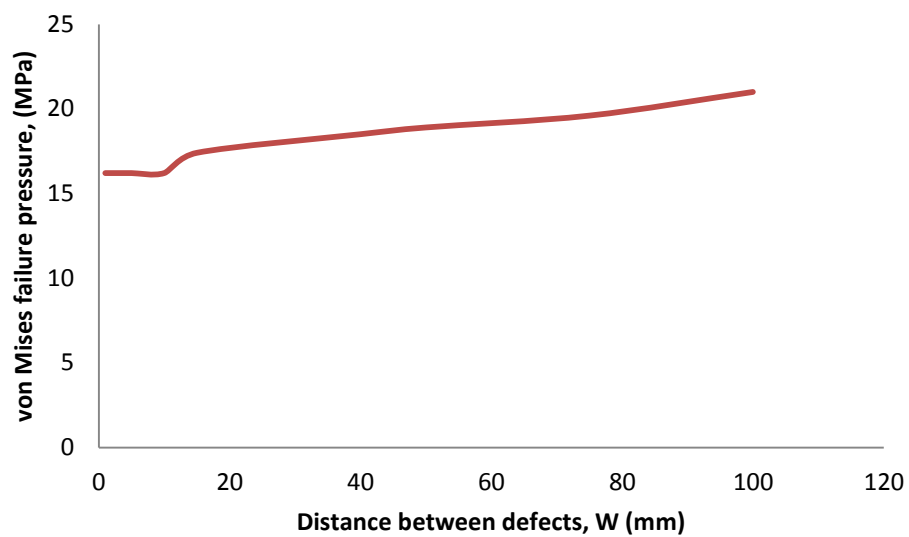
Figure 4.3: Graph of von Mises failure pressure versus distance between defects of 100 mm defect length
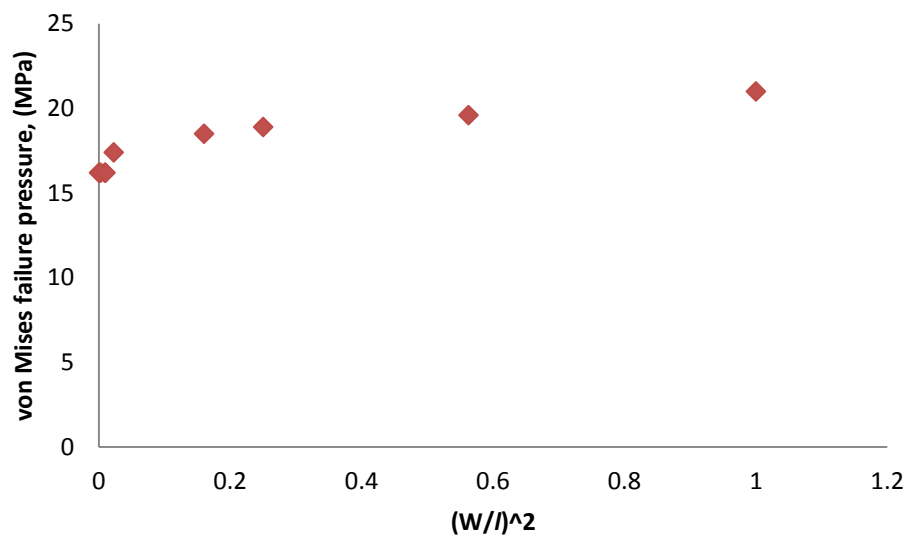
Figure 4.4: Graph of von Mises failure pressure versus $\left(W/l\right)^2$ of 100 mm defect length
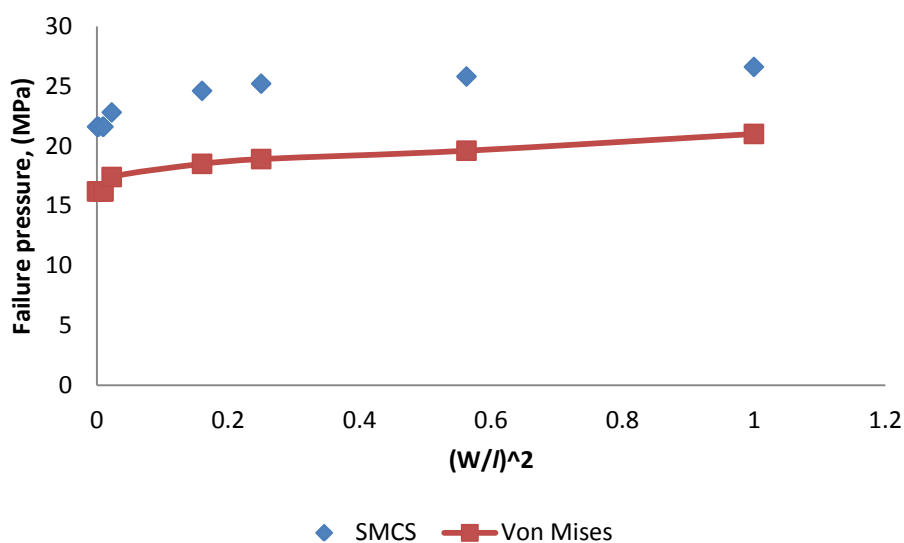
Figure 4.5: Graph of comparison between SMCS and von Mises for failure pressure versus $\left(W/l\right)^2$ of 100 mm defect length

According to figure 4.1, the maximum failure pressure is 26.6 MPa with distance between defects of 100 mm and minimum failure pressure is 21.6 MPa with distance between defects of 1 mm. However, for von Mises graph, it shows that maximum failure pressure is 21 MPa while minimum failure pressure is 16.2 MPa. After comparing the two graphs, it shows that the larger distance between defects will have the highest values of failure pressure. Furthermore, from result of comparing both graphs, it also shows the SMCS failure pressure prediction is always higher than von Mises stress failure pressure prediction. However, the failure pressure for distance between defects of 1, 3, 5, and 10 mm are same. This is due to the distance between defects are too small compared to the length of defects. Hence, the multiple defects acts as a single defect.
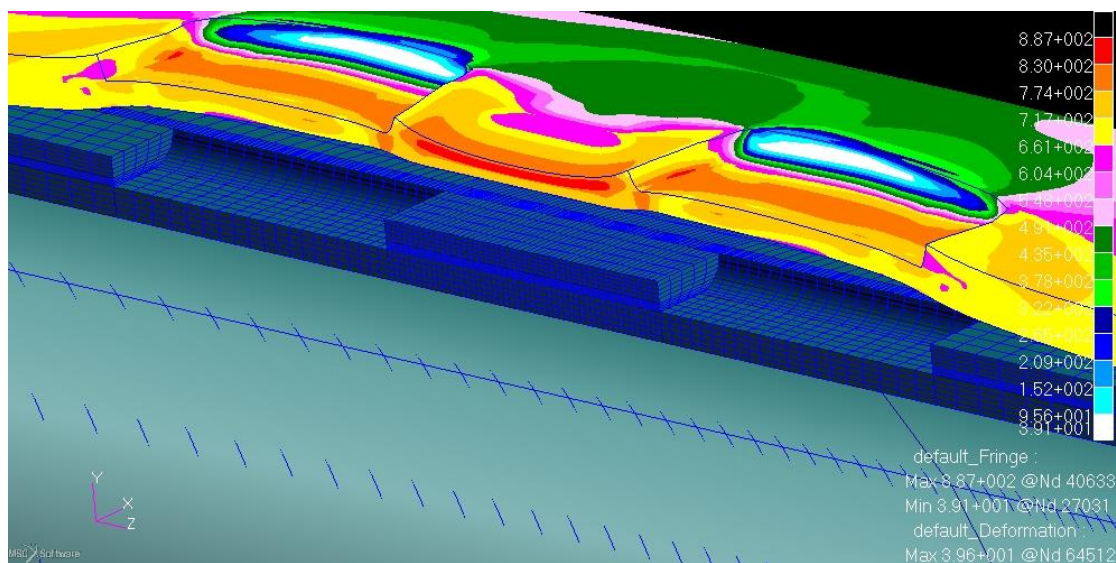
Figure 4.6: SMCS stress distribution of 100 mm distance between defects
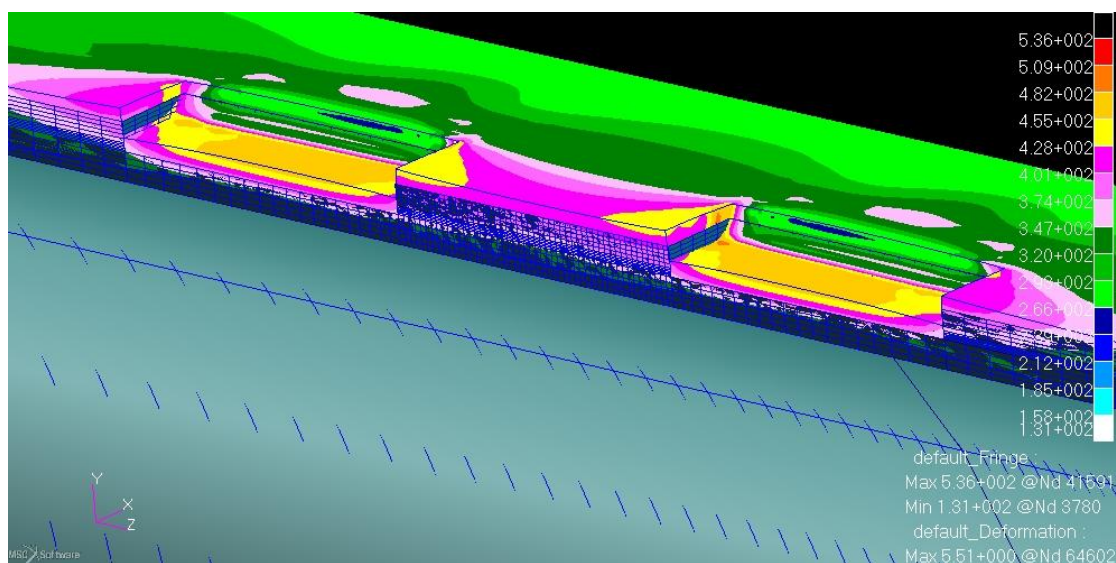

Figure 4.7: von Mises stress distribution of 100 mm distance between defects

Figure 4.6 and 4.7 show the stress distribution of SMCS and von Mises at the parameter of 100 mm defect length and distance between defects.

4.2.2 **Comparison of failure pressure between SMCS and von Mises to different distance between defects with same defect length of 200 mm.**

The analysis for this section is to increase the defect length to 200 mm. The results and analysis of failure pressure for using Stress Modified Critical Strain model and Von Mises stress with different distance between defects of the same defect length is presented. The results of failure pressure with different distance between defects are plotted in Figure 4.8 and 4.10. However, the smoothen trend line of the graph is represented in Figure 4.9 and 4.11 whereby the x-axis is replaced by a new parameter. Meanwhile, the comparison of graph for SMCS and von mises are shown in Figure 4.12. Furthermore, Table 4.2 reveals failure pressure for different distance between defects with evaluation by SMCS and von Mises. The graph indicated clearly that two of the plot give a similar pattern where the larger distance between defects has higher values of failure pressure just like previous analysis that is being discussed before this.

Table 4.3: Comparison of failure pressure between SMCS and von Mises to different distance between defects with same defect length of 200 mm

|			SMCS	von Mises
Defect length, l (mm)	Distance between defects, W (mm)	$\left(\dfrac{\text{Distance between defects}, W}{\text{Defect length}, l}\right)^2$	Failure Pressure (MPa)	Failure Pressure (MPa)
200	5	0.000625	18.8	15
200	10	0.0025	18.8	15
200	15	0.005625	19.2	15
200	50	0.0625	20.4	16.2
200	75	0.140625	21	16.8
200	100	0.25	21.4	17.3
200	150	0.5625	21.8	17.8
200	200	1	22.4	18.4
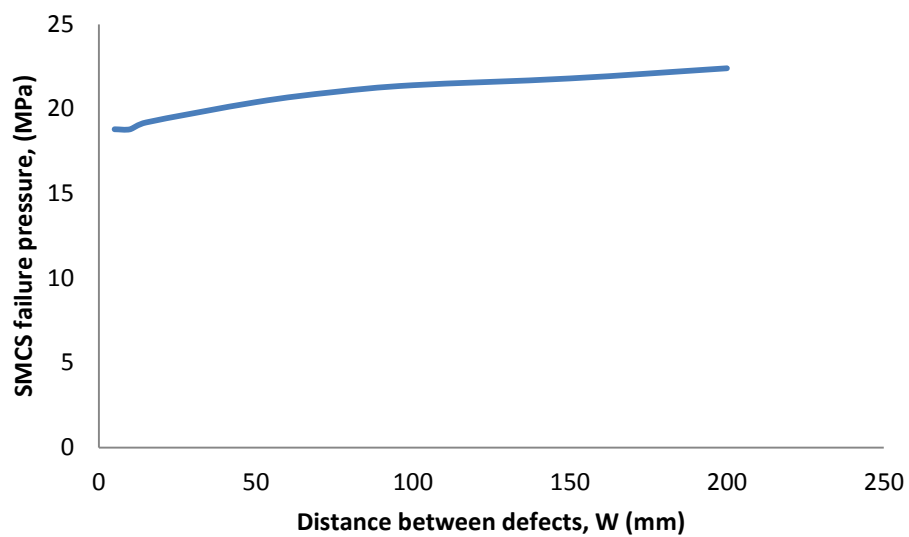
Figure 4.8: Graph of SMCS failure pressure versus distance between defects of 200 mm defect length
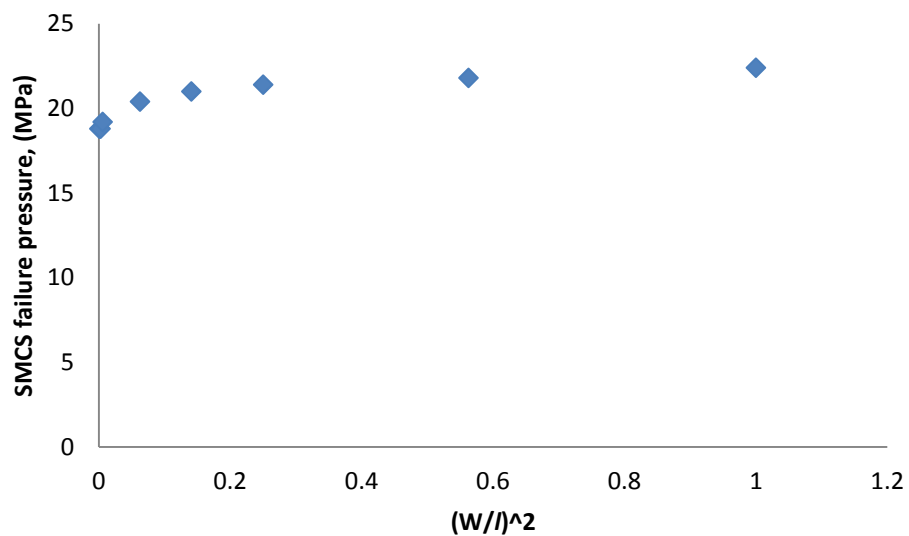
Figure 4.9: Graph of SMCS failure pressure versus $\left(W/_l\right)^2$ of 200 mm defect length
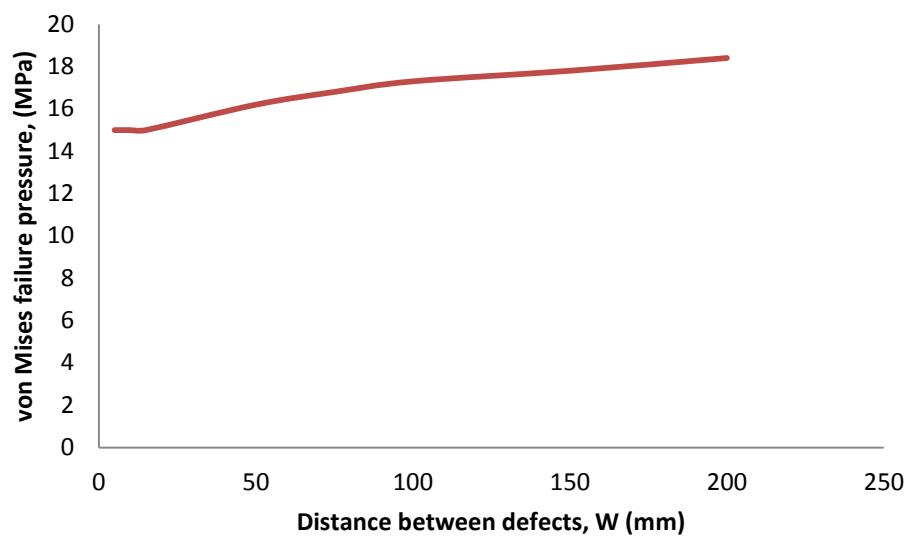
Figure 4.10: Graph of von Mises failure pressure versus distance between defects of 200 mm defect length
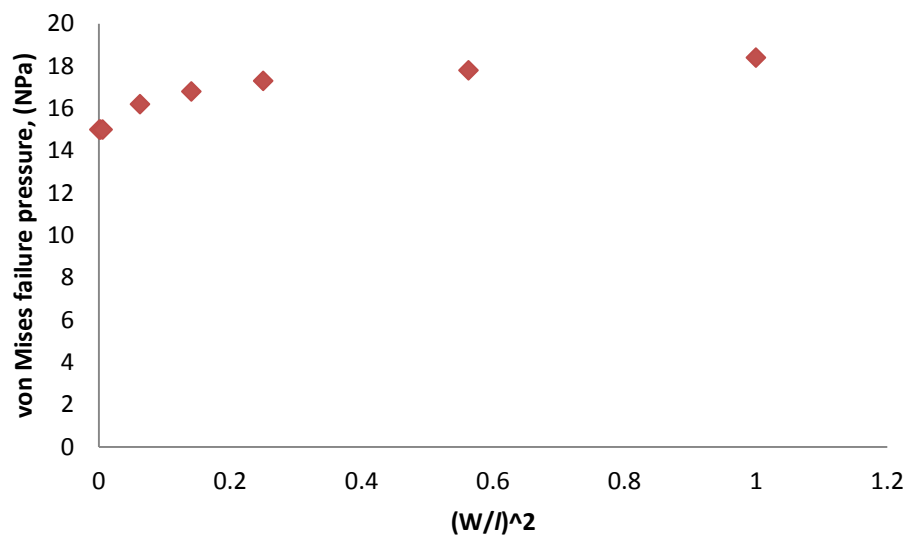
Figure 4.11: Graph of von Mises failure pressure versus $\left(W/l \right)^2$ of 200 mm defect length
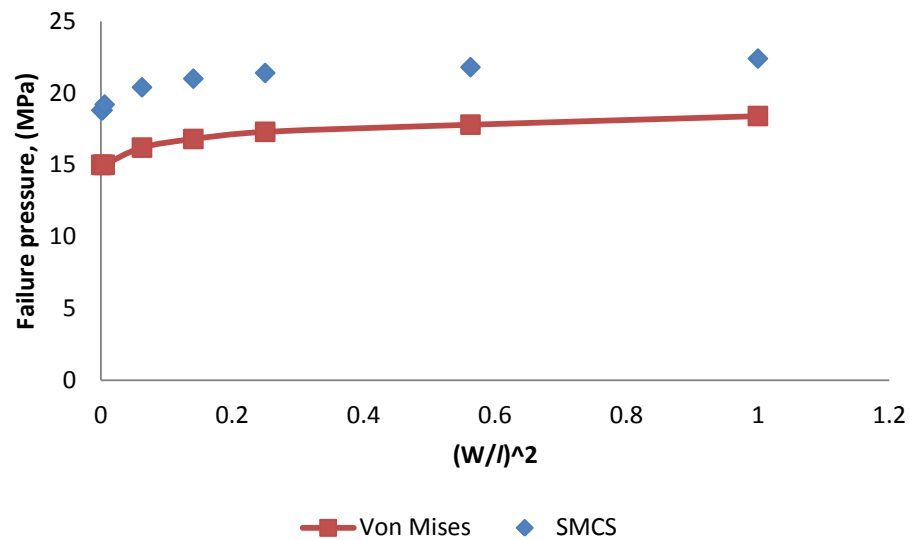
Figure 4.12: Graph of comparison between SMCS and von Mises of failure pressure versus $\left(\frac{W}{l}\right)^2$ of 200 mm defect length

According to Figure 4.8, the maximum failure pressure is 22.4 MPa with distance between defects of 200 mm and minimum failure pressure is 18.8 MPa with distance between defects of 5 mm. However, for von misses graph, it shows that maximum failure pressure is 18.4 MPa while minimum failure pressure is 15 MPa. After comparing the two graphs, it shows that the larger distance between defects will have the highest values of failure pressure. Furthermore, from result of comparing both graphs, it also shows the SMCS failure pressure prediction is always higher than von Mises stress failure pressure prediction. However, the failure pressure for distance between defects of 5, 10 and 15 mm are same. This is due to the distance between defects are too small compared to the length of defects.
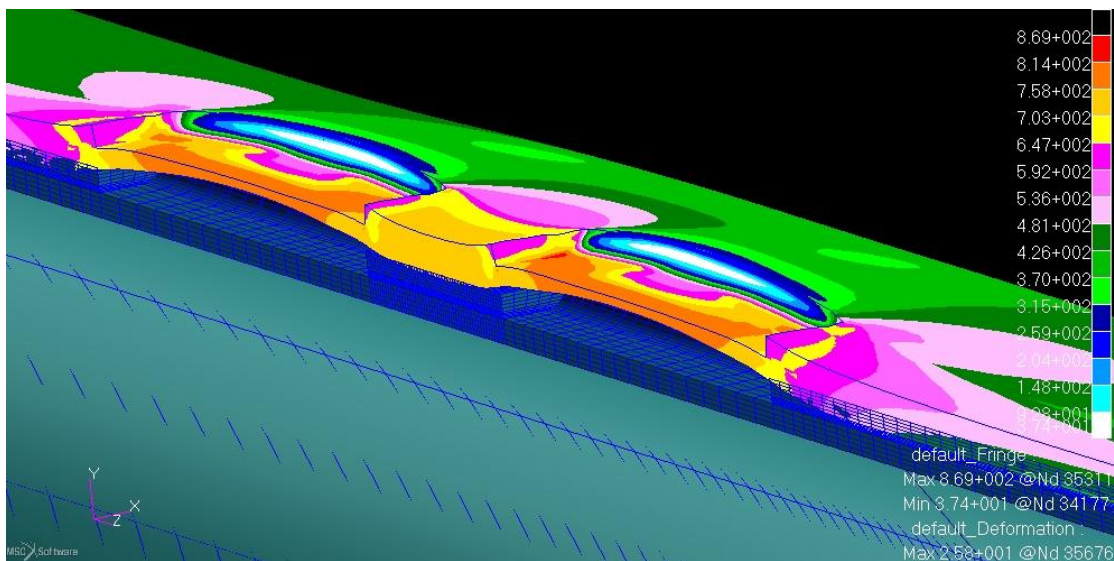
Figure 4.13: SMCS stress distribution of 200 mm distance between defects
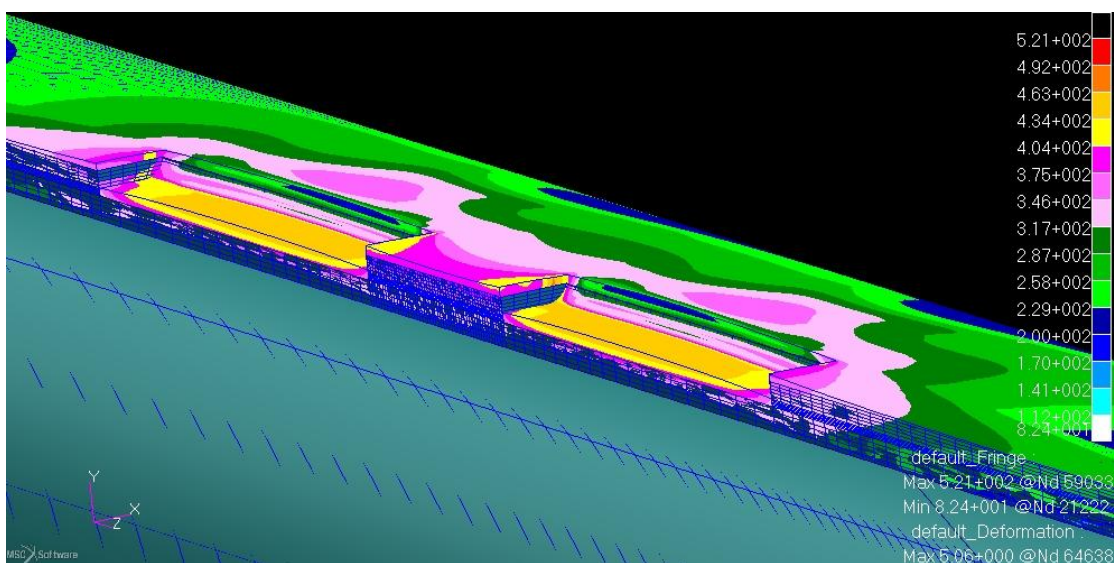

Figure 4.14: von Mises stress distribution of 200 mm distance between defects

Figure 4.13 and 4.14 show the stress distribution of SMCS and von Mises at the parameter of 200 mm defect length and 100 mm of distance between defects.

4.2.3 Comparison of failure pressure between SMCS and Von Mises to different distance between defects with same defect length of 300 mm.

The distance of defect grows increase to 300 mm in this section. The results and analysis of failure pressure for using Stress Modified Critical Strain model and von Mises stress with different distance between defects of the same defect length is presented. For results of failure pressure with different distance between defects are summarized in Figure 4.15 and 4.17. However, for Figure 4.16 and 4.18, the x-axis is represented by a new parameter which smoothen the trend line of the curve. Meanwhile, the comparison of graph for SMCS and von Mises are shown in Figure 4.19. Furthermore, Table 4.4 shows failure pressure for different distance between defects for SMCS and von Misses. The two plots show approximately same pattern where the larger distance between defects have higher values of failure pressure.

Table 4.4: Comparison of failure pressure between SMCS and von Mises to different distance between defects with same defect length of 300 mm

| Defect length, l (mm)	Distance between defects, W (mm)	$\left(\dfrac{\text{Distance between defects}, W}{\text{Defect length}, l}\right)^2$	SMCS Failure Pressure (MPa)	von Mises Failure Pressure (MPa)
300	5	0.000278	17.28	13.68
300	10	0.001111	17.64	13.68
300	15	0.0025	17.64	13.68
300	50	0.027778	18.8	14.9
300	100	0.111111	19.5	15.4
300	150	0.25	20	15.8
300	225	0.5625	20.5	16.2
300	300	1	21	16.6
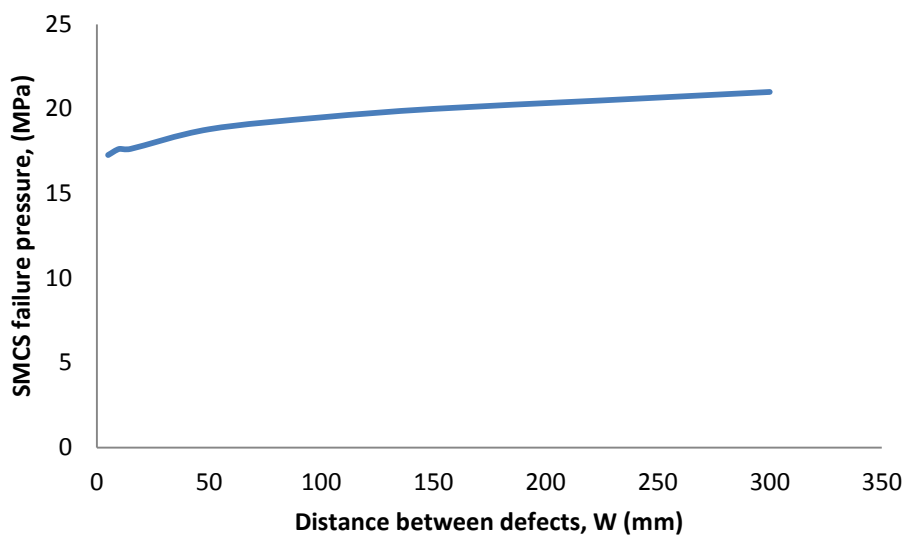
Figure 4.15: Graph of SMCS failure pressure versus distance between defects of 300 mm defect length
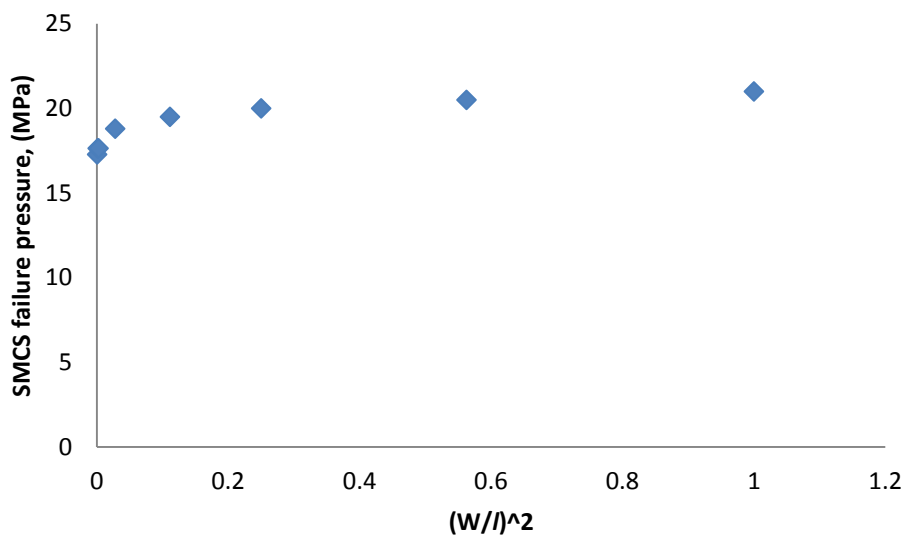
**Figure 4.16:** Graph of SMCS failure pressure versus $\left(W/_l\right)^2$ of 300 mm defect length
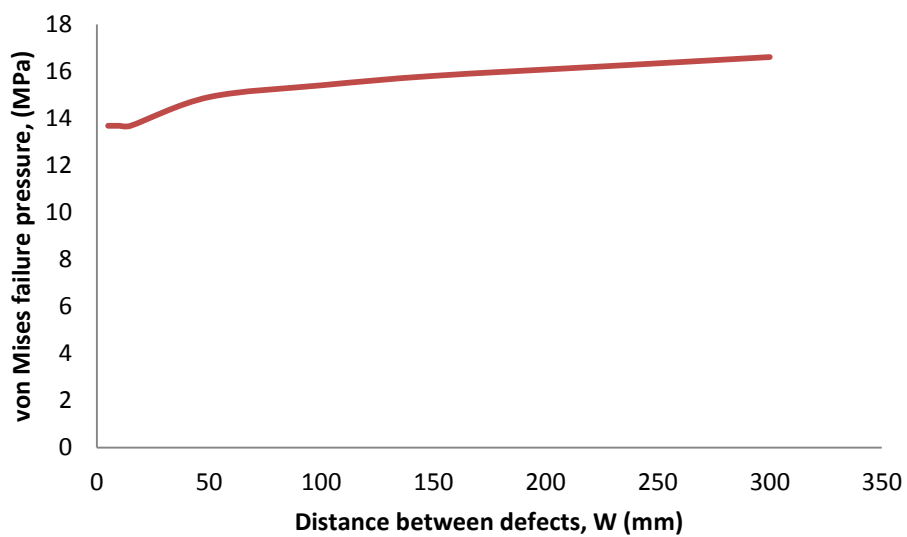
Figure 4.17: Graph of von Mises failure pressure versus distance between defects of 300 mm defect length
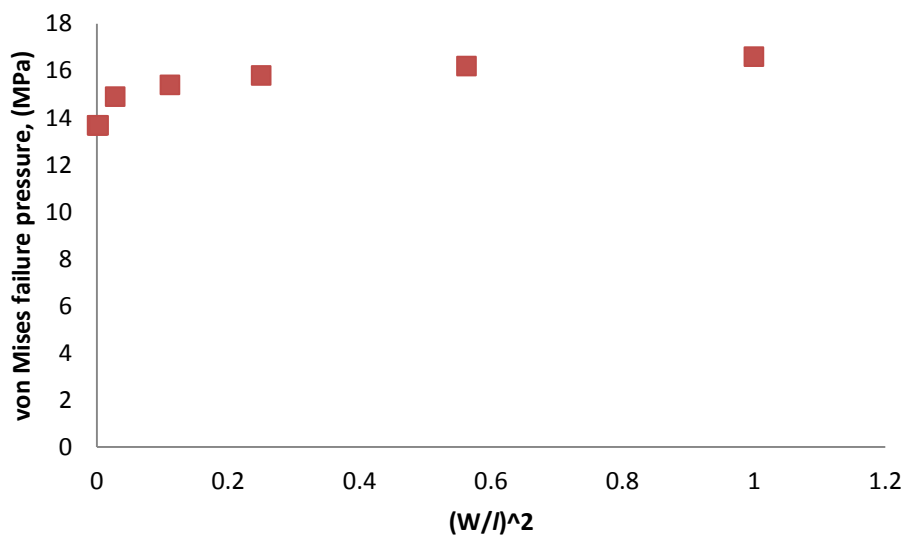
Figure 4.18: Graph of von Mises failure pressure versus $\left(\frac{W}{l}\right)^2$ of 300 mm defect length
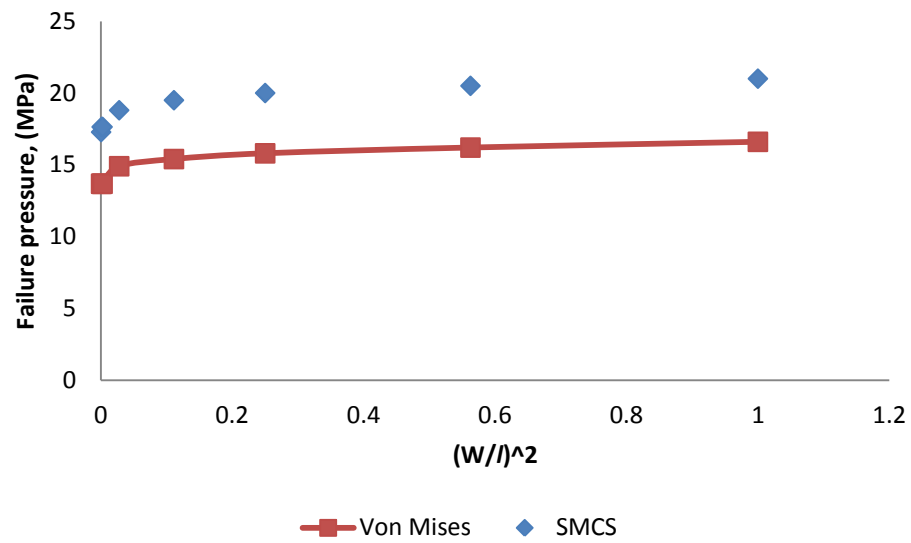
Figure 4.19: Graph of comparison between SMCS and von Mises of failure pressure versus $\left(W/_l\right)^2$ of 300 mm defect length

According to Figure 4.15, the maximum failure pressure is 21 MPa with distance between defects of 300 mm and minimum failure pressure is 17.28 MPa with distance between defects of 1 mm. However, for von Mises graph, it shows that maximum failure pressure is 16.6 MPa while minimum failure pressure is 13.68 MPa. After comparing the two graphs, it shows that the larger distance between defects will have the highest values of failure pressure. Furthermore, from result of comparing both graphs, it also shows the SMCS failure pressure prediction is always higher than von Mises stress failure pressure prediction. However, the failure pressure for distance between defects of 5, 10 and 15 mm are same. This is due to the distance between defects are too small compared to the length of defects.
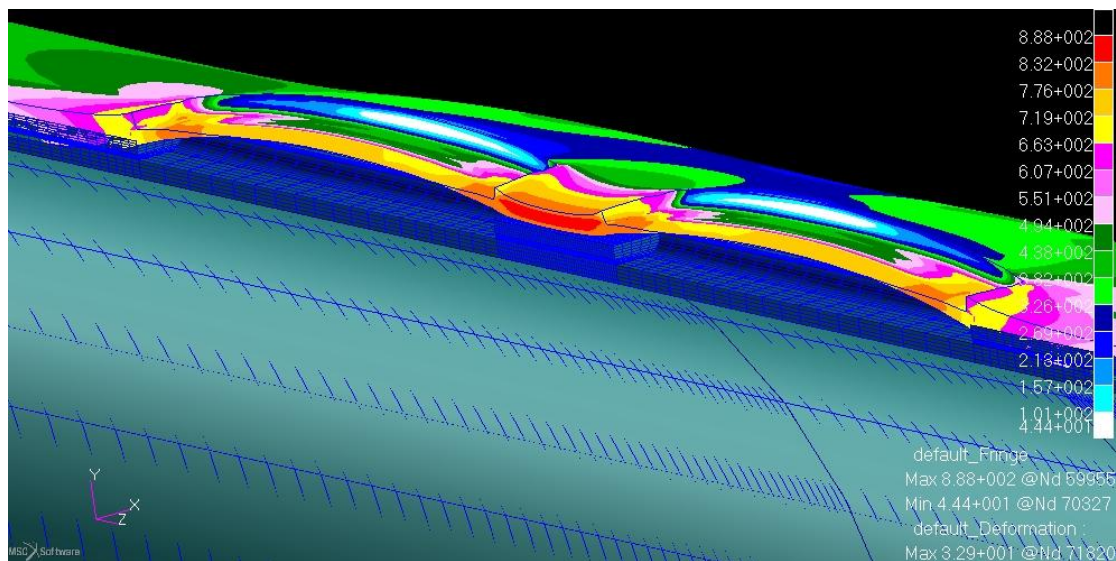
**Figure 4.20:** SMCS stress distribution of 300 mm distance between defects
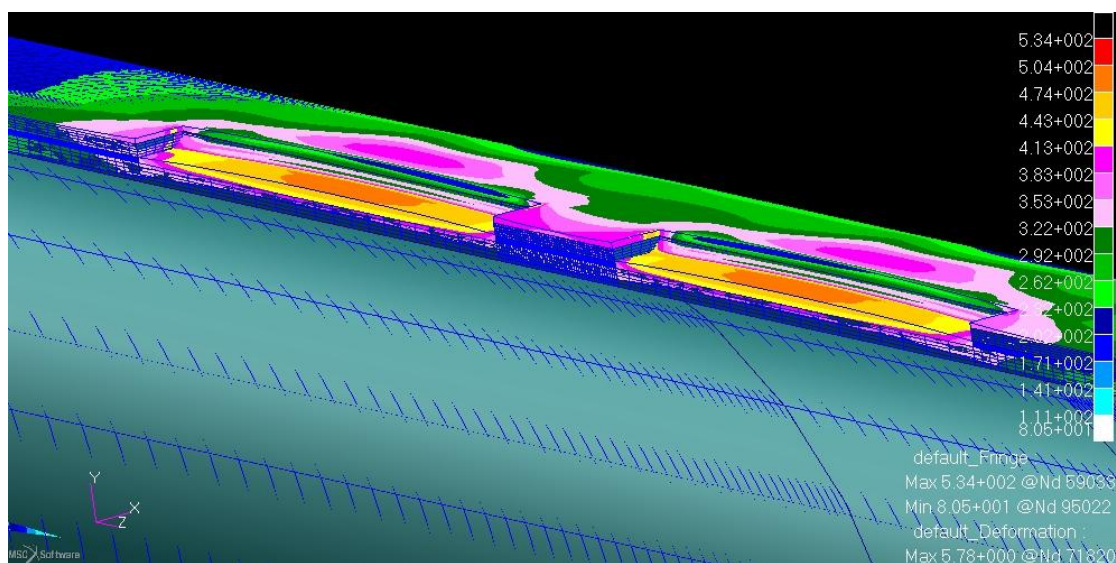
Figure 4.21: von Mises stress distribution of 300 mm distance between defects

Figure 4.20 and 4.21 show the stress distribution of SMCS and von Mises at the parameter of 300 mm defect length and 100 mm of distance between defects.

4.2.4 Comparison of failure pressure for different defect length
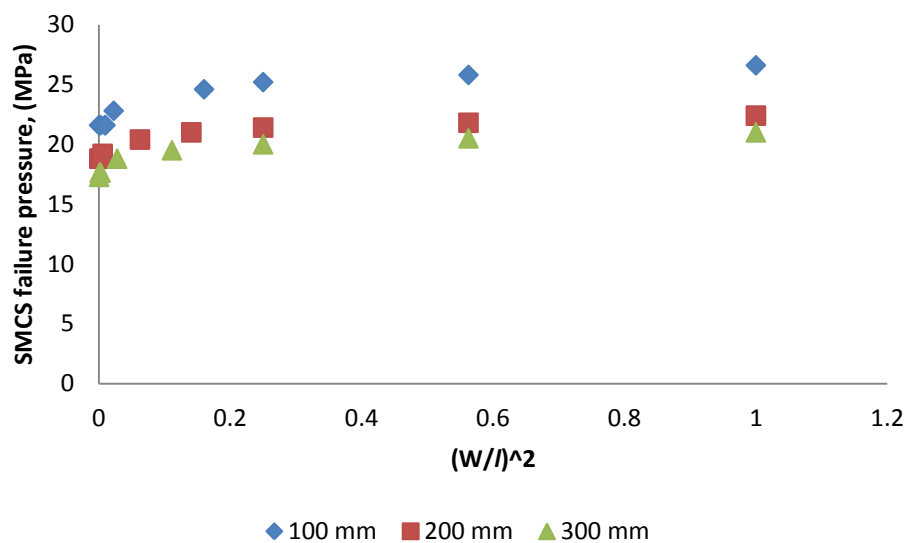
Figure 4.22: Graph of SMCS failure pressure versus $\left(W/_l \right)^2$ for three different defect
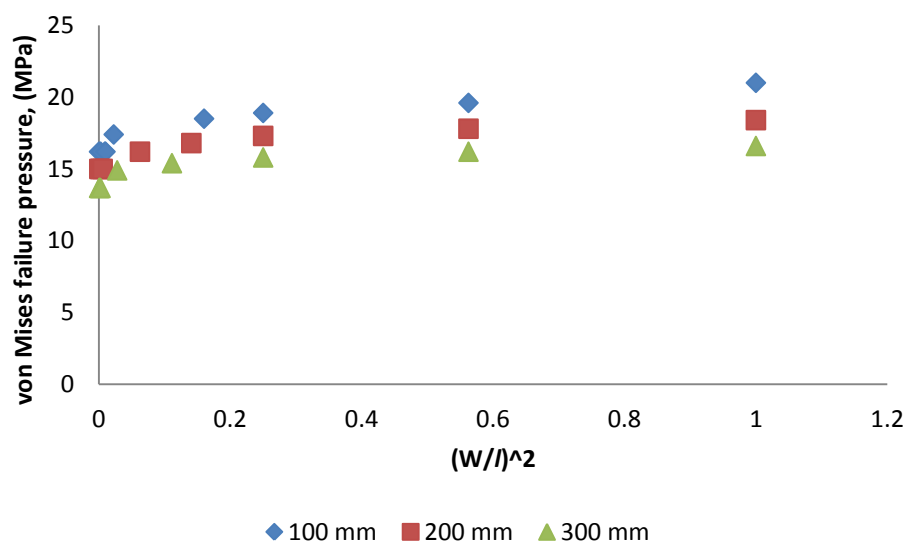
length

Figure 4.23: Graph of von Mises failure pressure versus $\left(W/_l \right)^2$ for three different

defect length

According to Figures 4.22 and 4.23, both graphs showed a similar pattern which is increasing, as the defect length increase, the stress intensity on it being scattered and dispersed. Hence, the failure pressure increase. However, the failure pressure for SMCS and von Mises varied. Failure pressure for SMCS is higher for the three different defect length compared to von Mises. The failure pressure in SMCS for 200 mm defect length differs from the normal trend line. It's slightly lower than the usual compared to the von Mises.

4.2.5 Comparison of failure pressure between SMCS and von Mises to different defect length with same distance between defects of 5 mm.

The results and analysis of failure pressure for using stress Modified Critical Strain Model and von Misses stress with a different defect length of the same distance between defects is presented. For results of failure pressure with different defect length are summarized in Figure 4.24 and 4.25. Figure 4.24 shows the failure pressure of SMCS while figure 4.25 shows the failure pressure of von Mises. Meanwhile, the comparison of graph for SMCS and von mises are shown in Figure 4.26. Furthermore, Table 4.5 shows failure pressure for different defect length for SMCS and von Mises. The two plots show approximately same pattern where the larger defect length has higher values of failure pressure.

Table 4.5: Comparison of SMCS and von Mises to different defect length with the same distance between defects of 5 mm

|		SMCS	von Misses
Distance between defects, W (mm)	**Defect Length, l (mm)**	**Failure Pressure (MPa)**	**Failure Pressure (Mpa)**
5	100	21.6	16.2
5	200	18.8	15
5	300	17.28	13.68
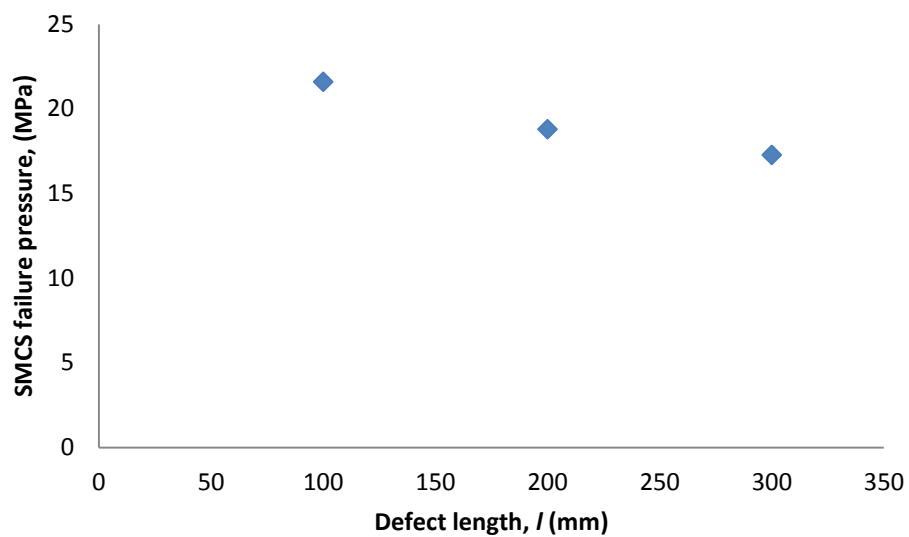
Figure 4.24: Graph of SMCS failure pressure versus defect length of 5 mm distance between defects
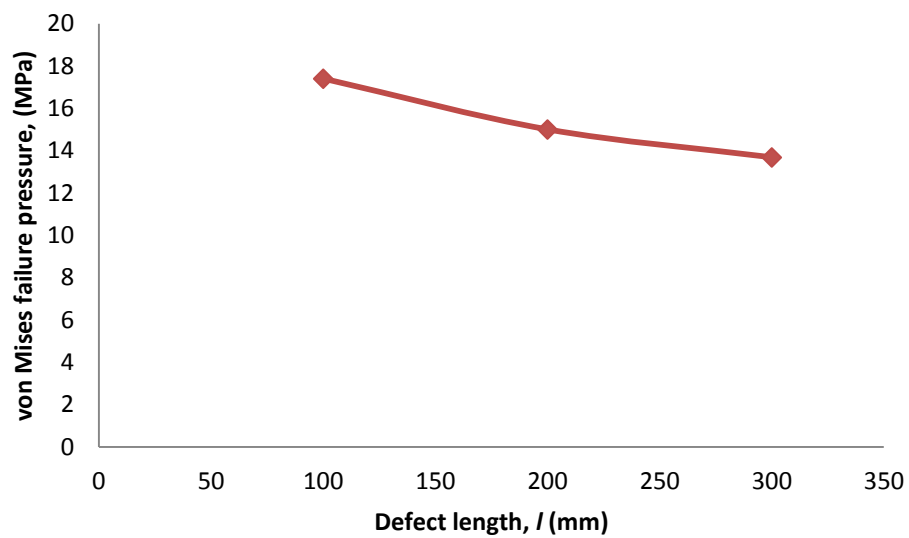

Figure 4.25: Graph of von Mises failure pressure versus defect length of 5 mm distance between defects
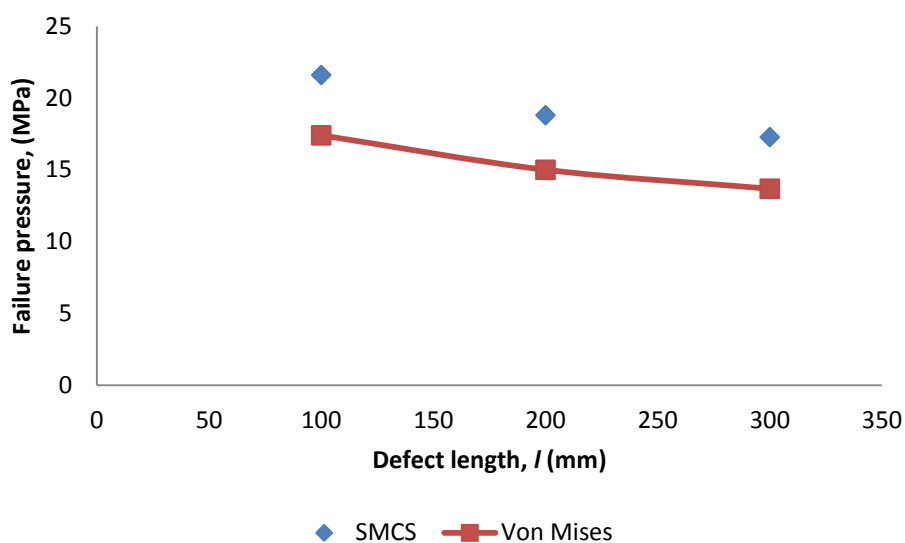
Figure 4.26: Graph of comparison between SMCS and von Mises of failure pressure versus defect length of 5 mm distance between defects

According to Figure 4.24, the failure pressure increase with the decreased of defect length. The maximum failure pressure is 21.6 MPa with a defect length of 100 mm and minimum failure pressure is 17.28 MPa with a defect length of 300 mm. von Mises failure pressure shows the similar pattern. Though, the failure pressure of SMCS is always higher than von Mises.
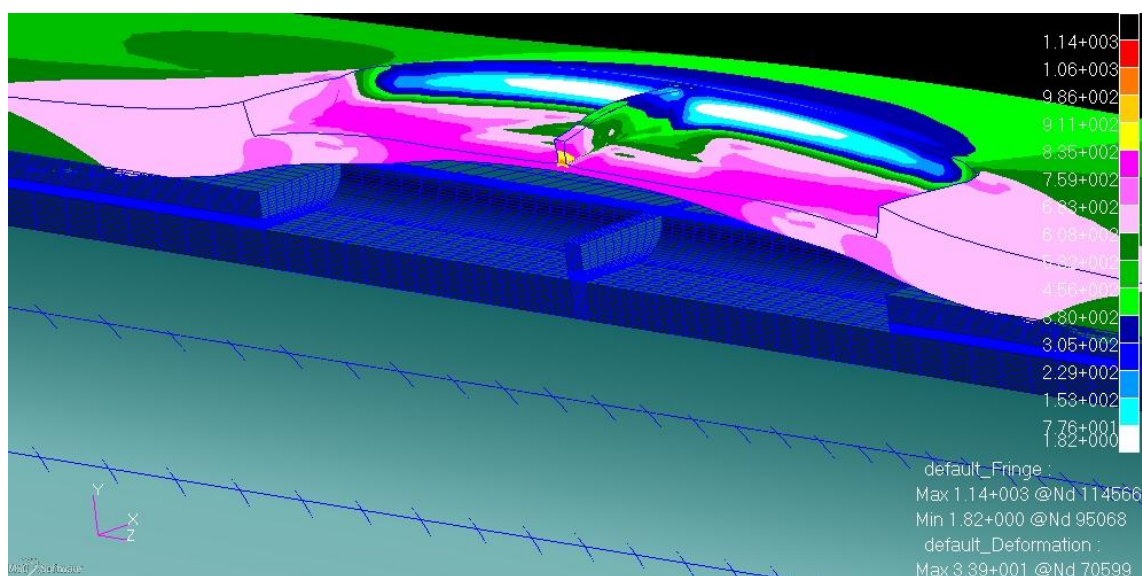

**Figure 4.27:** SMCS stress distribution of 100 mm defect length
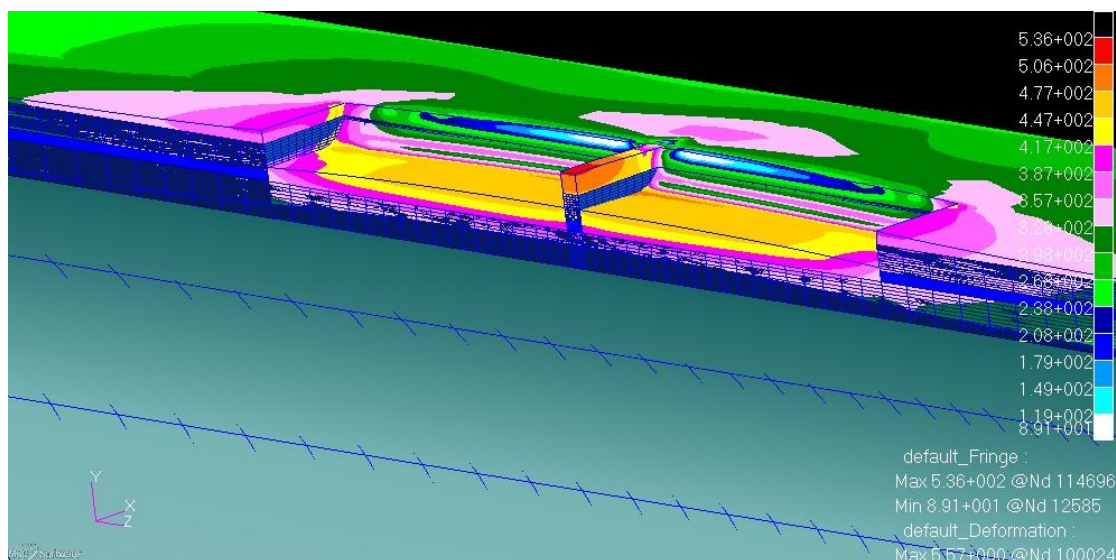
Figure 4.28: von Mises stress distribution of 100 mm defect length

Figure 4.27 and 4.28 show the stress distribution of SMCS and von Mises at the parameter of 100 mm defect length and 5 mm of distance between defects.

4.2.6   Comparison of failure pressure between SMCS and von Mises to different defect length with same distance between defects of 50 mm.

The results and analysis of failure pressure for using stress Modified Critical Strain Model and von Misses stress with a different defect length of the same distance between defects is presented. For results of failure pressure with different defect length are summarized in Figure 4.29 and 4.30. Figure 4.29 shows the failure pressure of SMCS while Figure 4.30 shows the failure pressure of von Mises. Meanwhile, the comparison of graph for SMCS and von mises are shown in Figure 4.31. Furthermore, Table 4.6 shows failure pressure for different defect length for SMCS and von Mises. The two plots show approximately same pattern where the larger distance between defects have higher values of failure pressure.

Table 4.6: Comparison of SMCS and von Mises to different defect length with the same distance between defects of 50 mm

Distance between defects, *W* (mm)	Defect Length, *l* (mm)	SMCS Failure Pressure (MPa)	von Misses Failure Pressure (MPa)
50	100	25.2	18.9
50	200	20.4	16.2
50	300	18.8	14.9
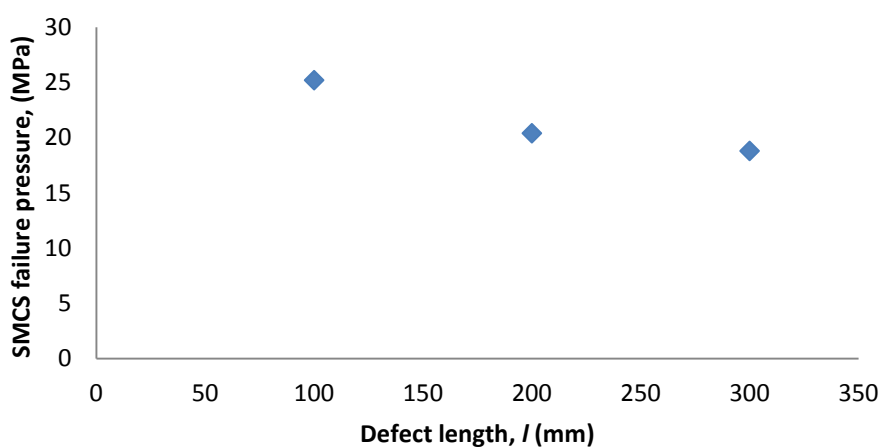
Figure 4.29: Graph of SMCS failure pressure versus defect length of 50 mm distance between defects
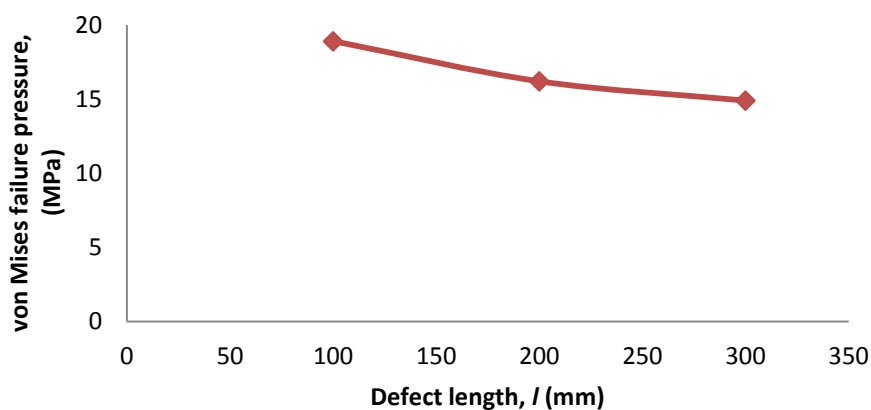
Figure 4.30: Graph of von Mises failure pressure versus defect length of 50 mm distance between defects
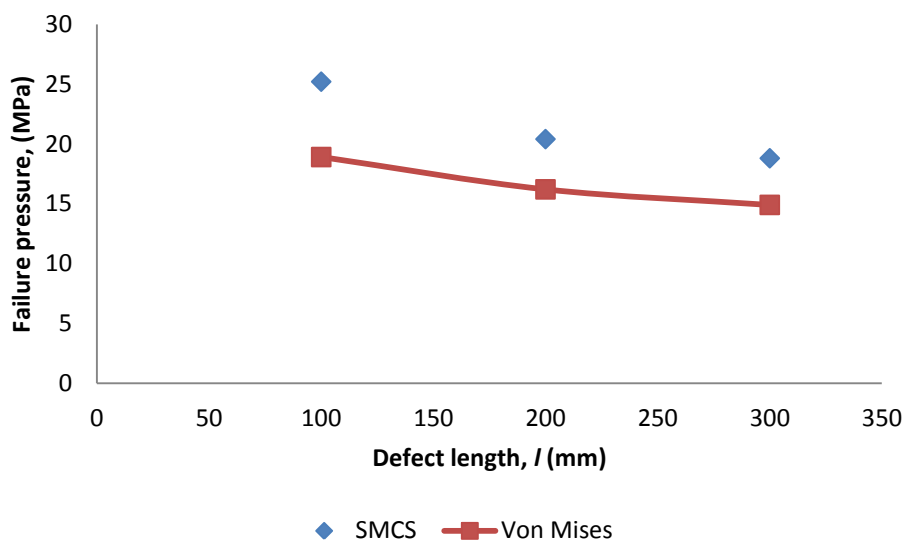
Figure 4.31: Graph of comparison between SMCS and von Mises of failure pressure versus defect length of 50 mm distance between defects

According to Figure 4.29, the failure pressure decrease with the increased of defect length. The maximum failure pressure of SMCS is 25.2 MPa with a defect length of 100 mm and minimum failure pressure is 18.8 MPa with a defect length of 300 mm. von Mises failure pressure shows the similar pattern. Though, the failure pressure of SMCS is always higher than von Mises.
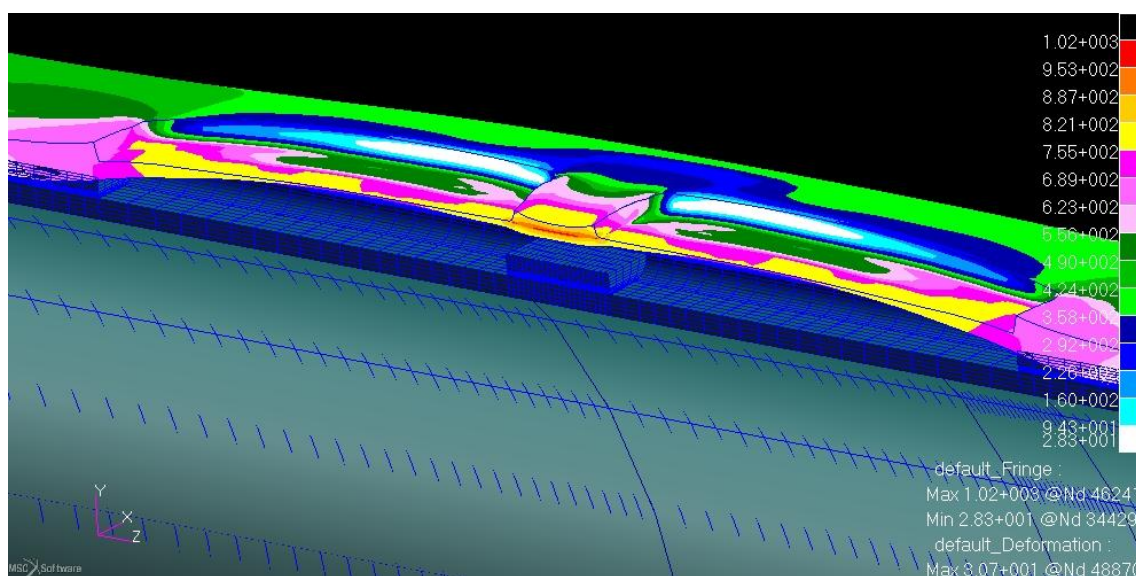
Figure 4.32: SMCS stress distribution of 200 mm defect length
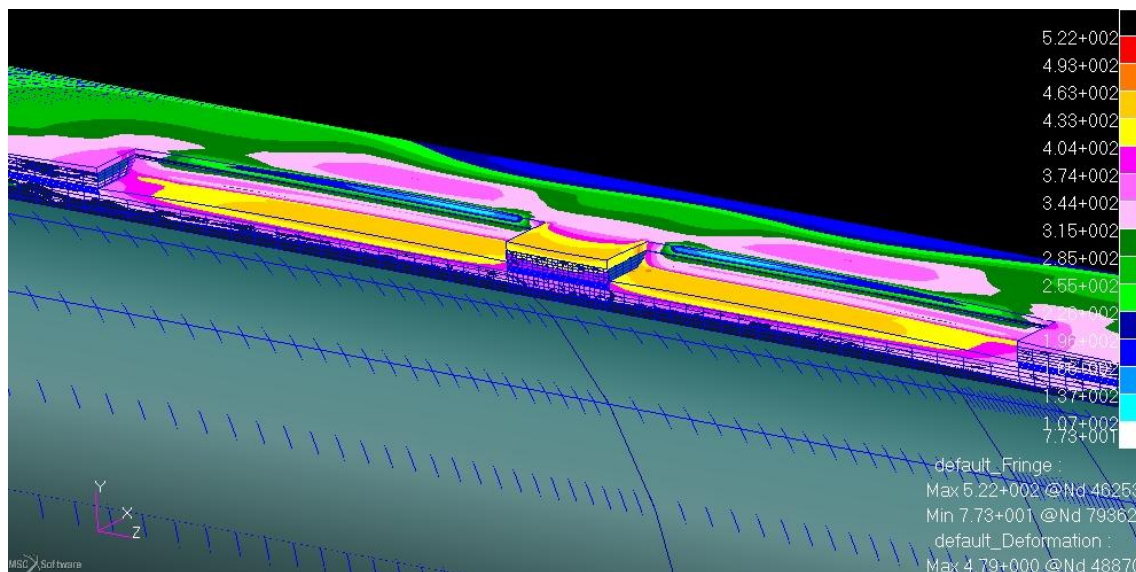
Figure 4.33: von Mises stress distribution of 200 mm defect length

Figure 4.32 and 4.33 show the stress distribution of SMCS and von Mises at the parameter of 200 mm defect length and 50 mm of distance between defects.

4.2.7 Comparison of failure pressure between SMCS and von Mises to different defect length with same distance between defects of 100 mm.

The results and analysis of failure pressure for using stress Modified Critical Strain Model and von Misses stress with a different defect length of the same distance between defects is presented. For results of failure pressure with different defect length are summarized in Figure 4.34 and 4.35. Figure 4.34 shows the failure pressure of SMCS while figure 4.35 shows the failure pressure of von Mises. Meanwhile, the comparison of graph for SMCS and von Mises are shown in figure 4.36. Furthermore, Table 4.7 shows failure pressure for different defect length for SMCS and von Mises. The two plots show approximately same pattern where the larger distance between defects have higher values of failure pressure.

Table 4.7: Comparison of SMCS and von Mises to different defect length with the same distance between defects of 100 mm

Distance between defects, W (mm)	Defect Length, l (mm)	SMCS Failure Pressure (MPa)	von Misses Failure Pressure (MPa)
100	100	26.6	21
100	200	21.4	17.3
100	300	19.5	15.4
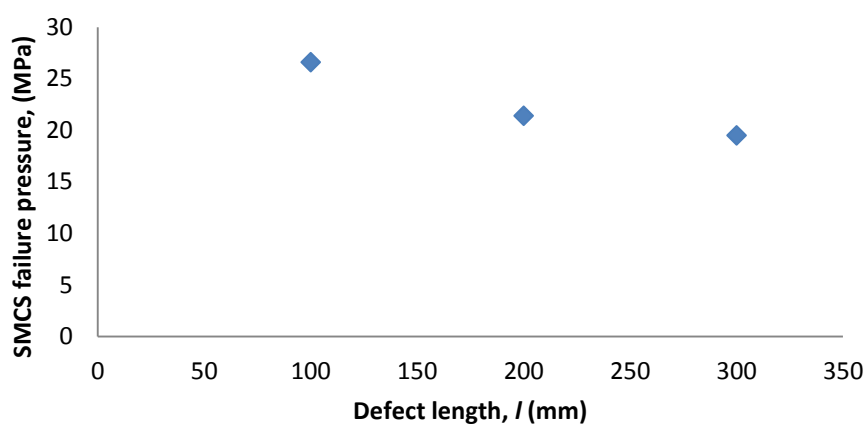
Figure 4.34: Graph of SMCS failure pressure versus defect length of 100 mm distance between defects
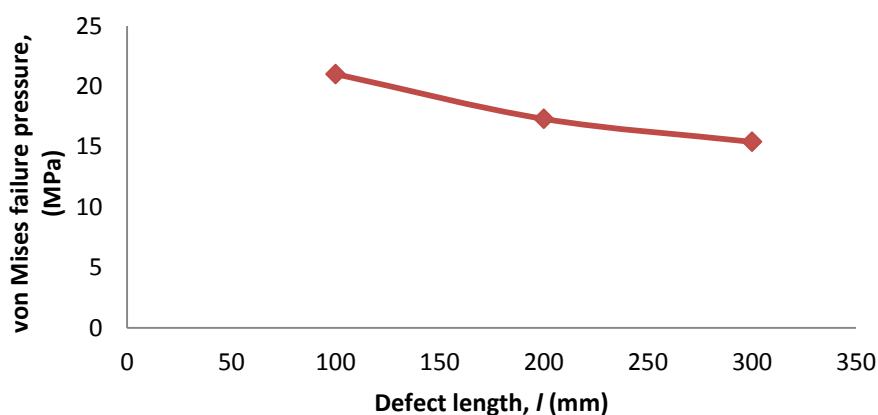
Figure 4.35: Graph of von Mises failure pressure versus defect length of 100 mm distance between defects
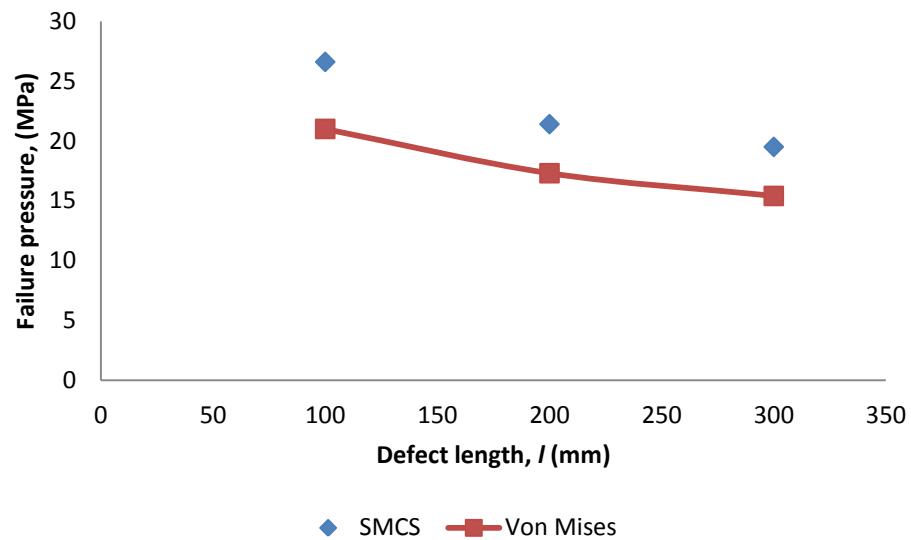
Figure 4.36: Graph of comparison between SMCS and von Mises of failure pressure versus defect length of 100 mm distance between defects

According to Figure 4.34, the failure pressure decrease with the increased of defect length. The maximum failure pressure of SMCS is 26.6 MPa with a defect length of 100 mm and minimum failure pressure is 19.5 MPa with a defect length of 300 mm. von Mises failure pressure shows the similar pattern. Though, the failure pressure of SMCS is always higher than von Mises.
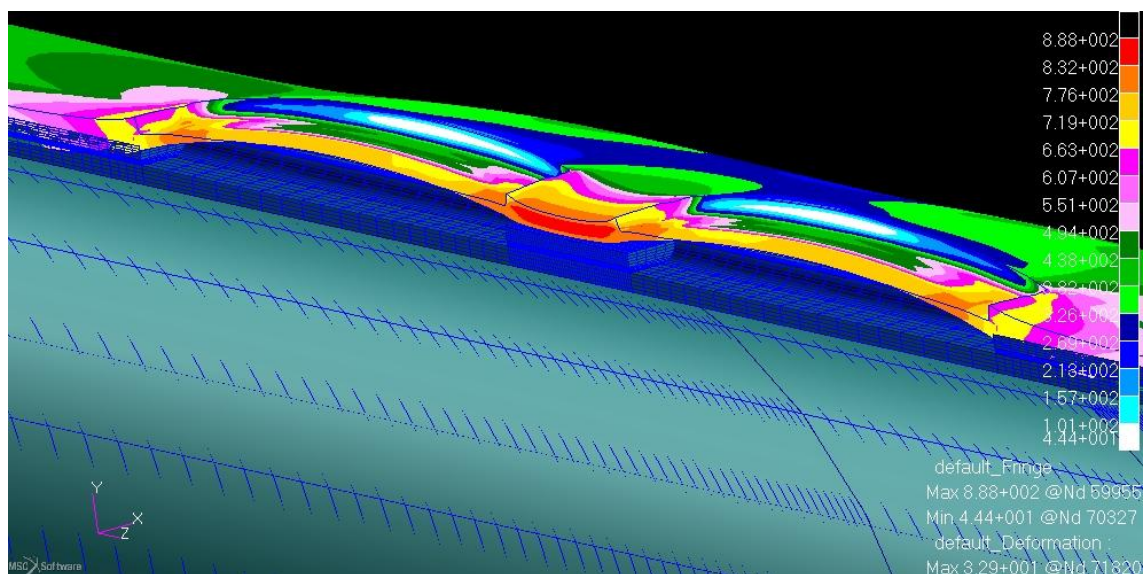

Figure 4.37: SMCS stress distribution of 300 mm defect length
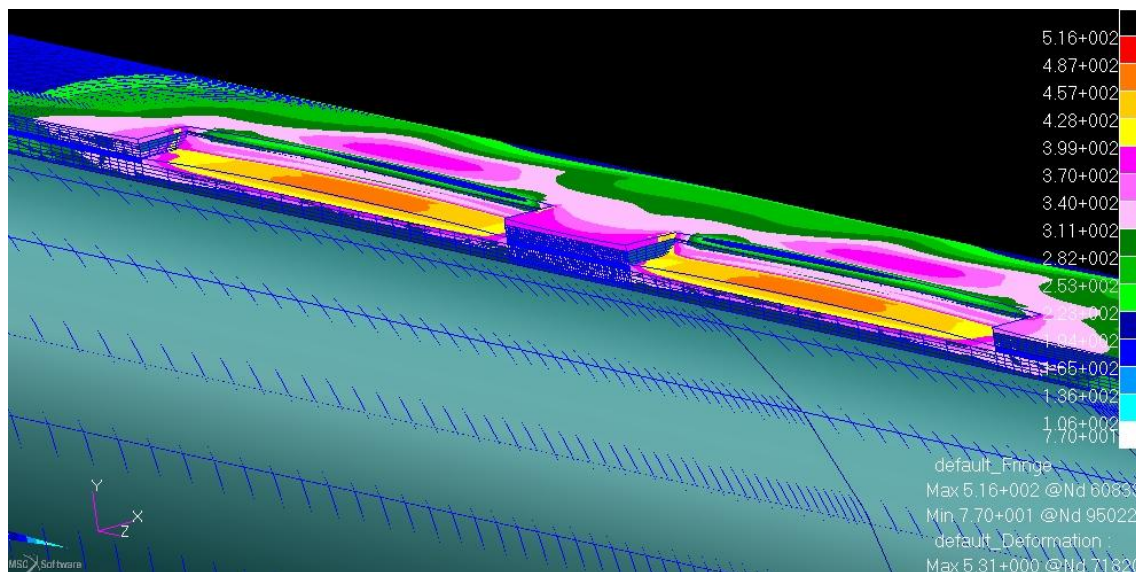
**Figure 4.38:** von Mises stress distribution of 200 mm defect length

Figure 4.37 and 4.38 show the stress distribution of SMCS and von Mises at the parameter of 300 mm defect length and 100 mm of distance between defects.

4.2.8 Comparison of failure pressure for different distance between defects
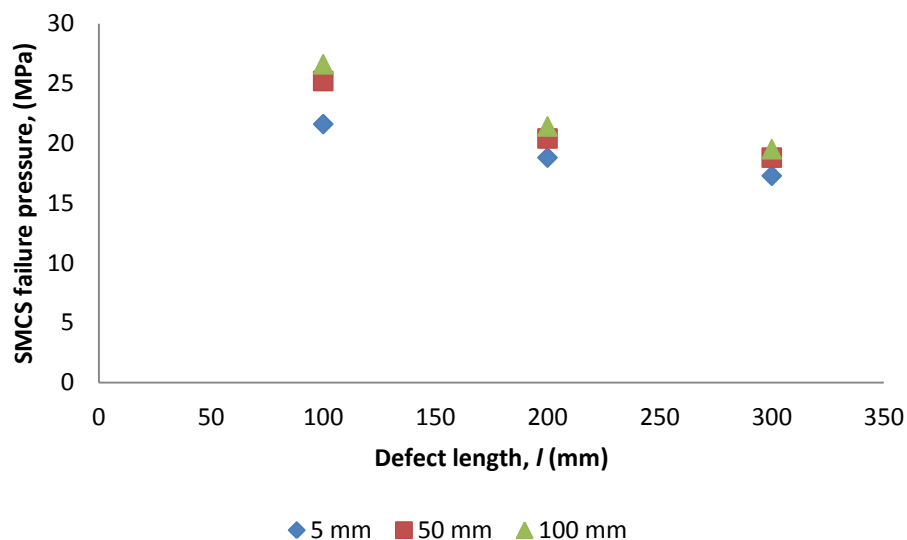
Figure 4.39: Graph of SMCS failure pressure versus defect length for different distance between defects
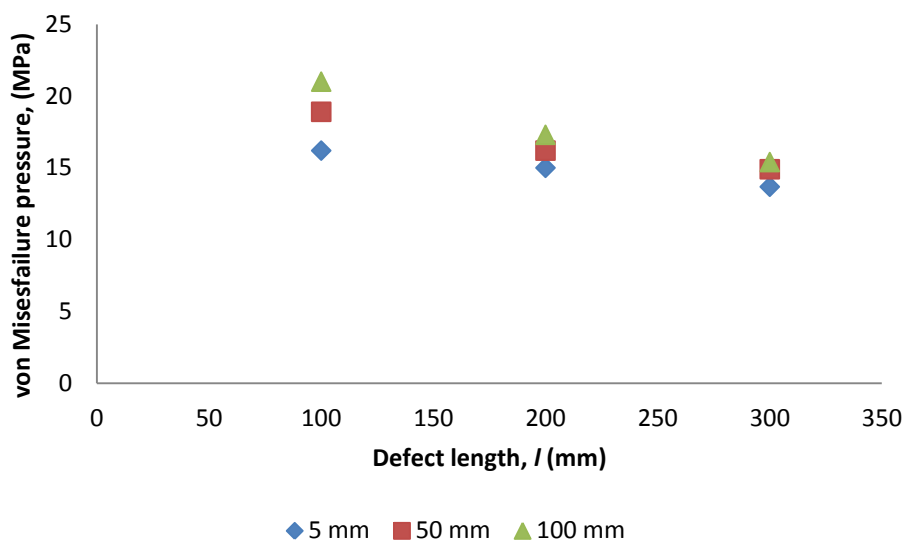
Figure 4.40: Graph of von Mises failure pressure versus defect length for different distance between defects

According to Figures 4.39 and 4.40, both graphs showed a similar pattern which is decreasing, as the distance between defect increase, it can sustain more and more stress intensity. Hence, the failure pressure increase. However, the failure pressure for SMCS and von Mises varied. Failure pressure for SMCS is higher for the three different defect length compared to von Mises. As the distance between defects exceed 150 mm, the failure pressure for SMCS and von Mises decrease slightly.

4.2.9 Comparison of failure pressure between design codes and FEA to different defect length with same distance between defects of 5 mm.

In this section, the failure pressure for different defect length is calculated and compared with the FEA results. The available design code is ASME-B31G, Modified ASME-B31G and DNV-RP-F101. As discussed in the introduction, the design codes are only valid for single defect. Therefore, the values that suitable for the calculation provided that distance between defects is much lower than the defect length. For example, distance between defects of 5 mm with a defect length of 100 mm is valid for the calculation.

Table 4.8: Comparison of failure pressure between design codes and FEA to different defect length with same distance between defects of 5 mm

Defect length, l (mm)	Failure pressure (MPa)			
	ASME B31G	Modified ASME B31G	DNV-RP-F101	FEA
100	10.1452	11.1302	20.0367	21.6
200	9.2591	9.7632	16.6593	18.8
300	8.9378	9.2717	15.3292	17.28

For distance between defects of 5mm (assume as single defects)
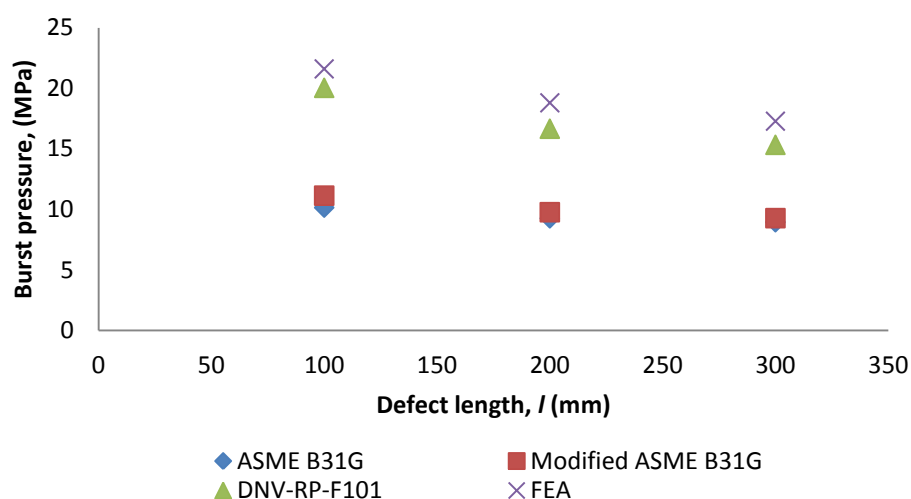
Figure 4.41: Graph of comparison between design codes and FEA of failure pressure versus defect length

According to Figure 4.41, the failure pressure is maximum for FEA, followed by DNV-RP-F101, Modified ASME-B31G and ASME-B31G. Recently developed methods such as DNV-RP-F101 are based on equations fitted to the results of a large number of finite element analyses of blunt, part wall defects, these analyses incorporated a failure criterion validated against actual failure pressure tests. The DNV-RP-F101 method was developed to be mean fits to the experimental and numerical data, and so should be the most accurate method. The modified ASME-B31G is more accurate than the original ASME-B31G.

4.2.10 Comparison of failure pressure between PCORCC and FEA to different defect length with same distance between defects of 5 mm.

In this section, the failure pressure for different defect length is calculated using PCORCC and compared with the FEA results. The equation has the parameter of defect length, l which has the same situation as the design. Therefore, the values that suitable for the calculation provided that distance between defects is much lower than the defect length. For example, distance between defects of 5 mm with a defect length of 100 mm is valid for the calculation.

Table 4.9: Comparison of failure pressure between PCORCC and FEA to different defect length with same distance between defects of 5 mm

Defect length, l (mm)	Failure pressure	
	PCORCC	FEA
200	17.8870	21.6
400	15.1212	18.8
600	13.5233	17.28

For distance between defects of 5mm (assume as single defects)
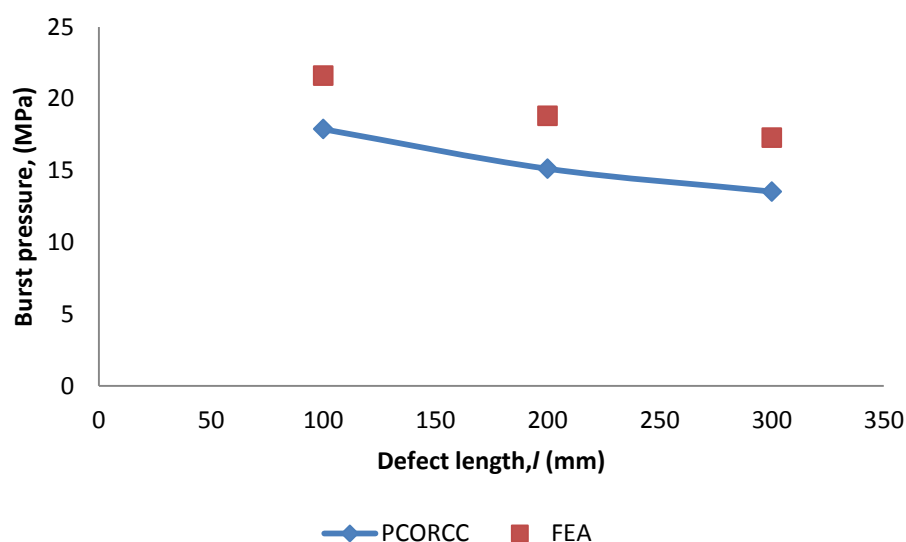
Figure 4.42: Graph of comparison between PCOPCC and FEA of failure pressure versus defect length

According to Figure 4.42, the maximum failure pressure for FEA is 21.6 MPA while the minimum failure pressure is 17.28. The PCORCC shows the same trend line. Though, the failure pressure for FEA result is always higher than PCORCC. The result proved that PCORCC equation is conservative.

4.3   STRESS CONTOUR

This section showed the stress contour of SMCS and von Mises at different pressure level. Figure 4.43 shows the stress contour of SMCS while Figure 4.44 shows the stress contour of von Mises.
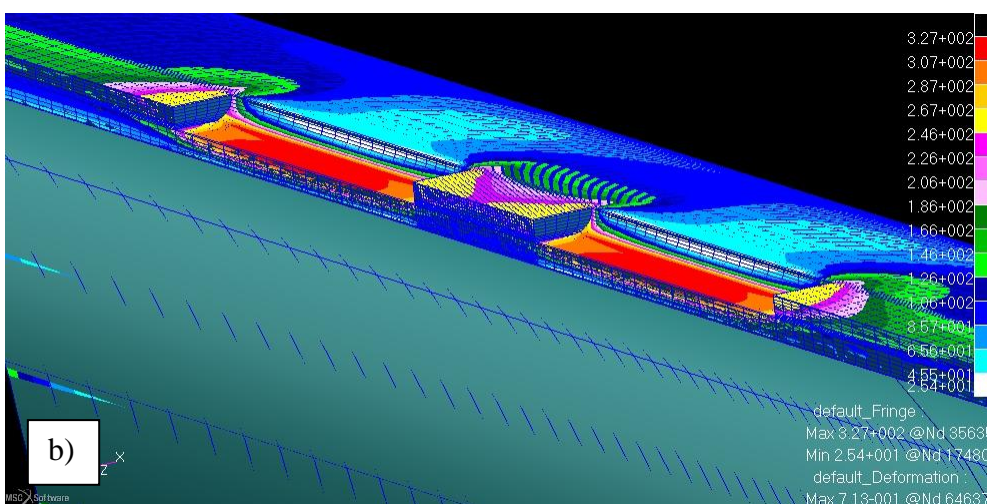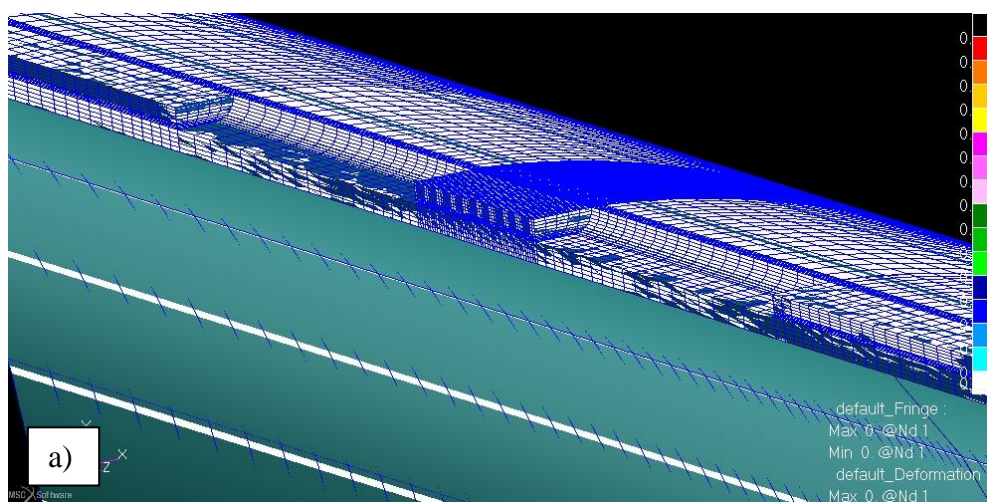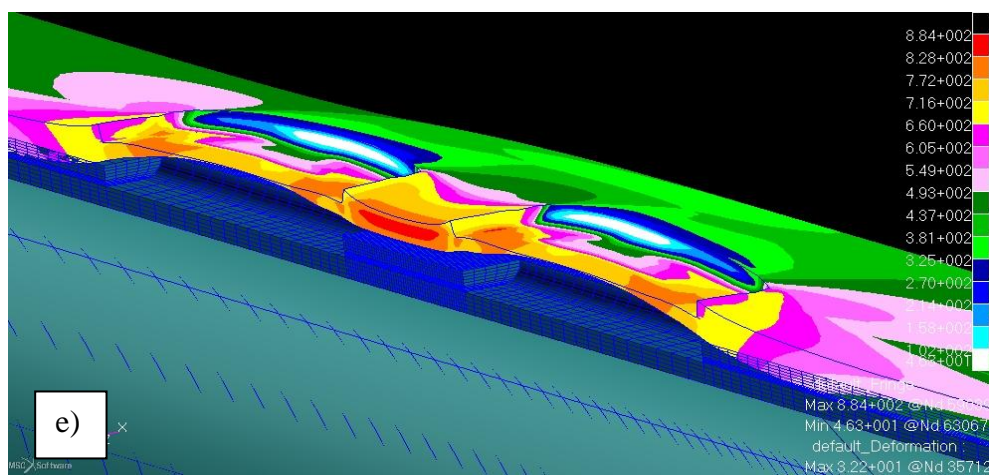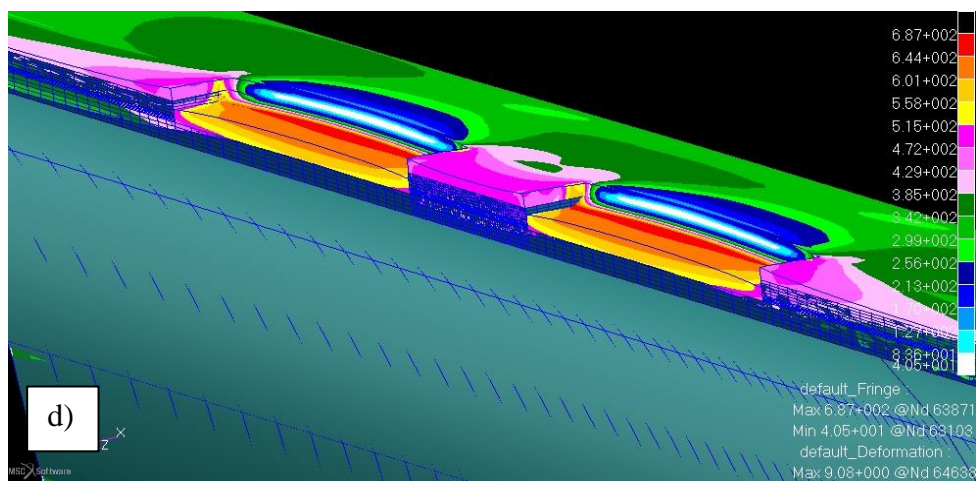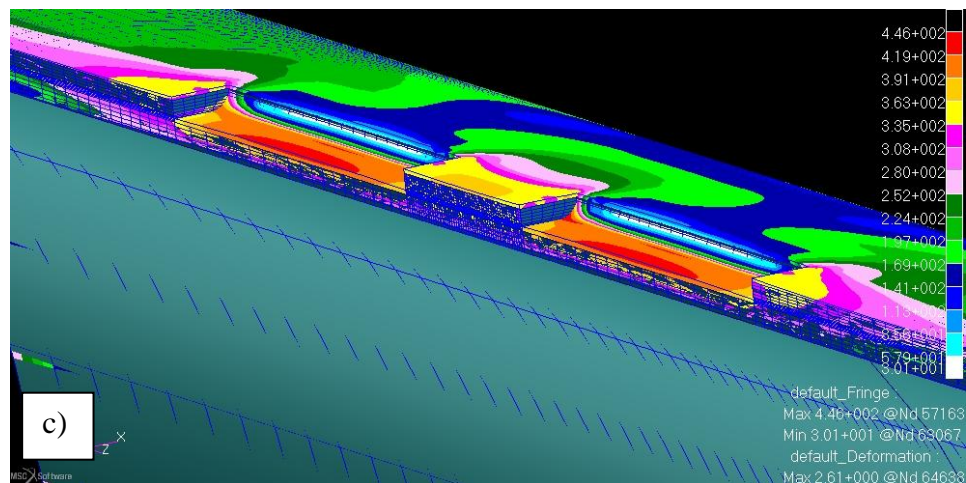
Figure 4.43: SMCS stress contour at different pressure level: a) 0 MPa, b) 5.4 MPa, c)10.8 MPa, d) 16.2 MPa and e) 21.4 MPa
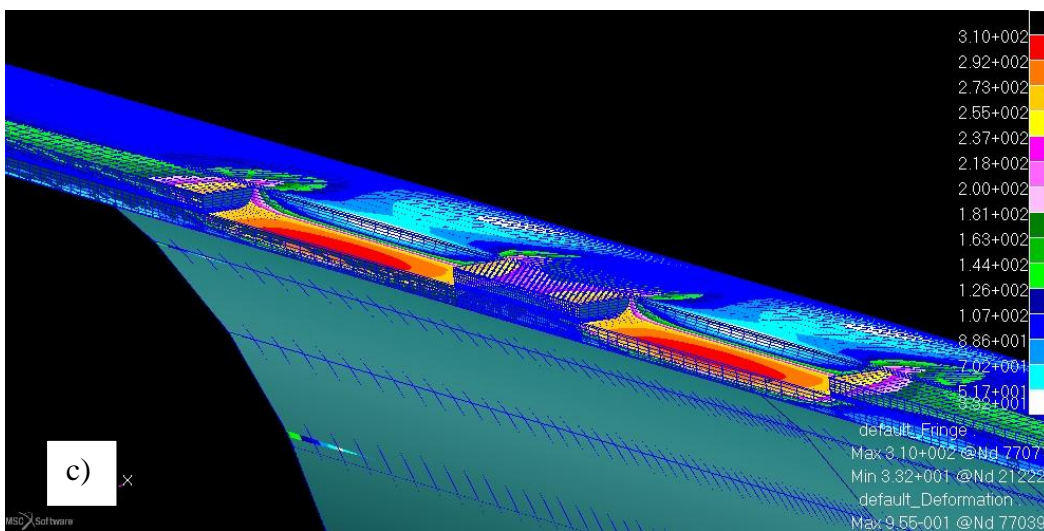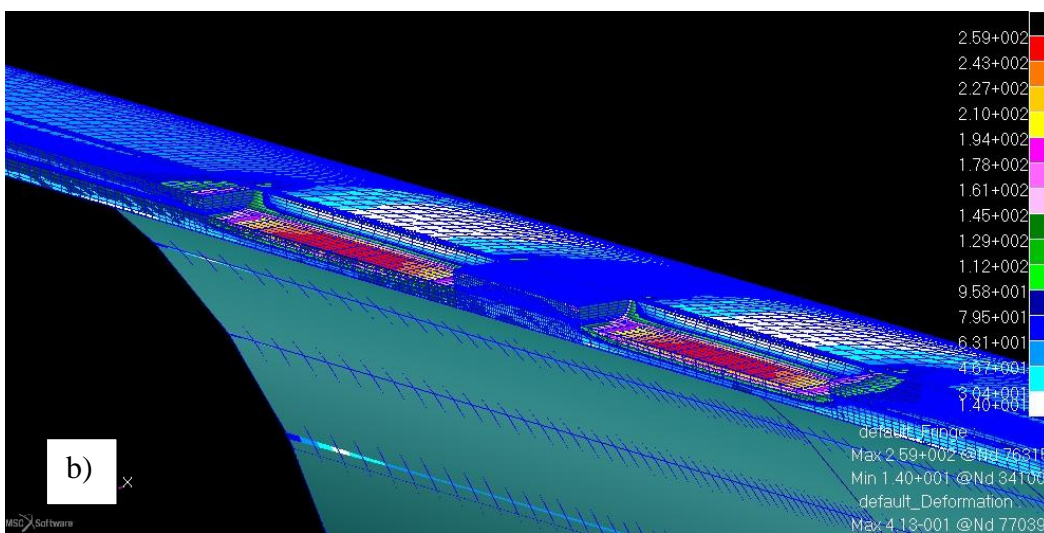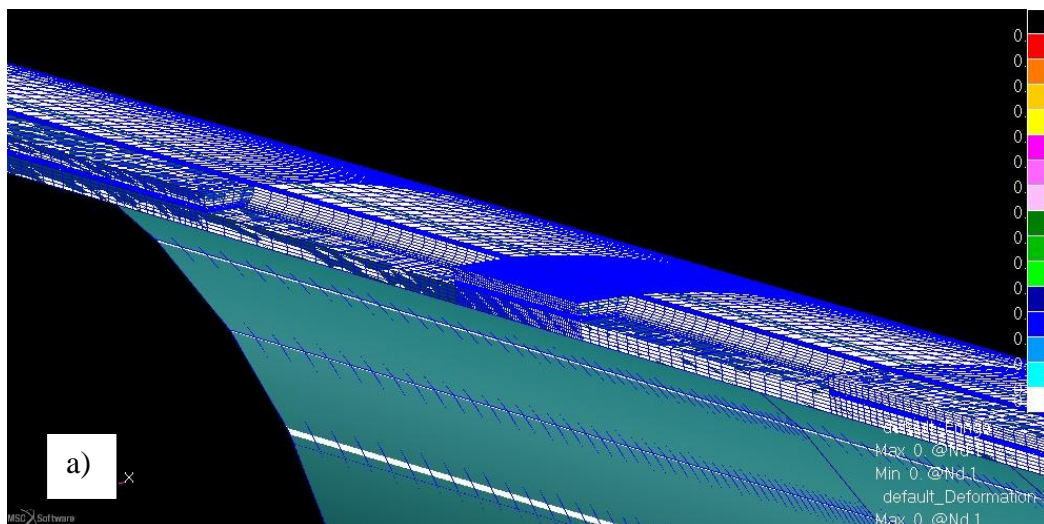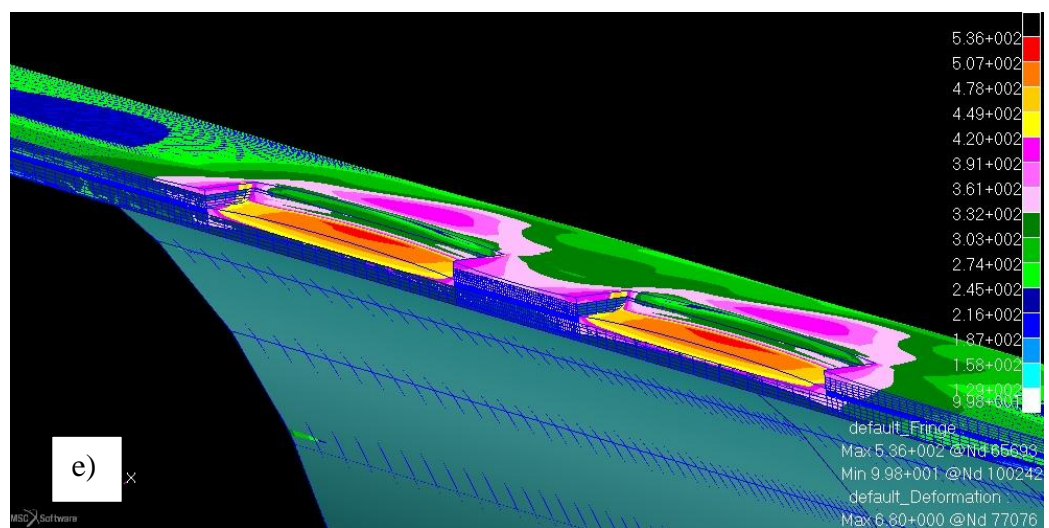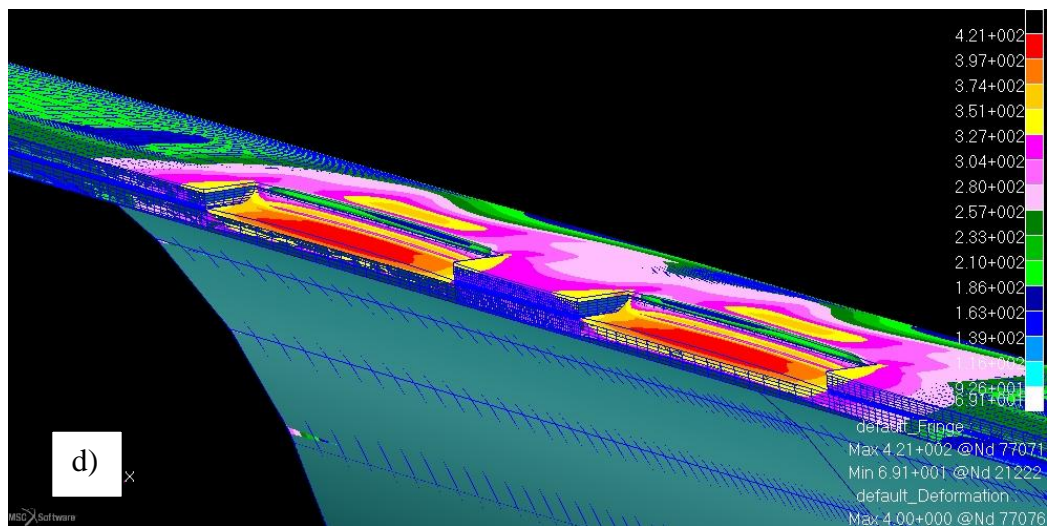
Figure 4.44: Stress contour at different pressure level: a) 0 MPa, b) 2.8 MPa, c) 5.6 MPa, d) 8.4 MPa and e) 13.6 MPa

CHAPTER 5

CONCLUSION AND RECOMMENDATION

5.1   INTRODUCTION

This chapter presents the conclusion of this study based on findings from the simulation process and the direct calculation. The objectives of the research will also be evaluated and the recommendations to improve the research in the future are also included.

5.2   CONCLUSION

Pipeline engineers and operators frequently encounter the need to repair and replace corroded pipeline sections. Therefore, the major concern of the operators is whether the integrity of the pipeline is affected by corrosion defects or not. Aiming to answer this question, a numerical model based on a finite element method and estimated the pressure capacity of API X42 with corroded defects.

The effect of multiple corrosion for this research restricted to the defect length and distance between defects. As the defect length increase, the stress intensity on it had been decreased, and the failure pressure decreases. However, the distance between defects is inversely proportional to the failure pressure increase. There is more pressure needed to overcome the barrier of the pipeline. There are two types of criteria used to evaluate the failure pressure which is SMCS and von Mises. The failure pressure for SMCS is always higher than the von Mises.

Though design codes are useful to evaluate the failure pressure with available equation and parameter, it's only valid for the single defect. For this research, however, some of the value still can use in the design codes. For example, the distance between defects that too small can be assumed that the multiple defects act as a single defect such as 1, 3, 5 and 10 mm compared to much larger of defect length. Compared to available design codes, FEA results always showed the highest values compared to the others. Meanwhile, for the PCORCC equation, the problem was similar to the design code and only valid for small distance between defects. Eventually, the equation could be applied.

5.3   RECOMMENDATION

This report will highlight on simple understanding for beginners. Hence a lot of description of every chapter used simple English language for easier understanding and clarity. Furthermore, this report also consists of the step by step method in order for readers to understand the effect of multiple defects on corroded pipeline. There are some recommendation and all of these suggestions are important to make sure better result will be obtained in the future research.

Due to insufficient time, the evaluation of failure pressure only be done by simulation. The results can only compare between SMCS and von Mises. Therefore, experiment on this multiple defects of failure pressure should be conducted. The experimental data are the most reliable. Hence, the simulation data can be compared. As a result, the percentage of error for simulation analysis can be calculated for comparison between experimental results and finite element analysis.

In this research, due to the restriction of design codes to single defect, the multiple defects of failure pressure unable to be calculated. However, the design codes valid when the distance between defects is small enough to assume the defect as a single defect. Therefore, the design codes should be improved with addition of parameter such as distance between defects in future research.

REFERENCES

API, 2004. " Specification for Line Pipe." American Petroleum Institute

ASTM Standard E8-08, 2008, "Standard Test Method for Tension Testing of Metallic Material". American and Society for Testing and Materials.

Beavers JA, Thompson NG, 2006. "External Corrosion of Oil and Natural Gas Pipelines." *ASM Handbook*. Volume 13C, Corrosion: Environments and Industries.

Beer FP, Johnston ER, DeWolf JT, Mazurek DF, 2009. "Mechanics of Materials." 5th ed. McGrawHill.

Bridgman PW, 1944, "Trans. Am. Society Material", 32, p.553.

Budynas RG, Nisbett JK, 2011. "Shigley's Mechanical Engineering Design." 9th ed. McGrawHill.

Corrosion Doctors (n.d.). Citing Websites. *Eight Forms of Corrosion*. Retreived Dec 1, 2012, from http://corrosion-doctors.org/Corrosion-History/Eight.htm.

CorrView International (n.d.). Citing Websites. *Forms of Corrosion*. Retreived Nov 30, 2012, from http://www.corrview.com/the-corrosion-threat/forms-of-corrosion.

Cosham A, Hopkins P, 2003. "The Effect of Dents in Pipelines-Guidance in the Pipeline Defect Assessment Manual." *ICPVT*-10. July 7-10.

Cosham A, Hopkins P, Macdonald KA, 2007. "Best practice for the assessment of defects in pipelines − Corrosion." *Engineering Failure Analysis*, **14**, pp 1245-1265

Darling D. (n.d.). Citing Websites. *The Encyclopedia of Science*. Retreived Nov 28, 2012, from http://www.daviddarling.info/encyclopedia/C/corrosion.html.

Hancock JW, and Mackenzie AC, 1976. "On The Mechanisms Of Ductile Failure In High-Strength Steels Subjected To Multi- Axial Stress-States", *J. Mech. Phys. Solids*, 24, pp. 147 to 169.

Hopkins P, 2002. "The Structural Integrity Of Oil And Gas Transmission Pipelines." *Comprehensive Structural Integrity*. Volume 1. Elsevier Publishers.

Lee YK et al., 2005. "The Prediction of Failure Pressure of Gas Pipeline with Multi Corroded Region." *Materials Science Forum* Vols. 475-479 pp 3323-3326

Oh CK, Kim YJ, Baek JH, Kim WS, 2007. "Development of stress-modified fracture strain failure of API X65 steel." *Int J Fact*, **143**:119-133

Oh CK, Kim YJ, Baek JH, Kim YP, Kim WS, 2007. "Ductile failure analysis of API X65 pipes with notch-type defects using a local fracture criterion." *International Journal of Pressure Vessels and Piping*, **84**, pp 512-525

Xu LY and Cheng YF, 2012, "Reliability and Failure Pressure Prediction of Various Grades of Pipeline Steel in the Presence of Corrosion Defects and Pre-strain", *International Journal of Pressure Vessels and Piping*, 89,pp.75-84

APPENDIX A

PSM 1

| No.	Activities	1	2	3	4	5	6	7	8	9	10	11	12	13	14
1	Identify problem	▓													
2	Identify objective, scope and problem statement		▓												
3	Literature Review			▓	▓	▓	▓	▓							
4	Design of experiment					▓	▓	▓							
5	Specimen preparation														
6	Experiment setup														
7	Perform tensile test								▓	▓	▓				
8	Analysing data/results									▓	▓	▓	▓		
9	Report preparation												▓	▓	
10	Presentation														▓

PSM 2

No.	Activities	1	2	3	4	5	6	7	8	9	10	11	12	13	14
1	Determine true stress-strain diagram	▓													
2	Development of Failure Criteria		▓	▓	▓										
3	Simulation setup				▓	▓									
4	Structure modelling					▓									
5	Boundary condition						▓								
6	Run the simulation							▓	▓	▓					
7	Analysis of result									▓	▓	▓			
8	Discuss on result												▓		
9	Report preparation								▓					▓	
10	Presentation														▓

APPENDIX B

APPENDIX C

FOUNDRY LABORATORY
FACULTY OF MECHANICAL ENGINEERING
UNIVERSITI MALAYSIA PAHANG

Universiti
Malaysia
PAHANG

Chemical Results

Date: 26/11/2012

Sample ID: Material:

Customer: Dimension:

Commision: Filler metals:

Lab-no.:   Heat treatment:

Reference no.:   Heat-no:

Spectrometer Foundry-MASTER   Grade :

	Fe	C	Si	Mn	P	S	Cr	Mo
1	98,3	0,232	0,257	0,987	< 0,0030	< 0,0030	0,0419	< 0,0050
2	98,3	0,264	0,254	0,987	< 0,0030	< 0,0030	0,0417	< 0,0050
3	98,3	0,266	0,258	0,985	< 0,0030	< 0,0030	0,0386	< 0,0050
Ava	98,3	0,254	0,256	0,986	< 0,0030	< 0,0030	0,0407	< 0,0050

	Ni	Al	Co	Cu	Nb	Ti	V	W
1	0,0372	0,0316	0,0019	0,0205	0,0065	< 0,0020	< 0,0020	< 0,0150
2	0,0358	0,0313	0,0024	0,0237	0,0054	< 0,0020	< 0,0020	< 0,0150
3	0,0376	0,0327	0,0019	0,0247	0,0058	< 0,0020	< 0,0020	< 0,0150
Ava	0,0368	0,0319	0,0020	0,0230	0,0059	< 0,0020	< 0,0020	< 0,0150

	Pb	Sn	B	Ca	Zr	As	Bi
1	< 0,0250	< 0,0020	< 0,0010	> 0,0010	< 0,0020	< 0,0050	< 0,0300
2	< 0,0250	< 0,0020	< 0,0010	> 0,0010	< 0,0020	< 0,0050	< 0,0300
3	< 0,0250	< 0,0020	< 0,0010	> 0,0010	< 0,0020	< 0,0050	< 0,0300
Ava	< 0,0250	< 0,0020	< 0,0010	> 0,0010	< 0,0020	< 0,0050	< 0,0300

Test by: Verify by: